Graduate School of Systemic Neurosciences
LMU Munich

Regulation of cerebral blood flow in health and disease

Matilde Balbi

Dissertation der Graduate School of Systemic Neurosciences

der Ludwig-Maximilians-Universität München

PhD thesis

Munich, 30 July 2015

Supervisor: Prof. Dr. Nikolaus Plesnila

Second reviewer: Dr. Leda Dimou

Date of the oral defense: 10.11.2015

Table of Contents

List of abbreviations

5-HT	serotonin
AA	arachidonic acid
AC	adenylyl cyclase
ACD	age related cerebrovascular dysfunction
ACh	acetylcoline
ATP	adenosine 3’5‘triphosphate
AVD	age related vascular dementia
BBB	blood brain barrier
BK	calcium-sensitive big potassium channels
Ca^{2+}	calcium
CADASIL	cerebral autosomal dominant arteriopathy with subcortical infarcts and leukoencephalopathy
cAMP	cyclic adenosine 3‘ 5‘ monophosphate
CARASIL	cerebral autosomal recessive arteriopathy with subcortical infarcts and leukoencephalopathy
CBF	cerebral blood flow
cGMP	cyclic guanine monophosphate
CNS	central nervous system
CO_2	carbon dioxide
COX	cyclooxygenase
CPP	cerebral perfusion pressure
CTGF	connective tissue growth factor
CSD	cortical spreading depolarization
CVR	cerebrovascular resistance
EBI	early brain injury
EDHF	endothelium-derived hyperpolarizing factor

EET_S	epoxyeicosatrienoic acids
EFS	electrical field stimulation
EGF	epidermal growth factor
eNOS	endothelium nitric oxide synthase
GABA	gamma-aminobutyric acid
GOM	granular osmiophilic material
H^+	hydrogen
HTRA1:	high temperature requirement A serine peptidase 1
ICP	intracranial pressure
IGF	insulin like growth factor
K^+	potassium
K_{ATP}	ATP-sensitive potassium channel
K_{ir}	inward-rectifier potassium channels
L-Arg	L-arginine
mAchR	muscarinic acetylcholine receptor
MCA	middle cerebral artery
mGluR	metabotropic glutamate receptor
MRI	magnetic resonance imaging
NE	norepinephrine
nNOS	neuronal nitric oxide synthase
NO	nitric oxide
Notch3ECD	Notch3 extracellular domain
Notch3ICD	Notch3 intracellular domain
NOS	nitric oxide synthase
NVC	neurovascular coupling
NVU	neurovascular unit
O_2	oxygen

PDGF-Rβ	beta-type platelet-derived growth factor receptor
PG	prostaglandin
PGD_2	prostaglandin D_2
PGE_2	prostaglandin E_2
PGH_2	prostaglandin H_2
PGI_2	prostaglandin I_2
PKA	protein kinase A
PNS	peripheral nervous system
rCBF	regional cerebral blood flow
ROS	reactive oxygen species
SAH	subarachnoid hemorrhage
sGC	soluble guanylyl cyclase
SMC	smooth muscle cell
SVD	small vessel disease
TGF-β	transforming growth factor β
VSM	vascular smooth muscle

Abstract

Due to limited capacity for substrate storage and high metabolic rate of brain tissue, a precise regulation of cerebral blood flow (CBF) is critical for the maintenance of constant nutrient and oxygen supply to the brain. This thesis explores the function of pial and parenchymal microcirculation in nitric oxide-dependent and neuronal activity-induced regulation, under physiological and pathological conditions using aged mice and mouse models for acute injury (subarachnoid hemorrhage—SAH) and small vessel disease (CADASIL and CARASIL). For this purpose, I established an experimental protocol using laser Doppler flowmetry as well as one- and two-photon in-vivo imaging, which allowed me to measure regional changes in CBF as well as individual artery diameter, respectively, in response to CO_2 administration and forepaw stimulation. By visually examining pial arteries, my investigation found age-related impairments in nitric oxide-dependent response to CO_2 at an earlier stage (8 months) than previous reports. My investigation of SAH revealed for the first time that intraparenchymal vessels show severe functional impairments after SAH. While reactivity to CO_2 is completely blunted, vasodilation upon neuronal activation following forepaw stimulation remains unchanged for up to 3 hours after SAH, suggesting that SAH induces a significant and selective dysfunction of NO-mediated vasodilation. Small vessel diseases are inherited or sporadic angiopathies of the brain that lead to white matter lesions, lacunar infarcts and dementia. Cerebral autosomal dominant arteriopathy with subcortical infarcts and leukoencephalopathy, CADASIL, and its recessive counterpart, CARASIL, are the only available animal models to study small vessel diseases. A decrease CBF response to CO_2 was found in 12-month old CADASIL mice, and decreases in vessel dilation and CBF response to CO_2 administration and neuronal activation were observed in CARASIL mice. Failures in the CADASIL and SAH models in NO-dependent regulation but not neuronal activity-induced regulation suggest that these mechanisms run along separate biochemical pathways. These results elucidate cerebrovascular regulatory processes and further the knowledge base required for comprehensive and efficient therapy.

1 Introduction

The brain is one of the most complex organs in the body, known for its high specialization, structural and functional hierarchy, and large metabolic demand (Kalaria 1996). From the time the embryonic brain first develops, the brain never ceases to be active and hungry for energy sources (Grigg, Kelly et al. 1987; Prayer, Kasprian et al. 2006). Neuronal activity requires vast amounts of energy, larger than what neighboring glial cells may be able to deliver from their limited glycogen storage capabilities (Gruetter 2003; Brown and Ransom 2007). Therefore, the main energy substrates are continuously extracted from the blood stream: glucose at an average rate of 10% and oxygen at a rate between 50 and 70% (Ohta, Meyer et al. 1992). Due to constant neuronal activity, the average cerebral blood flow (CBF) required under normal resting metabolic conditions is of about 800 mL/min, or 57 mL/100g-tissue/min, which corresponds to approximately 15% of total resting cardiac output (Ohta, Meyer et al. 1992). The brain accounts for 20% of total body oxygen consumption in adults despite contributing to just 2% of body weight (Kalaria 1996). However, different regions of the brain have different energy requirements, driven specifically by neuronal activity. Central white matter, constituted primarily by axonal tracts without synapses, consumes approximately one third of the energy used by gray matter (Sokoloff 1977), where synapses account for large portions of signaling energy use: 59% in the cortex and 30% in the cerebellum, in terms of glucose uptake (Attwell and Laughlin 2001; Howarth, Peppiatt-Wildman et al. 2010). In order to constantly match the brain's high energy demand under resting conditions as well as during activation, cerebral perfusion needs to be maintained at a high level independent of fluctuations of systemic blood pressure and to increase during neuronal activity through a homeostatic process known as autoregulation (Aaslid, Lindegaard et al. 1989). Additionally, to efficiently supply the precise amount of energy substrates required to satisfy specific metabolic needs, neurons, glial cells and blood vessels communicate with each other to regulate cerebral blood flow and vessel permeability as a function of location and neuronal activity in a process known as neurovascular coupling (NVC) (Gordon, Mulligan et al. 2007).

Any supply-and-demand imbalance between CBF and activity of the brain quickly affects cerebral function (Kimelberg 2004; Hawkins and Davis 2005; Zlokovic

2005). This is demonstrated by the fact that interruption of blood flow results in loss of consciousness within 5 to 10 seconds as a result of cerebral ischemia. If blood flow is not restored promptly, it may result in permanent brain damage (Iadecola 2004). Thus, to prevent the devastating consequences of ischemia and satisfy the high metabolic demands of the brain, cerebral circulation is endowed with several specialized regulation features (Iadecola 1998).

1.1 Regulation of CBF

CBF is determined by both cerebral perfusion pressure (CPP) and cerebrovascular resistance (CVR). CPP can be calculated from the difference between blood pressure and internal cerebral pressure. CVR is determined by the diameter of the intracranial arteries and blood viscosity (Markus 2004). Arterial pressure is a major determinant of CBF (Faraci and Heistad 1998), but it fluctuates widely during daily-life activities, which could induce dangerous increases or decreases in CBF (Cipolla 2007). To maintain stable blood flow, cerebral circulation has well-developed routes for collateral circulation, such as the communications between the basilar and internal carotid arteries at the circle of Willis, which play an important protective role providing means of irrigation that compensate for each other (Riggs and Rupp 1963). Collateral supply also occurs through anastomoses between the external carotid artery branches and intracerebral circulation (Vander Eecken and Adams 1953). In conditions were CPP remains constant, any change in CBF must result from a change in CVR (Markus 2004). Thus, under normal circumstances, there is a direct correlation between CBF and intracranial vessel diameter: CBF will increase as vessels dilate and decrease as vessels constrict. There are two major mechanisms that regulate CBF by adjusting vessel diameter, autoregulation and functional hyperemia.

1.1.1 Autoregulation

Cerebral autoregulation is the homeostatic process whereby intracerebral arteries and arterioles maintain a constant CBF in the face of changing CPP by

changing their diameter to adjust CVR. It maintains a leveled CBF in physiological situations, such as exercise, and in pathological conditions, such as hypotension (Iadecola 1993). This protects the brain from fluctuations in arterial pressure, keeping a near constant blood flow within the range of 60–150 mmHg (Cipolla 2007). When the limits of autoregulation are reached, CBF passively complies with changes in perfusion pressure. Specifically, when CPP falls below the lower limit of autoregulation, the decrease in CBF results in hypoperfusion (Hossmann 1994) and needs to be compensated by an increase in oxygen extraction from the blood (Iadecola 1998). Clinical signs are not seen until the decrease in perfusion exceeds the ability of increased oxygen extraction to meet metabolic demands. At this stage, clinical signs of hypoperfusion occur, including dizziness, altered mental status, and may eventually result in irreversible tissue damage (Hossmann 1994; Iadecola 2004). On the other hand, if mean arterial pressure increases beyond the upper limit of autoregulation, resistance arteries in the brain are not able to sustain vasoconstriction (Strandgaard and Paulson 1990) which leads to dilation along the entire length of the arterioles, and a passive increase in CBF. An early sign of functional disruption is the so called “sausage stringing” appearance, where the vessel is characterized by an alternating pattern of dilated segments, representing regions of passive dilation, and focal regions of constrictions (Markus 2004). These changes can be associated with damage of the cerebrovascular endothelium and disruption of the blood brain barrier (BBB).

The mechanisms of cerebral autoregulation are not completely understood. Myogenic, metabolic and neurogenic factors have been hypothesized to play a role. The myogenic hypothesis describes how smooth muscle in the resistance arteries responds directly to alteration in perfusion pressure by contracting during an increase in pressure (Kontos, Wei et al. 1978). Autoregulation of cerebral blood flow when pressure fluctuates beyond the upper limit of the autoregulatory curve is most likely due to myogenic behavior of cerebral smooth muscles, which constrict in response to elevated pressure and dilate in response to decreased pressure (Mellander 1989; Osol, Brekke et al. 2002). The metabolic hypothesis states that the reductions in cerebral blood flow stimulate the release of vasoactive substances from the brain, affecting arterial dilation. These vasoactive substances include hydrogen (H^+), potassium (K^+), oxygen (O_2), and adenosine (Chillon, Ghoneim et al. 1997). A

neurogenic factor, neuronal nitric oxide, has also been shown to modulate cerebral blood flow autoregulation, suggesting that intrinsic innervation may play a role in the underlying mechanism (Talman and Nitschke Dragon 2007).

1.1.2 Functional hyperemia

The high metabolic demand of neuronal tissue requires close coordination between neuronal activity and blood flow within the brain parenchyma (Hamel 2006; Drake and Iadecola 2007). Functional hyperemia, or neural activity coupling with CBF, is the mechanism by which blood flow is regulated at a local level. Hyperemia is activated in physiological situations, such as reading, calculating, or any other mental exercise (Gordon, Mulligan et al. 2007). It can also be triggered in pathological situations, such as seizures, when metabolic demand increases in a specific brain area (Itoh and Suzuki 2012). Vascular adjustments underlying increases in CBF involve relaxation of both local arterioles and upstream arteries supplying the activated area (Cox, Woolsey et al. 1993; Kleinfeld, Mitra et al. 1998; Takano, Tian et al. 2006). It has been estimated that nearly every neuron in the human brain is connected to its own capillary (Zlokovic 2005). Subcortical microvessels are innervated by neighboring principal neurons and interneurons from within the brain parenchyma and are unique in their apposition to astrocytic end-feet that surround arterioles (Kulik, Kusano et al. 2008). Upstream dilation prevents a drop in microvascular pressure in the dilated vessels of the activated region and avoids a blood ‘grab’ from adjacent vascular territories.(Faraci and Heistad 1998; Kulik, Kusano et al. 2008) Neurons whose cell bodies are located within the subcortical brain regions (e.g., nucleus basalis, locus ceruleus, raphe nucleus) project to cortical microvessels to control local blood flow through neurotransmitter release—e.g., Acetylcholine (ACh), norepinephrine (NE), serotonin (5-HT) (Hamel 2006). Neurotransmitter release stimulates receptors on astrocytes, endothelium, or smooth-muscle cells (SMC) to constrict or dilate, thereby regulating local blood flow in concert with neuronal demand (Iadecola 2004; Hamel 2006; Drake and Iadecola 2007). Hemodynamic neurovascular coupling ensures a strong increase in cerebral blood flow and an acute increase in neuronal glucose uptake upon increased neural activity.

1.2 Anatomy

The regulation of CBF through vasodilation and vasoconstriction is performed by a group of cells closely related to each other called neurovascular unit (NVU). Components of this NVU include neurons, astrocytes, blood vessels and extracellular matrix components. These cells, through their intimate anatomical and chemical relationship, monitor neuronal activity and metabolism and trigger necessary vascular responses to supply required substrates (Hawkins and Davis 2005; Weiss, Miller et al. 2009).

1.2.1 Neurons

Neurons are the building blocks of the electrical circuitry of the brain. As such, they possess sophisticated homeostatic mechanisms to regulate their intrinsic, synaptic and metabolic properties (Koehler, Gebremedhin et al. 2006; Banerjee and Bhat 2007). Intrinsic conductance is subject to activity dependent regulation in a negative feedback loop that maintains a basal level of electrical activity and prevents cell death due to excitotoxicity (Franklin, Fickbohm et al. 1992). Manipulations that either increase or decrease synaptic activity are accompanied by alterations in synaptic strength over the course of several hours that counteract the changes in activity (Kirov and Harris 1999). To regulate their energy supply, active synapses send signals to different segments of the cerebral vasculature through neuronal-astrocytic-vascular apposition (Chedotal, Cozzari et al. 1994; Abounader and Hamel 1997; Vaucher, Tong et al. 2000) either directly or through an interneuron, so as to elicit an increase in CBF as a function of neural activity within seconds and highly restricted to the activated region (Cox, Woolsey et al. 1993; Silva, Lee et al. 2000).

Interneurons constitute a class of neurons responsible for communication between larger, principal neurons in the central nervous system (CNS) acting as integrators of neuronal activity (Chedotal, Cozzari et al. 1994). In the context of neurovascular coupling, interneurons have been demonstrated to make direct contact with cortical microvessels and astrocytic processes (Cauli, Tong et al. 2004; Haydon and Carmignoto 2006; Cauli and Hamel 2010). Depending on the type and frequency of the stimulus, afferent signals in the cortex engage specific populations

of interneurons, which release vasoactive substances, namely neuropeptide Y (Abounader, Villemure et al. 1995; Cauli, Tong et al. 2004), and somatostatin (Long, Rigamonti et al. 1992), capable of directly dilating or constricting arterioles, as well as neurotransmitters that indirectly affect vascular tone through the modulation of excitatory neurons or astrocytes (Dunn and Nelson 2014).

1.2.2 Astrocytes

Astrocytes are uniquely positioned to monitor and modify synaptic activity and contribute to the increase in CBF produced by neural activity (Harder, Zhang et al. 2002). Anatomically, neurovascular communication takes place mainly through the astrocytic end-foot. The end-foot is a peculiar anatomical structure, consisting of a highly specialized astrocyte extension that is in contact with the surface of SMCs and pericytes (Kacem, Lacombe et al. 1998). The end-foot provides a broad contact surface with SMCs or pericytes, wrapping them and acting as a fast and efficient surface for the action of neurotransmitters and neuromodulators. The significance of these interactions to the regulation of CBF was first substantiated by the demonstration that astrocytes could synthesize vasodilatory messengers, particularly epoxyeicosatrienoic acids (EETs) generated from P450 arachidonic acid epoxygenase activity (Alkayed, Birks et al. 1996), that were involved in CBF response to glutamate (Alkayed, Birks et al. 1997; Harder, Roman et al. 1998). NVU astrocytes are able to detect neuronal levels of glutamate and gamma-aminobutyric acid (GABA), thanks to their metabotropic glutamate receptors (mGluRs), leading to increases in intracellular calcium (Ca^{2+}) and cyclooxygenase (COX) activation. They are also able to convert those signals into vasomotor commands through arachidonic acid (AA) products such as prostaglandin E_2 (PGE_2) (Zonta, Angulo et al. 2003; Pelligrino, Vetri et al. 2011; Duchemin, Boily et al. 2012). Another pathway activated in astrocytic end-feet following Ca^{2+} increases is the large-conductance, Ca^{2+}-sensitive big potassium channels (BK) that induces K^+ release, activation of smooth muscle inwardly rectifying potassium channels (K_{ir}) and relaxation (Filosa, Bonev et al. 2006). Studies performed in brain slices show that direct electrical stimulation of neuronal processes raises calcium in astrocytic end-feet and causes dilation of nearby arterioles (Filosa, Bonev et al. 2004). However, whether dilation or constriction occurs seems to depend on the level of calcium and resting tone

(Mulligan and MacVicar 2004). Astrocytes have a great capacity for propagating calcium waves, forming extensive and specialized networks of intercommunication (Cornell-Bell, Finkbeiner et al. 1990). They communicate simultaneously with neurons and blood vessels (Lopez-Bayghen and Ortega 2011; Santello, Cali et al. 2012), establishing connections that not only enable the interplay between neurons but also between capillaries and pericytes at a physical and chemical level through the release of gliotransmitters (Haydon and Carmignoto 2006; Petzold and Murthy 2011).

1.2.3 Blood vessels

Willis (1664) gave the first anatomical description of the arterial circle at the base of the brain, but no physiological study on this structure was performed until 1912 when Kramer studied the distribution of blood to the brain in the living animal by injecting methylene blue directly into the carotid or vertebral arteries. Two pairs of large arteries provide the vascular supply of the brain: carotid and vertebral pairs. The vertebral arteries merge to form the basilar artery and the basilar artery together with the internal carotid arteries merge to form the circle of Willis at the base of the brain (Mc and Potter 1951). Large cerebral arteries arising from the circle of Willis branch out into smaller pial arteries that travel on the surface of the brain across the subarachnoid space (Iadecola and Nedergaard 2007). Pial vessels form an effective collateral network such that occlusion of one vessel does not significantly decrease cerebral blood flow. Pial arteries receive perivascular innervation from the peripheral nervous system, which forms a network of varicose fibers within the adventitial layer that decreases in density upon entering the Virchow–Robin space and then disappears in vessels within the brain parenchyma (Chedotal and Hamel 1990). Arteries have a continuous elastic membrane on which endothelial cells rest (internal elastic lamina) and several SMC layers—typically more than three.

Pial arteries give rise to penetrating arteries and arterioles that enter the brain parenchyma. Penetrating arterioles lie within the Virchow–Robin space, which is a continuation of the subarachnoid space and varies considerably in depth between species (Jones 1970). As penetrating arterioles extend deeper into the brain, the Virchow-Robin space disappears, and their basal lamina forms direct contact with

perivascular astrocytic processes (end-feet), becoming parenchymal arterioles (Palay 1991). Penetrating and parenchymal arterioles are long and largely unbranched such that occlusion of an individual arteriole results in significant reductions in flow and damage to the surrounding local tissue (Nishimura, Schaffer et al. 2007). Parenchymal arterioles receive innervations from within the brain tissue with nerve afferents from subcortical neurons or local cortical interneurons that project to the perivascular space surrounding the arteriole (Estrada, Mengual et al. 1993). However, the targets of most terminals are astrocytes surrounding the arterioles in the brain neuropil (Estrada, Mengual et al. 1993; Cohen, Molinatti et al. 1997). While parenchymal arterioles have only one layer of smooth muscle (Iadecola and Nedergaard 2007) they possess greater basal tone and are unresponsive to some neurotransmitters that can have large effects on upstream vessels, such as NE or 5-HT (Cipolla, Li et al. 2004). Arterioles give rise to capillaries, which are comprised of a layer of endothelial cells resting on the basal lamina and pericytes, perivascular cells containing contractile elements analogous to SMCs (Palay 1991). The total length of capillaries in human brain is about 400 miles, and the capillary surface area available for molecular transport is about 20 m^2 (Begley and Brightman 2003). The microvascular density in the CNS is associated with the rate of metabolic activity of different regions (Villringer and Dirnagl 1995; Malonek, Dirnagl et al. 1997). Regions with the highest synaptic activity and metabolic demand are endowed with higher levels of vascularization, which is evident when comparing gray matter to white matter: capillaries constitute up to 0.5% of volume in the optic chiasm and up to 2% in areas of the sensory cortex (Lierse and Horstmann 1965).

1.2.3.1 Endothelial cells

As in peripheral organs, endothelial cells are involved in regulation of vessel diameter, adhesion of inflammatory cells, regulation of ion and water transport, angiogenesis, and thrombus formation (Zlokovic 2008). Brain endothelial cells are, however, unique in that they are sealed by tight junctions—a feature that creates the blood brain barrier. Endothelial cells produce trophic and vasoactive mediators, including nitric oxide (NO), prostaglandin I_2 (PGI_2), and endothelium-derived hyperpolarizing factor (EDHF), all of which decrease vascular tone in order to increase cerebral blood flow (Furchgott and Zawadzki 1980; Faraci and Heistad

1998). Specifically, since NO synthase (NOS) is calcium–dependent,(Sobey and Faraci 1997) production of NO by endothelial NOS (eNOS) is primarily activated by calcium-dependent binding of calmodulin. Thus, many factors that increase intracellular calcium activate eNOS. Whether NO is produced basally or is induced, NO diffuses to vascular smooth muscle (VSM) where it causes vasodilation primarily by activating soluble guanylyl cyclase (sGC) (Sobey and Faraci 1997). Activation of sGC results in increased levels of cyclic guanine monophosphate (cGMP), which in turn activates protein kinase G (PKG), causing relaxation of SMC by opening BK channels and reducing intracellular calcium (Robertson, Schubert et al. 1993). PGI_2 is normally produced by COX-1 from AA and diffuses to VSM where it activates adenylyl cyclase (AC), causing increased production of cyclic adenosine monophosphate (cAMP) and thus relaxation. EDHF is a potential product of AA metabolism. EDHF diffuses to vascular muscle where it activates K^+ channels and causes closure of Ca^{2+} channels. Increased activity of K^+ channels produces hyperpolarization and relaxation of vascular muscle (Faraci and Heistad 1998) (Figure 1).

1.2.3.2 Pericytes

Pericytes belong to the vascular smooth muscle cell lineage. They are located in capillaries between endothelial cells and astrocytic end-feet and might encircle 30% to 70% of the capillary wall (Allt and Lawrenson 2001) at a pericyte to endothelia ratio in the brain of 1:3 compared to 1:100 in striated muscles (Armulik, Genove et al. 2010; Peppiatt, Howarth et al. 2006). They provide mechanical stability to microvessels by matrix deposition and by releasing and activating signals that promote the development and maturation of endothelial cells (Sa-Pereira, Brites et al. 2012). Recent studies have shown that pericytes are contractile cells with contractile proteins that, being juxtaposed to cerebral capillaries, regulate brain capillary blood flow through contraction and relaxation in response to neuronal activity (Peppiatt, Howarth et al. 2006). In this regard, pericytes may function similarly to SMC in arterioles and small pial arteries in the brain, which regulate CBF through vasoconstriction and vasodilation (Chow, Bell et al. 2007). It has been suggested that endothelial cells might aid in communication between pericytes, as they are connected by gap junctions, and have a large flow of adenosine

triphosphate (ATP), which is a well-known promoter of remote communication between neural syncytia even at long distances (Wu, Shen et al. 2006).

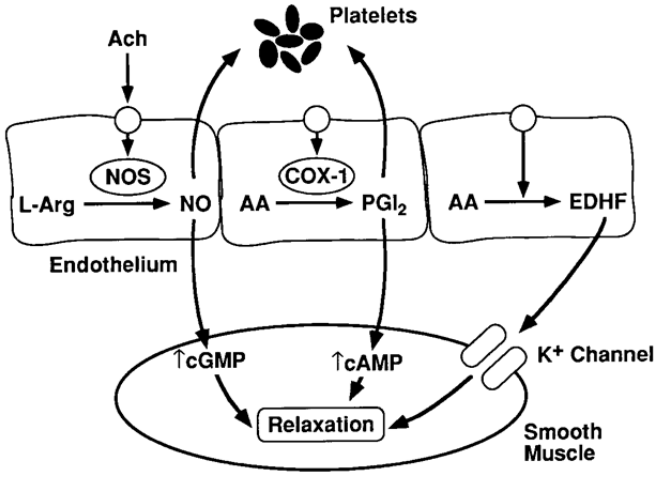

Figure 1: Some mechanisms of endothelium-dependent relaxation of cerebral vascular muscle. NO is produced by NOS from amino acid L-arginine (L-Arg). NO diffuses to vascular muscle where it activates soluble guanylate cyclase, causing increased production of cGMP, which results in relaxation. PGI_2, once produced, diffuses to vascular muscle increasing the production of cAMP which results in relaxation. EDHF Increases activity of potassium channels produces hyperpolarization and relaxation of vascular muscle (Kim and Filosa 2012).

1.3 Vasoactive factors

Communication between depolarized neurons and glia require vasoactive factors that act together to regulate CBF (Iadecola 2004). Cerebral endothelial cells, pericytes, and smooth-muscle cells are the target of these signals and transduce them into coordinated vascular adjustments that ultimately lead to an increase in CBF. Therefore, any regulation in CBF evoked by brain activity is accomplished by the coordinated action of multiple mediators that originate from different cells and act at different levels of the cerebral vasculature.

1.3.1 Ions released

Extracellular K^+ ion concentration increases following the outflow of K^+ during neuronal membrane repolarization. Elevations in extracellular K^+ up to 8–10 mM cause dilation of arterioles both *in vitro* and *in vivo* (Nguyen, Winn et al. 2000). This

effect is mediated by the opening of K^+ channels, primarily of the inward rectifier type, on the membrane of arterial SMCs (Nguyen, Winn et al. 2000), leading to their hyperpolarization and subsequent relaxation. During sustained activation, ATP depletion could lead to opening of ATP-sensitive K^+ channels (K_{ATP}) on vessels. Therefore, K_{ATP} channels have been implicated in the mechanisms of neurovascular coupling (Nguyen, Winn et al. 2000). Furthermore, K_{ATP} could also participate in neurovascular coupling by mediating vasodilation stimulated by agents that increase (cAMP), such as adenosine or PGI_2 (Faraci and Sobey 1998). Extracellular acidification following neuronal activity is the result of CO_2 and lactic acid metabolic production. The vasodilatory effect of increased concentrations of H^+ is also mediated, at least in part, by the opening of pH sensitive K^+ channels (Faraci and Sobey 1998). It has also been suggested that activity-induced reductions in extracellular Ca^{2+} may produce vasodilation (Heuser 1978).

1.3.2 Products of neuronal activation

Vasoactive factors can also be secreted following activation of neurotransmitter receptors and the consequent cascade of intracellular signaling. A widely accepted hypothesis is that some vasodilators are primarily synthesized by distinct neuronal populations; these include COX2-derived prostanoids (Niwa, Maruyama et al. 2000) produced by some Layer II–III pyramidal cells (Yamagata, Andreasson et al. 1993), NO (Gotoh, Kuang et al. 2001) produced by subpopulations of cortical GABA interneurons (Kubota, Hattori et al. 1994), and VIP (Yaksh, Wang et al. 1987), Ach (Scremin, Rovere et al. 1973), and corticotropin-releasing factor (De Michele, Touzani et al. 2005) synthesized by bipolar/bitufted GABAergic interneurons (Chedotal, Cozzari et al. 1994). Synthesis of these vasoactive factors is triggered by changes in intracellular Ca^{2+} associated with glutamate receptor activation. The increase in Ca^{2+} activates Ca^{2+}-dependent enzymes such as NOS, the enzyme responsible for the oxygen-dependent conversion of L-arginine to NO and L-citrulline.(Moncada 1992) Out of the three isoforms of NOS, two exist in the brain with neuronal (nNOS) and endothelial (eNOS), expressed in neurons and cerebral endothelium, respectively (Szabo, Hardebo et al. 1991). The increase in CBF in the somatosensory cortex induced by sensory stimulation is associated with NO release and attenuated by nNOS inhibitors (Lindauer, Megow et al. 1999).

Moreover, in the cerebral cortex, the effect of nNOS inhibition on functional hyperemia can be reversed by application of exogenous NO. This finding suggests that the presence of NO is required for vasodilation (Lindauer, Megow et al. 1999). NO produced by eNOS in vascular endothelial cells in response to muscarinic ACh receptors (mAChR) stimulated by neuronally released ACh may also contribute to the CBF response to neuronal activation (Elhusseiny and Hamel 2000). Increase in intracellular Ca^{2+} may also activate phospholipase A2, leading to production of AA. AA is then metabolized by the COX pathway, producing vasodilatory prostaglandins (PGI_2, PGE_2, PGD_2) (Garavito and Mulichak 2003). Although there are several isoforms of COX (COX-1, -2, and -3) (Garavito and Mulichak 2003), COX-2 is the main isoform involved in functional hyperemia. COX-2 is present in axon terminals and dendritic processes, separated from penetrating arterioles and capillaries by glial processes (Wang, Hitron et al. 2005). Functionally, the CBF increase evoked by somatosensory stimulation is attenuated by COX-2 inhibitors or in COX-2 null mice, whereas COX-1 does not participate in the response (Niwa, Araki et al. 2000; Niwa, Haensel et al. 2001). The COX-2 metabolites responsible for the vasodilation may include vasodilatory prostaglandins. Specifically, PGI_2 is synthesized from prostaglandin H_2 (PGH_2) by PGI_2 synthase, which can activate adenylate cyclase and increase cAMP and protein kinase A (PKA) in smooth muscle, resulting in vasodilation (Smith, Garavito et al. 1996). Other AA products involved in functional hyperemia include metabolites of the P450 pathway, such as EETs (Peng, Carhuapoma et al. 2002).

1.3.3 Products of energy metabolism

A sudden increase in energy demand during synaptic activity could result in a relative lack of O_2 and glucose, which may in turn have a role in triggering the hemodynamic response (Attwell and Iadecola 2002). However, the reduction in brain O_2 concentration at the site of activation is small and transient and cannot account for sustained increases in blood flow (Ances 2004). Furthermore, the CBF response to neuronal activation is not altered by hypoglycemia or hypoxia, suggesting that lack of glucose or O_2 is not the primary factor triggering vasodilation (Attwell and Iadecola 2002). On the other hand, adenosine, a potent vasodilator produced during ATP catabolism, is involved in neurovascular coupling in the cerebellum (Li and Iadecola

1994) and the cerebral cortex (Ko, Ngai et al. 1990). Lactate produced during brain activation could also be an important mediator of functional hyperemia by increasing H^+ concentration and promoting vasodilation (Attwell and Iadecola 2002). However, the increase in lactate is small and transient, and cannot fully account for the increase in flow produced by neural activity (Attwell and Iadecola 2002). Carbon dioxide (CO_2) has a profound but reversible effect on cerebral blood flow, such that hypercapnia causes marked dilation of cerebral arteries and arterioles and increased blood flow, whereas hypocapnia causes constriction and decreased blood flow(Reivich 1964). The potent vasodilatory effect of CO_2 is demonstrated by the finding that in humans, 5% CO_2 inhalation causes an increase in cerebral blood flow by 50% while 7% CO_2 inhalation causes a 100% increase in cerebral blood flow (Kety and Schmidt 1948). Although several mechanisms involved in hypercapnic vasodilation have been proposed, the major mechanism appears to be related to a direct effect of extracellular H^+ on vascular smooth muscle (Kontos, Wei et al. 1977).

None of the vasoactive messengers implicated in neurovascular coupling can individually account for the hemodynamic response, as shown by genetic invalidation (Iadecola 1992) or pharmacological inhibition (Lindauer, Megow et al. 1999; Hoffmeyer, Enager et al. 2007). Likely, the activated pathways operate in an integrated manner, and under specific circumstances, some may even act as modulators rather than mediators of the perfusion responses, as documented for NO in the somatosensory cortex (Lindauer, Megow et al. 1999).

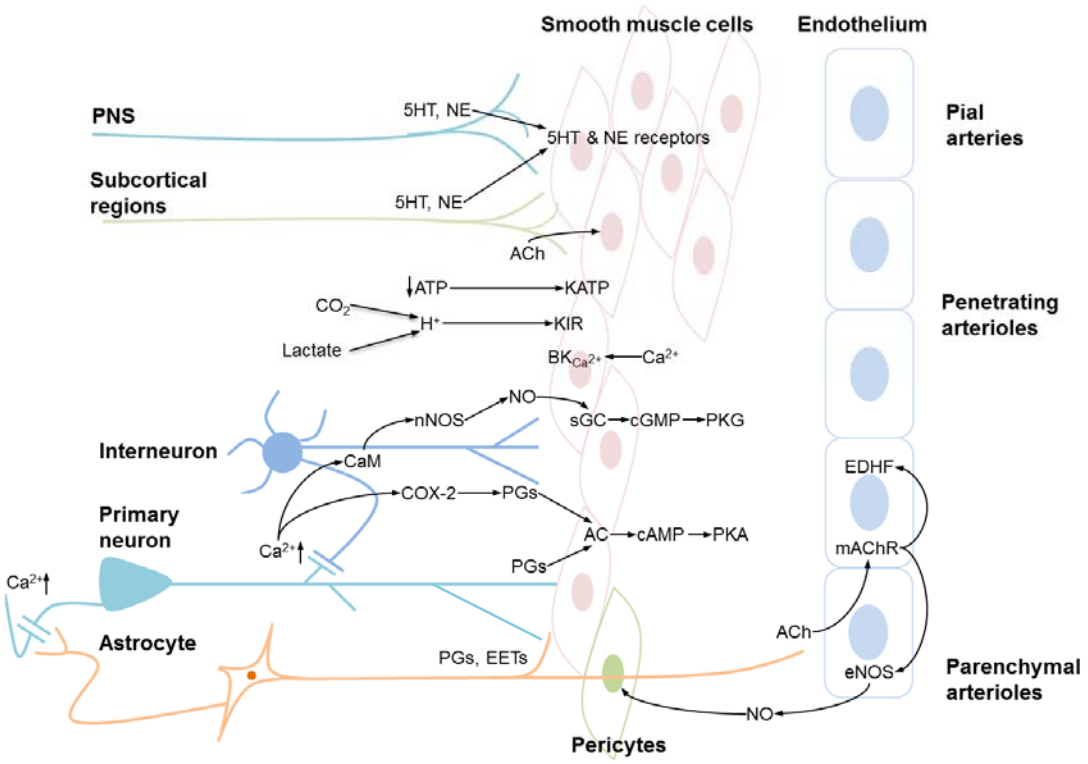

Figure 2. Schematic of cerebral blood flow regulation. Neurons from the peripheral nervous system (PNS) deliver 5-HT and NE to SMCs of pial arteries, inducing vasodilation. Neurons from subcortical regions (dorsal raphe nucleus, nucleus ceruleus, etc.) deliver 5-HT, NE and ACh to SMCs of penetrating arterioles. Metabolic byproducts such as CO^2 and lactate increase pH levels, and the resulting H^+ trigger the opening of K_{ir} channels. Intracellular increases in Ca^{2+} result in the opening of BK channels. Excess extracellular potassium enters through either variety of potassium channels and in turn repolarizes or hyperpolarizes and relaxes SMCs. An increase in intracellular Ca^{2+} in interneurons triggers both the calmodulin and COX-2 pathways. Calmodulin promotes nNOS and ultimately NO release to SMCs, where it binds to sGC to promote cGMP and thereby PKG activity to induce vasodilation. In some primary neurons, an increase in intracellular Ca^{2+} also activates the COX-2 pathway, which results in transformation of AA into PGs, which bind to AC in SMCs to promote cAMP and thereby PKA activity to dilate the blood vessel. A decrease in ATP due to neuronal activity results in the opening of K_{ATP} channels. Astrocytes innervate parenchymal arterioles, releasing vasodilatory factors such as prostaglandins (PGs) and EETs to SMCs or ACh to the endothelium where they bind to mAChR to activate both the EDHF pathway and the eNOS pathway, resulting in NO release into pericytes.

1.4 Neurovascular coupling in health and disease

Dysfunction of cerebral regulation as a result of increasing age, acute hemorrhagic events, or age-related structural and functional alterations in small cerebral blood vessels increases neuronal degeneration and susceptibility to hypoxia and ischemia.

1.4.1 Healthy aging

Aging is associated with a reduction in resting CBF and a dysfunction of the mechanisms regulating the cerebral circulation (Farkas and Luiten 2001; Kalaria, Maestre et al. 2008), leading to an increased risk of stroke, cerebral white matter lesions, and cognitive decline (Poels, Steyerberg et al. 2012). Changes in systemic circulation and degenerative changes in extracerebral resistance arteries (Kalaria 1996) may shift the lower and upper limits of the autoregulatory plateau to cause hypertensive encephalopathy or cerebral hypoperfusion, which lead to the disruption of microvascular flow, damage to the cerebral endothelium, breach of the BBB, and edema (Kalaria 1996). These alterations reduce cerebral perfusion, deplete cerebrovascular reserves, and increase the susceptibility of the brain to vascular insufficiency and ischemic injury (Farkas and Luiten 2001). In the cerebral cortex and hippocampus, cerebral capillaries are reduced in number and have thickened and fibrotic basement membranes (Farkas and Luiten 2001). White matter vessels (diameter: 100 μm) of aged individuals appear more tortuous—a phenomenon not observed in gray matter vessels (Kalaria 2009). Pericytes, which replace smooth-muscle cells in capillaries, undergo a degenerative process, whereas endothelial cells appear elongated and exhibit a reduced number of mitochondria (Farkas and Luiten 2001).

1.4.2 Subarachnoid hemorrhage

Subarachnoid hemorrhage (SAH) is characterized by the rupture of a cerebral aneurysm at the base of the skull with subsequent release of blood into the subarachnoid space—the cerebrospinal fluid-filled space between the pia and the arachnoid (Pobereskin 2001; Skrifvars and Parr 2012). SAH is a rare subtype of

stroke with an incidence of 10 cases per year per 100.000 people, or 5% of all first-ever strokes (Cahill and Zhang 2009). Overall, 20-25% of patients die almost immediately after hemorrhage as a consequence of acute intracranial hypertension as the blood is released in the subarachnoid space with a pressure almost equal to systolic blood pressure (Pobereskin 2001). From the remaining 75% of patients, 15% die after several days, while the remaining 60% die within 48 h of the initial bleeding (Weir, Grace et al. 1978) due to rebleedings (25%) or subsequent events (35%) (Pobereskin 2001). From those patients reaching a hospital, less than 8% fully recover. Regardless of the incidence, SAH is the subtype of stroke with the worst prognosis considering the relative young age at which SAH occurs as life losses before the age of 65 are comparable that of ischemic stroke, which has an incidence of 240 cases per year per 100.000 people (20 times more frequent) (Johnston, Selvin et al. 1998).

The pathophysiology of SAH can be divided into two distinct phases, early and delayed. Early brain injury (EBI) occurs within the first few days after SAH, when large cerebral vessels are still fully functional. It is characterized by a severe reduction in CBF (Schubert, Seiz et al. 2009) and can cause cortical spreading depolarization (CSD), and ischemic brain damage (Adams, Kassell et al. 1981) under normal or almost normal CPP. Ischemia results from the constriction of vessels at the level of cerebral microcirculation as observed in experimental animals (Herz, Baez et al. 1975; Sehba, Friedrich et al. 2007) and in patients (Uhl, Lehmberg et al. 2003). The events leading to early microvascular constrictions start with an acute vasoconstriction of the internal carotid artery, anterior cerebral artery and their A2 branches, as early as 5 minutes after hemorrhage (Bederson, Levy et al. 1998). This is followed by an acute constriction of intraparenchymal and pial micro vessels (10 to 30 micrometers) up to 24 hours after SAH (Sehba, Friedrich et al. 2007). Within the first 3 hours after SAH, over 70% of arterioles deriving from the middle cerebral artery (MCA) show pearl string-like constrictions that persist for at least 3 days after hemorrhage, suggesting that vessels are spastic. These events are associated with a loss of perfusion at the microcirculatory level indicating a much more severe microvascular deficit, namely microcirculatory stasis. The delayed phase of injury occurs later than four days after SAH and is associated with delayed spasms of large intracranial vessels (Macdonald and Weir 1991; Frontera, Rundek et

al. 2006). Vascular changes, such as subacute presence of microvasospasms and microthrombi (Sehba, Mostafa et al. 2005; Friedrich, Muller et al. 2012) along with the constriction of large intracranial vessels (Sehba, Friedrich et al. 2007) may prolong and exacerbate the perfusion deficits acutely caused by global ischemia and result in delayed focal cerebral ischemia. Despite the clinical relevance of these findings, the pathophysiology of SAH remains still unclear. We can still not account for presence of the global brain edema suffered by SAH patients (Helbok, Ko et al. 2011) or why glutamate levels increase after SAH only to decrease immediately after (Westermaier, Jauss et al. 2011). Another peculiarity is that patients surviving SAH suffer from pronounced memory deficits (Feiler, Friedrich et al. 2010). These changes may be associated with global ischemia due to extremely high increase in intracranial pressure and the cessation of cerebral perfusion during the vessel rupture (Mendelow 1993).

Among the different animal models for SAH, the procedure that reproduces early pathophysiology of SAH most adequately is the intravascular perforation model, where the Circle of Willis is perforated by an endovascular approach (Strbian, Durukan et al. 2008; Titova, Ostrowski et al. 2009). When the endovascular perforation of the Circle of Willis is induced, blood is released into the subarachnoid space at the skull base where it forms a large clot. As a consequence of the clot growth, intracranial pressure (ICP) starts to rise immediately after hemorrhage to values around 100 mmHg triggering an increase of blood pressure, the so-called Cushing reflex, thereby aggravating the bleeding (Hockel, Trabold et al. 2012). Intracranial hypertension results in a pathological decrease of CPP for up to 5 minutes, leading to a global reduction of cerebral blood flow for 2-3 minutes (Feiler, Plesnila et al. 2011; Hockel, Trabold et al. 2012). Local vasoconstriction along with activation of the coagulation cascade promote the formation of a blood clot at the bleeding site, which induces cessation of hemorrhage as indicated by a gradual decrease of ICP over the next 2-3 minutes to values around 30 mmHg. Consequently, CPP recovers to near normal values of 60 mmHg or more. Despite the recovery of CPP, CBF does not necessarily get back to baseline and may stay at low levels for up to 60 min after SAH (Hungerhuber, Zausinger et al. 2006; Hockel, Trabold et al. 2012). However, this early lack of CBF recovery after SAH is prevented when instead of anesthetics with a known blood pressure-lowering and

Cushing reflex-suppressive effect, such as halothane or isoflurane, anesthetic which maintain systemic blood pressure are used (Hockel, Trabold et al. 2012). This makes it difficult to understand whether the prolonged drop of CBF after SAH is a pure experimental phenomenon or indeed a component of the early pathophysiology of SAH. In vivo microdialysis shows that SAH results in metabolic changes in the brain parenchyma (Westermaier, Jauss et al. 2011) within 30 min after SAH, and the level of glutamate increases up to six fold and gradually returns to near baseline values within the next 1.5 hours. This increase in glutamate is paralleled by an increase in the lactate/pyruvate ratio, an indicator of tissue ischemia (Westermaier, Jauss et al. 2011). The posthemorrhagic brain shows a slow increase in brain water content from between three to six hours until at least three days after SAH (Thal, Sporer et al. 2009; Feiler, Friedrich et al. 2010), suggesting that the pathophysiology of SAH may be linked to opening of the BBB rather than to the initial posthemorrhagic global ischemia, given that brain edema formation following global ischemia is caused by ischemic cell swelling and thus disappears within minutes after reperfusion (Hossmann and Hossmann 1977).

1.4.3 Small vessel disease

Ischemic cerebral small vessel disease (SVD) describes a group of pathological processes with various etiologies affecting the penetrating cerebral arterioles, capillaries and venules and resulting in brain damage in the cerebral white and deep gray matter (Pantoni 2010). Diffuse arteriopathy of smaller penetrating arteries result in multiple subcortical lacunar infarctions, areas of white matter lesions defined as leukoaraiosis, large hemorrhages, and microbleeds (Ringelstein and Nabavi 2005). Age-related and hypertension-related small vessel diseases and cerebral amyloid angiopathy are the most common forms. However, other forms of the disease have a genetic base: several single-gene disorders causing cerebral SVD have been discovered, including cerebral autosomal dominant arteriopathy with subcortical infarcts and leukoencephalopathy, CADASIL, and its recessive counterpart, CARASIL.

1.4.3.1 CADASIL

CADASIL is a hereditary non-hypertensive ischemic cerebral SVD leading to vascular dementia. It is the most common hereditable cause of stroke and vascular dementia in adults (Joutel, Corpechot et al. 1996; Dichgans 2007; Chabriat, Joutel et al. 2009), with a prevalence of 1 to 2 cases per 100.000 (Markus, Martin et al. 2002) and it has been reported in all ethnic groups (Razvi, Davidson et al. 2005). It causes a type of stroke and dementia whose key features include recurrent sub-cortical ischemic events and vascular dementia associated with diffuse white-matter abnormalities (Chabriat, Vahedi et al. 1995). Pathological examination reveals multiple small, deep cerebral infarcts, a leukoencephalopathy, and a non-atherosclerotic, non-amyloid angiopathy involving mainly the small cerebral arteries (Baudrimont, Dubas et al. 1993). Severe alterations of vascular smooth-muscle cells are evident upon ultrastructural analysis (Ruchoux, Guerouaou et al. 1995). CADASIL is characterized by four cardinal manifestations. Migraine with aura occurs at an average age of 30 years. Ischemic events are present in 60-85% of patients, often preceded by transient ischemic attacks; the age of first ever strokes varies vastly between 40 and 60 years and are almost always subcortical and typically present as lacunar syndromes. Cognitive decline results in subcortical dementia between 50 and 60 years of age, and patients become bedridden and die around 65-70 years of age (Dichgans, Mayer et al. 1998; Opherk, Peters et al. 2004). Lastly, 20-30% of CADASIL patients suffer from mood disturbances (Chabriat, Vahedi et al. 1995).

CADASIL patients carry highly stereotyped mutations in the 33-exon NOTCH3 gene at 19p13.1-13.2., which alter the number of cysteine residues in the extracellular domain of the single pass transmembrane heterodimer receptor protein Notch3 (Joutel, Vahedi et al. 1997). Notch3 belongs to the Notch family, whose signaling pathways are indispensable during development of most organs (Joutel, Dodick et al. 2000). The postnatal expression of this protein is predominantly restricted to vascular smooth-muscle cells and pericytes (Joutel, Andreux et al. 2000). This receptor is initially synthesized as an approximately 280-kDa precursor, which is then constitutively cleaved by a paired basic amino acid cleaving enzyme, Furin, and the bipartite molecule is inserted to the plasma membrane. Notch3 consists of an extracellular domain (Notch3ECD) with 34 epidermal growth factor

(EGF)-like repeats followed by three notch/lin-12 repeats, a transmembrane domain, and an intracellular domain (Notch3ICD) which contains seven ankyrin repeats. The binding site of the ligand (in human Delta or Jagged) is at EGF repeats 10-11. Upon binding, Notch3ECD is cleaved external to the intramembranous domain. Thereafter intramembranous cleavage occurs and Notch3ICD enters the nucleus to release the repressor molecules CoR and HDAc and binds to a transcription regulator of the CSL family, RBP-Jk, activating transcription. CADASIL mutations are associated with vascular accumulation of Notch3ECD without associated Notch3ICD accumulation, at the plasma membrane of smooth-muscle cells and pericytes in close vicinity to or within granular osmiophilic material (GOM) deposits (Joutel, Andreux et al. 2000; Joutel, Favrole et al. 2001). Thickening and fibrosis of the arterial wall as well as transient but prominent alterations of smooth-muscle cells characterized this arteriopathy.

The earliest manifestation of CADASIL is leukoaraiosis: consistent magnetic resonance imaging (MRI) change preceding the onset of ischemic and cognitive symptoms by 10–15 years (Chabriat, Levy et al. 1998). Autopsy studies in patients with CADASIL demonstrated an arteriopathy that affected primarily the cerebral small penetrating and pial arteries. Distinct from other causes of SVD, vessels exhibit pathognomonic deposits of granular osmiophilic material of unknown composition (Kalimo, Viitanen et al. 1999; Miao, Paloneva et al. 2004). CADASIL patients have a predominant CBF reduction in cerebral white matter, and it becomes more apparent at ages above 30 years, when strokes begin to occur (Chabriat, Vahedi et al. 1995). Experimental studies have given similar results: transgenic mice expressing p.Arg90Cys-mutant human Notch3 showed reduced responses to hypercapnia, higher cerebrovascular resistance during hypertension and a lower limit of CBF autoregulation shifted towards higher blood pressure (Lacombe, Oligo et al. 2005). Moreover transgenic mice expressing rat p.R169C mutant Notch3 have shown cerebrovascular dysfunction with impaired neurovascular coupling and auto regulation of cerebral blood flow prior to the appearance of fibrosis and stenosis (Joutel, Monet-Lepretre et al. 2010).

1.4.3.2 CARASIL

The recessive counterpart of CADASIL, CARASIL, is a very rare disease with only 54 cases reported so far (Fukutake 2011). While most cases originated in Japan and China, there is a case report from the Caucasian population in the literature (Mendioroz, Fernandez-Cadenas et al. 2010). 50% of patients with CARASIL experience ischemic stroke, often of lacunar type and mainly in the basal ganglia or brainstem. This leads to progressive impairment of brain function and ultimately dementia, usually an age between 30 and 40 years. Patients first develop forgetfulness and gradually exhibit calculation disturbances, disorientation in time, personality changes including irritability and emotional lability. Prominent signs are premature diffuse baldness/alopecia, which predominantly affects male patients (Fukutake and Hirayama 1995; Fukutake 2011). and spondylosis. Alopecia is the most common initial symptom, present in 90% of patients. Hair loss is confined to the head; no obvious body hair loss is observed. Acute pain in the middle to lower back occurs in 80% of patients with CARASIL. MRI shows spondylotic deformations in the cervical spine. Onset of these deformations occurs generally in early adulthood (Fukutake and Hirayama 1995; Hara, Shiga et al. 2009).

High-temperature requirement A serine peptidase 1 (HTRA1) is the gene involved in the disease, with mutations reducing or eliminating the function of the HtrA1 enzyme. HtrA1 is ubiquitously expressed, plays an important physiological role in regulating the availability of insulin-like growth factors (IGFs), and is associated with diseases such as arthritis, cancer, age-related macular degeneration, and Alzheimer's diseases (Truebestein, Tennstaedt et al. 2011). It is composed of nine exons which encode a protein member of the trypsin family of serine proteases. This protein consists of 480 residues and has four functional domains. Exons 3 through 6 encode the main domain of a trypsin-like serine protease that represses signaling by the transforming growth factor-beta (TGF-β) family members (Hara, Shiga et al. 2009). This protein is a secreted enzyme that was proposed to regulate the availability of IGFs by cleaving IGF-binding proteins (Jacobo et al. 2013). The protein family participates in a variety of physiological processes, such as cell signaling and protein degradation, and is associated with the development of the musculoskeletal system (Hara, Shiga et al. 2009).

CARASIL's histopathology is characterized by arteriosclerosis of small penetrating arteries, without granular osmiophilic materials or amyloid deposition (Chabriat, Levy et al. 1998). Features of the disease are fibrous intimal proliferation, hyaline degeneration of the media, loss of vascular smooth-muscle cells, thickening and splitting of the internal elastic lamina, and concentric narrowing of the lumen. The small arterial changes are intense, leading to multifocal, confluent or diffuse ischemic changes. Experimental studies on circulatory disturbances in CARASIL have not been published.

2 Dysfunction of mouse cerebral arteries during early aging

2.1 Summary

The timeframe for onset of age-related vascular dementia (AVD) and which vascular components and functions are first affected is currently unknown. Considering how critical it is to maintain regulation of cerebral blood flow, I decided to investigate age-related functional decay in terms of vascular endothelial reactivity and neurovascular coupling in mice. To do this, cerebral vessels were dilated by inhalation of 5 and 10% CO_2 or by electrical stimulation of the forepaw. I measured regional changes in CBF by laser Doppler flowmetry and in individual artery diameter using two-photon and intravital microscopy. Regions of interest for intravital microscopy were selected on the criteria that they contain pial arterioles, venules and capillaries. CBF measurements did not reveal any vascular dysfunction up to 12 months of age in response to 5% CO_2, while only the 12-month-old group revealed a decreased response to 10% CO_2. By visually examining pial arteries, my investigation revealed age-related impairments in nitric oxide-dependent response to 5% CO_2 earlier at 8 months of age. In terms of neurovascular coupling, young mice maintained a strong CBF response while in 8 and 12 month old mice the response became weaker the longer the stimulation lasted. Components of the neurovascular unit are not altered by aging, and there was no difference in both resting and evoked end-foot calcium concentration between control and aged mice. These results suggest that aging does not affect cerebral vessel function simultaneously, but starts in pial microvessels months before global changes in CBF are detectable

Journal of Cerebral Blood Flow & Metabolism (2015), 1–9
© 2015 ISCBFM All rights reserved 0271-678X/15 $32.00
www.jcbfm.com

ORIGINAL ARTICLE

Dysfunction of mouse cerebral arteries during early aging

Matilde Balbi[1,2,5], Mitrajit Ghosh[1,5], Thomas A Longden[3], Max Jativa Vega[2], Benno Gesierich[1], Farida Hellal[1], Athanasios Lourbopoulos[1], Mark T Nelson[3] and Nikolaus Plesnila[1,2,4]

Aging leads to a gradual decline in the fidelity of cerebral blood flow (CBF) responses to neuronal activation, resulting in an increased risk for stroke and dementia. However, it is currently unknown when age-related cerebrovascular dysfunction starts or which vascular components and functions are first affected. The aim of this study was to examine the function of microcirculation throughout aging in mice. Microcirculation was challenged by inhalation of 5% and 10% CO_2 or by forepaw stimulation in 6-week, 8-month, and 12-month-old FVB/N mice. The resulting dilation of pial vessels and increase in CBF was measured by intravital fluorescence microscopy and laser Doppler fluxmetry, respectively. Neurovascular coupling and astrocytic endfoot Ca^{2+} were measured in acute brain slices from 18-month-old mice. We did not reveal any changes in CBF after CO_2 reactivity up to an age of 12 months. However, direct visualization of pial vessels by *in vivo* microscopy showed a significant, age-dependent loss of CO_2 reactivity starting at 8 months of age. At the same age neurovascular coupling was also significantly affected. These results suggest that aging does not affect cerebral vessel function simultaneously, but starts in pial microvessels months before global changes in CBF are detectable.

Journal of Cerebral Blood Flow & Metabolism advance online publication, 10 June 2015; doi:10.1038/jcbfm.2015.107

Keywords: aging; cerebral blood flow; CO_2 reactivity; *in vivo* microscopy; mice; neurovascular coupling

INTRODUCTION

Owing to the high energy demands of membrane potential repolarization, neuronal activation needs to be tightly matched to cerebral blood flow (CBF). Therefore, neurons, glia, and vascular cells of the neurovascular unit (NVU) interact to increase CBF in response to neuronal activation through a mechanism known as neurovascular coupling (NVC).[1] The resultant functional hyperemia ensures that neuronal energy demands are satisfied by the timely delivery of oxygen and glucose.

Aging is known to have profound effects on NVC and CBF, thereby contributing to an increased risk of stroke and possibly dementia.[2,3] Resting CBF and neuronal activity-mediated increases in CBF have been reported to decrease with age,[4,5] and decreases in resting CBF and cerebrovascular reactivity to neuronal activation are associated with an elevated risk of cerebrovascular disease.[6] Despite the importance of NVC for proper function of the brain and the profound effects of aging on CBF regulation, significant gaps remain in our knowledge of age-related cerebrovascular dysfunction (ACD). For instance, it is unknown if all cerebral vessels are affected by ACD simultaneously or if ACD starts in pial vessels and proceeds down to parenchymal vessels at a later stage as observed in animal models of small-vessel disease.[7] Therefore, the aim of the current study was to investigate the effect of aging on CBF regulation and reactivity of the cerebral microcirculation.

MATERIALS AND METHODS

Subjects

Animal breeding, housing, and all experimental procedures were conducted according to institutional guidelines of the University of Munich and were approved by the Ethical Review Board of the Government of Upper Bavaria and the Institutional Animal Care and Use Committee of the University of Vermont. *In vivo* experiments were conducted on 6-week, 8-month, and 12-month-old male and female FVB/N mice bred at the Center for Neuropathology, University of Munich (Munich, Germany) and are reported according to the ARRIVE criteria.

Two- to three-month-old male C57BL/6 mice were purchased from Jackson Laboratories (Bar Harbor, MA, USA) and 18-month-old male C57BL/6 mice were obtained from the National Institutes of Aging (USA). All animal cohorts were group housed and kept on a 12-hour light:dark cycle with *ad libitum* access to food and water.

Anesthesia and Physiologic Monitoring

For *in vivo* experiments on CO_2 reactivity, anesthesia was induced by intraperitoneal injection of midazolam (5 mg/kg; Braun, Melsungen, Germany), fentanyl (0.05 mg/kg; Janssen-Cilag, Neuss, Germany), and medetomidine (0.5 mg/kg; Pfizer, Karlsruhe, Germany) and was maintained for up to 4 hours by hourly injections of one-quarter of the initial dose, as previously described.[8–11]

For *in vivo* experiments on NVC mice were initially anesthetized with 2% isoflurane in 70% N_2O and 30% O_2. Later on isoflurane was gradually reduced over the course of 10 minutes to a range of 0.5% to 0.9% in 70% room air and 30% O_2, and at the same time, a continuous intraarterial

[1]Institute for Stroke and Dementia Research (ISD), University of Munich Medical Center, Munich, Germany; [2]Graduate School of Systemic Neurosciences (GSN), Ludwig-Maximilians University (LMU), Munich, Germany; [3]Department of Pharmacology, University of Vermont, Burlington, Vermont, USA and [4]Cluster of Systems Neurology (Synergy), Munich, Germany. Correspondence: Professor, Dr Nikolaus Plesnila, Institute for Stroke and Dementia Research (ISD), University of Munich Medical Center, Feodor-Lynen Straße 17, Munich 81377, Germany.
E-mail: nikolaus.plesnila@med.uni-muenchen.de
This work was supported by Solorz-Żaks foundation.
[5]These authors contributed equally to this work.
Received 13 February 2015; revised 22 April 2015; accepted 23 April 2015

infusion of ketamine (30 mg/kg/h, Inresa, Freiburg, Germany) was administrated.

Mice were orotracheally intubated and mechanically ventilated (Minivent, Hugo Sachs, Hugstetten, Germany). End-tidal pCO_2 was measured continuously with a microcapnometer (Capnograph, Hugo Sachs, Hugstetten, Germany) and kept constant between 20 and 30 mm Hg by respective adjustments to the ventilation frequency to obtain arterial blood gas values physiologic for FVB/N mice, which are ~10 mm Hg lower than in C57BL/6 mice.[8,12] A thermostatically regulated, feedback-controlled heating pad (FHC, Bowdoin, ME, USA) was used to maintain body temperature at 37°C. The left femoral artery was cannulated for continuous blood pressure monitoring and for infusion of 240 μL/h physiologic saline solution to prevent dehydration of the mice. Regional CBF (rCBF) was measured with a laser Doppler probe placed over the right somatosensory cortex (NVC) or over the territory of the left middle cerebral artery (CO_2 reactivity).

Imaging of Cerebral Microvessels *In Vivo*

A cranial window (4 × 4 mm) was drilled under constant cooling above the right parietal cortex leaving the dura mater intact as previously described.[11,13–16] Animals were placed under an epifluorescence microscope (Axio Scope Vario, Zeiss, Oberkochen, Germany) and the exposed dura mater was kept wet at all times with isotonic saline. The plasma was stained by an intraarterial injection of fluorescein isothiocyanate (FITC–dextran, molecular weight 150 kDa; 0.05 ml of a 0.5% solution; Sigma-Aldrich, Deisenhofen, Germany) and pial microvessels (diameter 20 to 40 μm) were visualized by epifluorescence imaging (excitation 470 nm; emission 527 nm) using a ×10 W N-Achroplan objective (Zeiss; numerical aperture (NA): 0.3). Four regions of interest containing arterioles, venules, and capillaries were investigated (Supplementary Figure S1A). Vessel diameters were quantified using a calibrated image analysis software (Zen, Zeiss) and expressed in percentage of baseline.

Neurovascular Reactivity to CO_2

Cerebral blood flow and diameter of pial vessels were examined for at least 10 minutes under physiologic, stable conditions, and the mean values obtained were taken as a baseline. Thereafter, CBF and vessel diameter were observed during inhalation of 5% CO_2 for 15 minutes as previously described.[17,18] After a break of 15 minutes the procedure was repeated with 10% CO_2 (Supplementary Figure S1B). The amount of inhaled CO_2 was measured by microcapnometry (Supplementary Figure S1C).

Forepaw-Evoked Neurovascular Coupling

The left forepaw was stimulated with two subdermally inserted needle electrodes with a diameter of 0.2 mm (Hwato, Suzhou, China) at an intensity of 2 mA for 0.3 ms (Digitimer, Hertfordshire, England). One stimulation cycle contained 96 stimulations and lasted for 16 seconds (6 Hz). The interval between two stimulation cycles was 40 seconds (Figure 1A). To identify the exact location of the somatosensory cortex representing the left forepaw, a train of 10 stimuli was applied and the rCBF response (Figure 1D) was assessed at five different locations within the somatosensory cortex. The region with the strongest synchronous response to stimulation was used for analysis and further for assessment of the microvascular response by *in vivo* microscopy.

To prove that our stimulation protocol indeed evoked neuronal activity, neuronal activation was assessed 3 seconds after the onset (Figure 1B) and 3 seconds after the end of each pulse train (Figure 1C) using custom-built cortical surface electrodes connected to an FE136 animal bioamplifier (ADInstruments, Oxford, UK). Only the recordings corresponding to the stimulus pulse trains showed the typical neuronal response to the single stimulus pulses with intervals of 167 ms.

Brain Slice Preparation and Imaging

Brain slices were prepared essentially as previously described.[19] Briefly, mice were killed by pentobarbital overdose and decapitated. The brain was rapidly removed into ice-cold artificial cerebrospinal fluid (aCSF) containing 124 mmol/L NaCl, 3 mmol/L KCl, 2 mmol/L $CaCl_2$, 2 mmol/L $MgCl_2$, 1.25 mmol/L NaH_2PO_4, 26 mmol/L $NaHCO_3$, and 4 mmol/L glucose; the aCSF used during slice preparation also contained 0.4 mmol/L ascorbic acid. Slices (160 μm) were prepared using a Leica VT1000 S vibratome (Leica, Buffalo Grove, IL, USA) and stored in oxygenated aCSF. Slices were then loaded with 10 μmol/L Fluo-4 AM (Invitrogen, Waltham, MA, USA) in aCSF containing 2.5 μg/mL pluronic acid for 1.5 hours at 32°C, and arteriolar diameter was measured and Ca^{2+} imaging was performed as previously described. Experimental solutions—gassed with 20% O_2, 5% CO_2, and balance N_2—contained 125 nm of the thromboxane analog U46619 to preconstrict arterioles (by 47% ± 4%, $n = 9$) and mimic physiologic tone. To enable offline quantification of endfoot $[Ca^{2+}]_i$, we treated a subgroup of slices with 10 μmol/L ionomycin and 20 mmol/L $[Ca^{2+}]_o$ to saturate loaded Fluo-4 AM (Invitrogen) and obtain a maximal fluorescence measurement. All other experiments were concluded by obtaining the passive vessel diameter by perfusing the slice with aCSF containing 50 μmol/L diltiazem, 200 μmol/L papaverine, 0 $CaCl_2$ and 5 mmol/L EGTA (in the absence of U46619) to allow assessment of arteriolar tone. The intensity and pulse pattern of electrical field stimulation remained constant throughout all experiments (a 3-second train delivering a 20 V, 50 Hz alternating square pulse of 0.3 ms duration).

Immunofluorescence Staining

Anesthetized mice were injected intraarterially with 30 μL of FITC-labeled tomato lectin, which stains vessels by direct binding to endothelial glycoproteins. Five minutes thereafter mice were transcardially perfused with sodium chloride and 4% paraformaldehyde. Brains were removed and fixed overnight in 4% paraformaldehyde. Coronal sections (50 μm thick) were made using a vibratome (Leica VS1200, Leica, Nussloch, Germany) and collected in phosphate-buffered saline. Free-floating sections from the rostral, medial, and dorsal brain were used for immunostaining. Sections were blocked with 3% bovine serum albumin for 60 minutes and incubated overnight at 4°C with the primary antibody in blocking solution. The following primary antibodies were used: for smooth muscle cells, Cy3-conjugated antialpha smooth muscle actin (1:100; Sigma-Aldrich, Taufkirchen, Germany, C6198); for pericytes, goat anti-platelet-derived growth factor receptor β (PDGFRβ) (1:100, R&D Systems, Wiesbaden, Germany, AF1042); for astrocytes, mouse anti-glial fibrillary acidic protein (GFAP) (1:100; Sigma-Aldrich, G3893); and for plasma protein (albumin), mouse antialbumin (1:100; Sigma-Aldrich, A6684). Sections were then washed three times in phosphate-buffered saline, blocked with 3% bovine serum albumin for 30 minutes, and incubated with fluorophore-conjugated secondary antibodies for 2 hours at room temperature. To visualize PGDFRβ-positive pericytes, sections were incubated in secondary Cy3-conjugated donkey antigoat antibody (1:100, Jackson ImmunoResearch, Suffolk, UK, 705165147); to visualize GFAP-positive astrocytes, sections were incubated in secondary Cy3-conjugated donkey antimouse antibody (1:100, Jackson ImmunoResearch, 715165150); and to visualize albumin, sections were incubated in secondary Cy3-conjugated donkey antimouse antibody (1:100, Jackson ImmunoResearch, 715165150). Sections were subsequently washed and mounted on slides using Fluoromount mounting medium (Sigma-Aldrich).

Imaging Acquisition and Analysis

All mounted sections were examined under a fluorescent (Axiovert 200M, Zeiss) or a confocal microscope (Leica TCS SP5 II, Wetzlar, Germany). Quantitative image analysis was performed by a blinded investigator using the software ImageJ (National Institute of Health, Bethesda, MD, USA). In each mouse, four regions of interests from the cortex were analyzed. This analysis was performed in three nonadjacent sections 100 μm apart from six animals per group. Capillaries were identified by positive FITC–lectin labeling and capillary density was quantified by subtracting the background and counting all FITC-positive pixels on maximum intensity projection confocal images using ImageJ. Smooth muscle cell coverage was determined by calculating the number of alpha-smooth muscle actin (α-sma)-positive pixels as a percentage of FITC–lectin-positive pixels per field (410 × 410 μm). Pericyte coverage was evaluated in the same way by the area occupancy of PDGFβR and lectin signals, respectively. Pericyte number was obtained by counting the number of PDGFβR-positive pericytes per mm^2 of selected field area. Astrocyte endfoot coverage was determined as a percentage of GFAP-positive astrocyte surface area covering lectin-positive capillary surface area per field. Extravascular albumin deposition was quantified on maximum intensity projection confocal images using ImageJ.

Statistical Analysis

Depending on whether data were normally distributed or not results are presented as mean ± s.e.m. or as median ± 75/25 percentile, respectively, and respective statistical tests were used to test for differences between groups/time points.

© 2015 ISCBFM

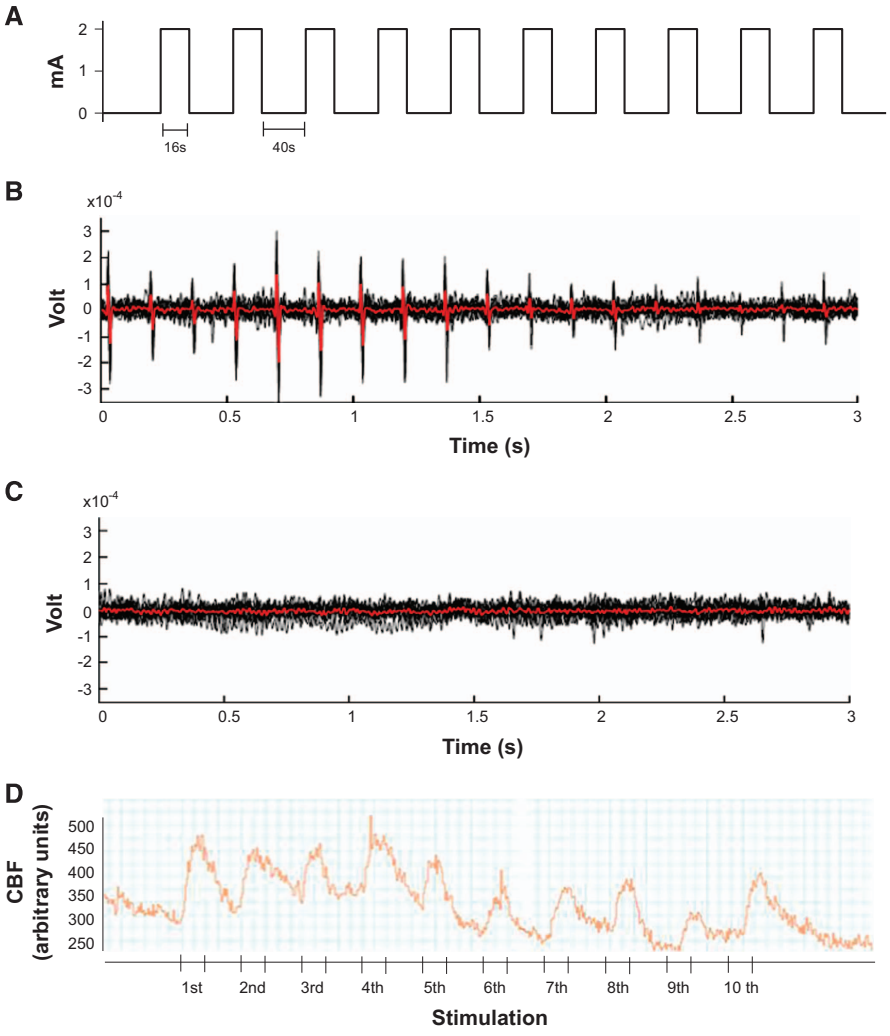

Figure 1. Experimental set up for the investigation of neurovascular coupling. (**A**) Representative recording of electrical pulses used to stimulate the forepaw. (**B** and **C**) Neuronal activity during (**B**) and after (**C**) forepaw stimulation. Original recordings are shown in black, the average of the first 3 seconds of 10 stimuli are shown in red. (**D**) Representative cerebral blood flow (CBF) increase in response to forepaw stimulation. Cerebral blood flow increased synchronous in response to the stimulation pattern shown in **A**.

For the *in vivo* study, statistical analysis was performed with a standard statistical software package (SigmaPlot 12.5; Systat Software, Erkrath, Germany). Differences across groups were evaluated using the Mann–Whitney rank sum test with the Bonferroni correction.

For the *in situ* study and immunohistologic experiments, statistical analyses were performed using Prism 5 (GraphPad Software, La Jolla, CA, USA). Time courses were analyzed using two-way repeated measures analysis of variance. Calcium concentration data were analyzed using one-way analysis of variance with Sidak's multiple-comparison test. Mean diameter data were analyzed using Student's unpaired *t*-test. Multiple group comparisons were analyzed using a one-way analysis of variance test followed by a Tukey's *post hoc* analysis. Data reported are mean ± s.e.m. A value of $P < 0.05$ was considered to be statistically significant.

Randomization and Blinding

All animals were randomly assigned to the procedures; the surgical preparation and data analysis were performed by a researcher masked toward the treatment of the animals.

RESULTS

In Vivo Physiologic Parameters

Body temperature, systemic blood pressure, and blood gases—factors shown to have strong effects on CBF[20]—were carefully monitored in all investigated mice. Parameters did not differ between groups and were within the physiologic range for FVB/N mice (Supplementary Table 1). These mice have a significantly lower pCO_2 than C57BL/6 mice anesthetized under the same conditions (Supplementary Figure S3) and a trend toward a lower arterial pH.[12] In keeping with this, we maintained endtidal pCO_2 at values ~20 to 30 mm Hg, which correspond to an arterial pH of ~30 to 40 mm Hg, i.e., the physiologic value for FVB/N mice.

Effect of Age on Neurovascular Response to CO_2 *In Vivo*

Inhalation of 5% or 10% CO_2 elicited the expected rCBF response in young (6 weeks old) FVB/N mice (Figures 2A and 2D, white symbols). In these animals, rCBF increased maximally by 20% and by 70% during 5% and 10% CO_2 inhalation, respectively. This response was similar in 8-month (Figures 2A and 2D, gray symbols) and 12-month-old mice (Figures 2A and 2D, dark gray symbols), indicating that the response of the whole cerebrovascular tree to CO_2 was not affected by age. In contrast to the CO_2-induced CBF response, dilation of pial vessels to CO_2 was significantly reduced in aged mice (Figure 3A). Although in young mice pial arterioles dilated as expected by 20% and 40% on inhalation of 5% and 10% CO_2, respectively (Figures 3B and 3E, white symbols), the increase in 8-month ($P = 0.001$ versus 6 weeks)

© 2015 ISCBFM

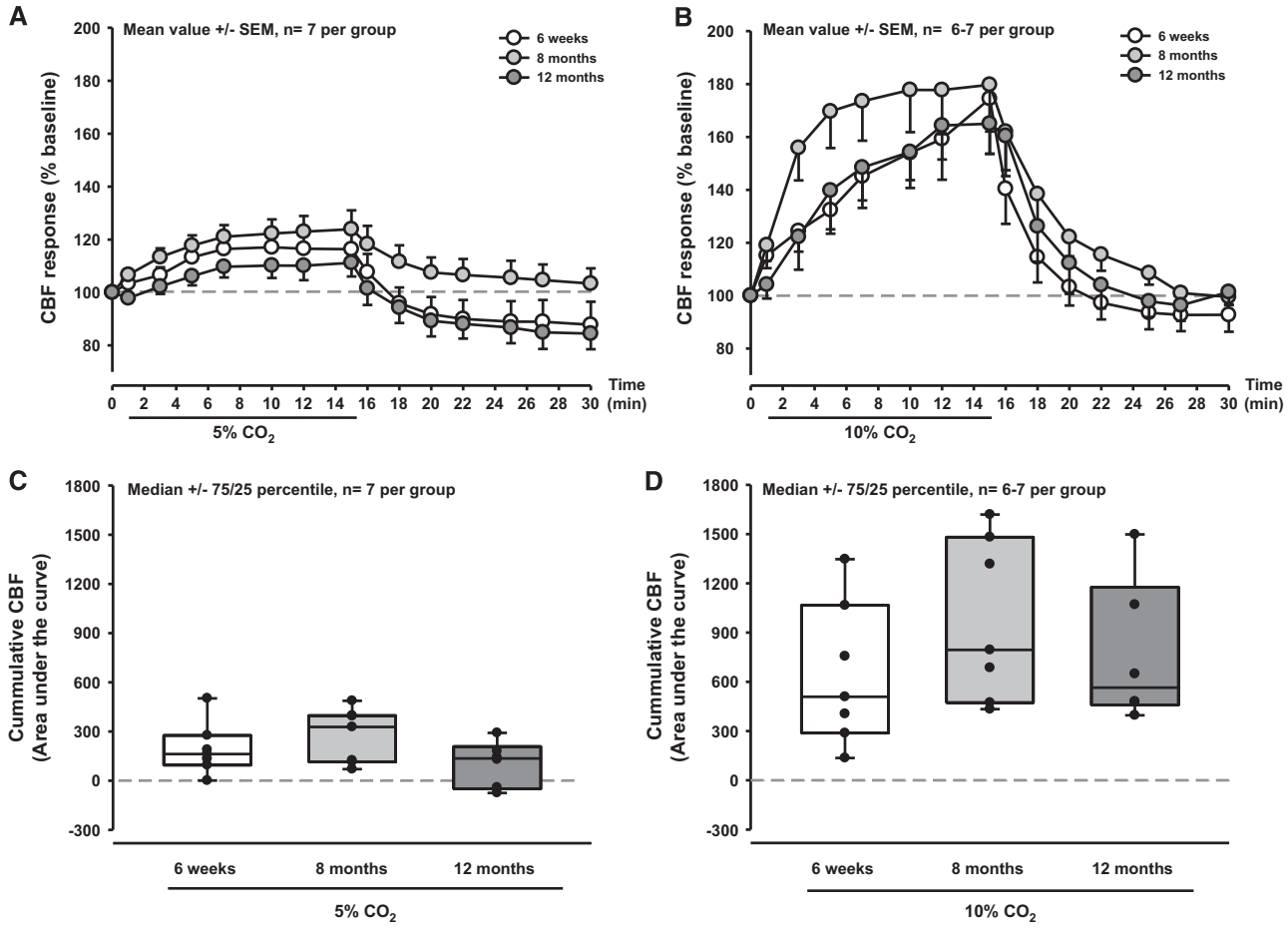

Figure 2. Cerebral blood flow (CBF) response to inhalation of CO_2 in young and aged mice. Cerebral blood flow response was not different in 6-week, 8-month, and 12-month-old-mice after inhalation of 5% (**A**) or 10% (**B**) CO_2 (means ± s.e.m.). (**C** and **D**) This was confirmed by area under the curve analysis and statistical evaluation. Median ± 75/25 percentiles; Mann–Whitney rank sum test; $n = 6$ to 7 per group.

and 12-month-old mice ($P = 0.001$ versus 6 weeks) was significantly smaller (Figures 3B and 3E, gray symbols). In 12-month-old mice, the response after application of 5% CO_2 was almost eliminated (Figure 3B, dark gray symbols) and analysis of individual vessels revealed that arteries in some animals even displayed an inverted response (Figure 3D, dark gray symbols), i.e., vasoconstriction instead of vasodilation. By doubling the concentration of inhaled CO_2 to 10%, we were able to dilate pial arterioles in 12-month-old mice (Figure 3C, dark gray symbols); however, the response was significantly attenuated ($P < 0.002$) and still showed an inverted response in some arteries (Figure 3E, dark gray symbols). These results show that exposure to CO_2, which results in vasodilation in young mice, is dramatically reduced in pial arterioles already at an age of 8 months.

Effect of Age on Neurovascular Coupling

Sensory stimulation of the forepaw with 10 consecutive stimulation cycles resulted in an increase of CBF by up to 40% in young mice (Figure 4A, white symbols). The first four stimuli had a weaker effect (20% to 30%); the maximum effect of 40% increase was reached only after the fifth stimulus. The response to the first four stimuli was not different between young and 8- or 12-month-old mice (Figures 4A and 4B), however, thereafter aged mice showed a significantly ($P < 0.04$ to 0.02) decreased response (Figures 4A and 4C). After the seventh stimulus, the CBF increase toward sensory stimulation in aged animals was completely eliminated. Six animals even display a decrease in CBF (Figure 4C). To ensure that sensation of the forepaw was not lost with age thereby resulting in reduced neuronal stimulation and subsequent NVC, we tested young and 7-month-old animals using a hot plate paradigm. All animals showed the same response (Supplementary Figure S4) suggesting not a loss of sensory input but age was responsible for the decline of NVC in old mice. Accordingly, these results point to a severe age-related neurovascular dysfunction already present after one-third of the life span of a mouse.[21]

Structural Changes of the Neurovascular Unit During Aging

To investigate whether structural changes of the NVU—e.g., loss of pericytes or opening of the blood–brain barrier[22]—are responsible for the observed functional deficits of aged cerebral vessels, we assessed and quantified important components of the NVU during aging by immunostaining (Figure 5A and Supplementary Figure S2B). We examined capillary density (lectin staining), coverage of arterioles with smooth muscle cells (*α*-sma), the coverage of capillaries with pericytes and the total number of pericytes in the microcirculation (PDGFR*β* expression), the coverage of capillaries with astrocytic endfeet (GFAP expression), and leakage of the blood–brain barrier by assessing the presence of blood plasma proteins in the brain parenchyma (antialbumin staining). We did not observe any significant change in the endothelium or in the structure of the NVU up to 12 months of

© 2015 ISCBFM

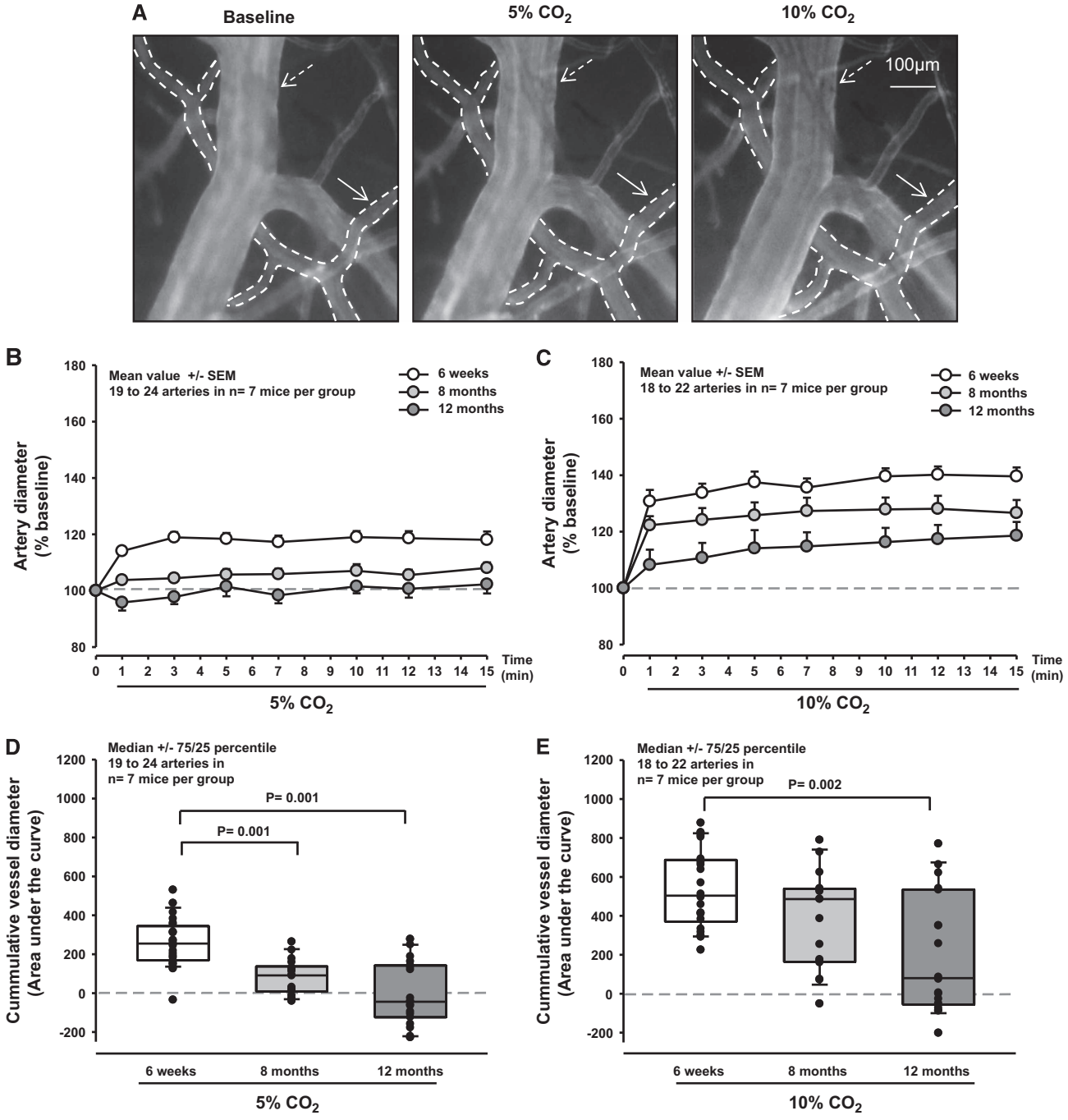

Figure 3. Diameter of pial arterioles in response to CO_2 in young and aged mice. (**A**) Intravital fluorescence microscopy of a pial vein (dotted arrow) and a pial arteriole (solid arrow) in a 6-week-old mouse before (left, baseline) and after inhalation of 5% (middle) and 10% (right) CO_2. The artery shows the expected dilation. (**B**–**E**) Pial artery diameter in response to inhalation of 5% (left) and 10% (right) CO_2 in 6-week, 8-month, and 12-month-old mice. Measurements of vessel diameter (**B** and **C**) as well as area under the curve analysis (**D** and **E**) revealed that vasodilation to CO_2 was significantly attenuated in old versus young mice. The response of pial arterioles of 12-month-old mice to 5% CO_2 was even completely lost. Median ± 75/25 percentile; Mann–Whitney rank sum test; 18 to 24 arteries in $n = 7$ mice per group.

age (Figure 5B and Supplementary Figure S2C), suggesting that structural integrity of the NVU is not affected by aging.

Neurovascular Coupling is Impaired *In Situ* in Aged Mice

To investigate the effects of aging on the function of penetrating arterioles, we used a brain slice model of NVC in which electrical field stimulation was used to initiate neurovascular signaling. By using this established paradigm,[19,23,24] we observed that the vasodilatory response to electrical field stimulation was abrogated at 18 months (Figures 6A and 6B). In fact, the prevailing response was a slight constriction in old mice (2- to 3-month-old: 30% ± 7% dilation, $n = 8$ arterioles, four mice; 18 months: −3% ± 8% constriction, $n = 10$ arterioles, five mice). A key step in NVC is an increase in concentration of astrocytic endfoot Ca^{2+}, which leads to the production or release of vasoactive factors onto the

© 2015 ISCBFM

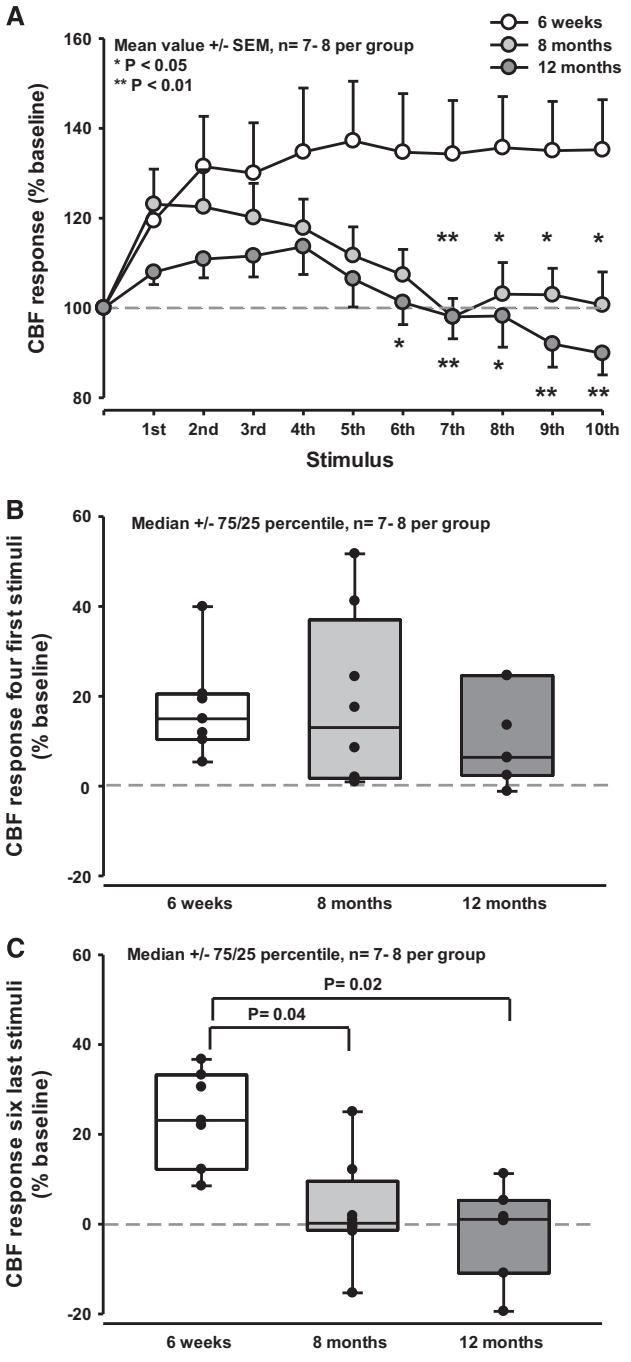

Figure 4. Neurovascular coupling in young and aged mice. (**A**) Response of cerebral blood flow (CBF) in somatosensory cortex to 10 consecutive stimulations of the contralateral forepaw. All mice showed a normal response to the first four stimuli. Young mice were able to maintain this response until the last stimulus, while in 8-month and 12-month-old mice the response became weaker the longer the stimulation lasted. In fact, 8-month and 12-month-old mice did not respond at all to the last four stimuli; pial arteries of 12-month-old mice even showed a tendency to constrict rather than dilate to forepaw stimulation. Mean value ± s.e.m. (**B** and **C**) Cerebral blood flow response to forepaw stimulation induced by the first four (**B**) and last six (**C**) stimuli. The increase in CBF was found to be significantly smaller during the last six stimuli in 8-month ($P = 0.04$) and 12-month-old mice ($P = 0.02$), compared with 6-week-old mice. Some old mice responded even with vasoconstriction. Median ± 75/25 percentile; Mann–Whitney rank sum test; $n = 7$ to 8 per group.

underlying pericytes or smooth muscle cells.[25] We observed no difference in either resting endfoot or the level of evoked endfoot calcium between young and 18-month-old mice (control resting: 92 ± 15 nmol/L, control evoked: 435 ± 93 nmol/L, $n = 6$ endfeet, four mice; aged resting: 98 ± 30 nmol/L; aged evoked 371 ± 70 nmol/L, $n = 6$ endfeet, four mice; Figures 6C and 6D).

DISCUSSION

The findings of the current study suggest that the function of cerebral vessels is differentially altered by aging and that cerebral vessels are structurally intact despite severe functional impairment. In addition, direct visualization of the pial microcirculation allowed us to detect neurovascular dysfunction to CO_2 inhalation much earlier that with regional measurements of CBF alone. Consistent with this, rCBF in response to forepaw stimulation was substantially reduced by 8 and 12 months, showing that the cerebral vasculature in mice is already functionally impaired in early adulthood.

An increase in CBF on neuronal activation, also termed functional hyperemia, is essential for the brain's proper function. Reduced hyperemia during brain activation limits the delivery of energy substrates and oxygen to activated neurons thereby resulting in mismatch of blood flow and metabolism, metabolic stress, and eventually neuronal damage as shown in various pathologic conditions, e.g., hypertension and Alzheimer's disease.[26,27] However, in addition to cerebrovascular and neurodegenerative diseases, physiologic aging was also reported to result in dysfunction of cerebral vessels. Aging is associated with a decrease of resting CBF[20] and aged vessels tend to display a reduced response to endothelium-dependent vasodilators.[28] It was suggested that the main underlying mechanism is the production of reactive oxygen species by reduced nicotinamide adenine dinucleotide phosphate oxidase in the vessel wall, where reactive oxygen species convert nitric oxide (NO) to peroxynitrite, thereby reducing the bioavailability of NO and damaging vascular structures.[13,29]

Despite these mechanistic insights, the spatiotemporal dynamics of ACD and its cellular and molecular basis remain poorly characterized. Functional hyperemia to whisker stimulation is reduced by ~40% in 12-month-old mice suggesting dysfunction of the neuron–astrocyte–pericyte/smooth muscle cell axis.[13] The results of the current study are in line with these findings, but detect an impaired NVC already at an age of 8 months. This was identified using trains of repetitive stimuli. By using this approach, we identified that after the first stimulus 6-week and 8-month-old mice reacted normally while 12-month-old mice showed a reduced CBF response. When repeating the stimulation up to ten times, however, it became apparent that vessels in 6-week-young mice maintained their CBF response over time, while 8-month and 12-month-old mice could not maintain their initial response level and showed almost no functional hyperemia. To the contrary, 6 of 16 of the old animals (38%) even showed inverse NVC, i.e., a reduction rather than an increase in CBF. Accordingly, NVC impairment seems to be a much earlier event than previously anticipated since it occurs already at 8 months of age, i.e., in the first third of a mouse's life.

Mechanistically, this vascular 'fatigue effect' could be explained by a structural damage to the NVU, by impaired neuron–astrocyte–vascular signaling, or by dysfunction within the vascular wall itself. To assess these hypotheses, we first investigated the NVU by quantifying capillary density, smooth muscle cell coverage of cerebral arterioles, pericyte and astrocytic endfeet coverage of capillaries, and leakage of the BBB by three-dimensional immunohistochemistry. None of these parameters was altered up to an age of 12 months suggesting that arterioles and capillaries are structurally completely intact while NVC is already impaired. To clarify whether neuron–astrocyte–vascular signaling might be

© 2015 ISCBFM

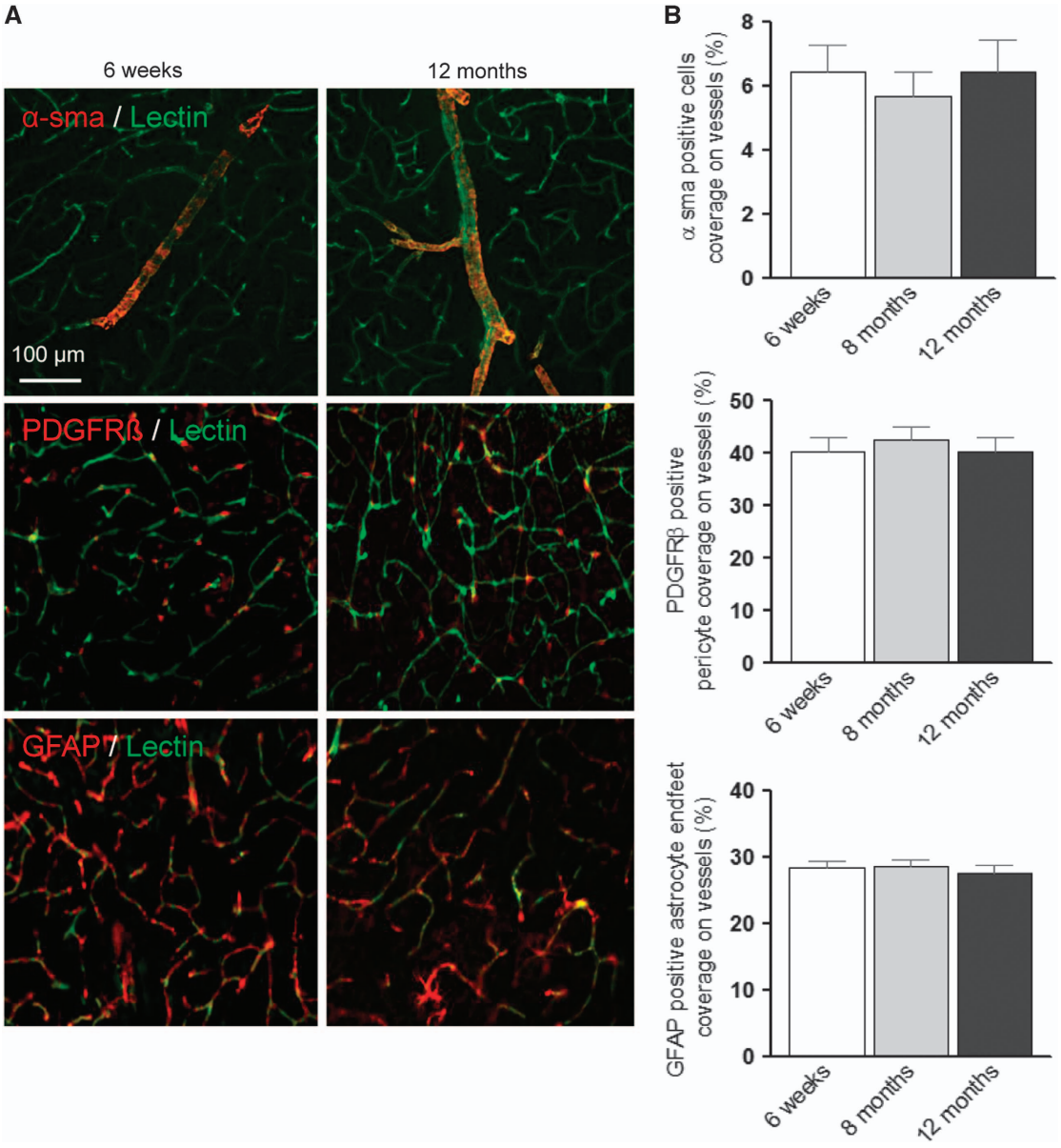

Figure 5. Quantification of the cellular components of the neurovascular unit in young and aged FVB/N mouse cortex. (**A**) Representative photomicrographs of immunostainings for smooth muscle cells (*α*-smooth muscle actin (*α*-sma)), pericytes (PDGF receptor-*β*), astrocytic endfeet (GFAP) together with endothelial staining with fluorescein isothiocyanate (FITC)–labeled tomato lectin. Scale bar represent 100 *μ*m. (**B**) Quantification of stainings shown in **A**. Components of the neurovascular unit are not altered by aging. Mean ± s.e.m.; $n = 6$ per group. GFAP, glial fibrillary acidic protein; PDGF, platelet-derived growth factor.

impaired, we performed experiments on isolated brain slices from aged mice. Vessels in control slices dilated robustly to neuronal activation, while vessels in slices from aged mice showed a response very similar to that observed *in vivo* at 12 months, namely a complete loss of NVC with a tendency toward vasoconstriction. However, the increase of astrocytic endfoot Ca^{2+} on neuronal activation was very similar to the response observed in slices from young mice. Accordingly, we conclude that aging principally affects the functionality of cerebral vessels without affecting neuronal–astrocytic signaling or the structure of the NVU, as also discussed above and suggested by others.[13,20,28,29]

The absence of an alteration in astrocytic endfoot Ca^{2+} levels, coupled with impairment of the reactivity of intracerebral arterioles, suggests that mechanisms downstream of this signaling step are affected by aging. One possible mechanism underlying the disturbance of NVC in the current study might be the impairment of potassium ion (K^+) signaling.[14,30] The Ca^{2+}-driven release of K^+ release from astrocytic endfeet plays a critical role in generating rapid vasodilation of cerebral parenchymal arterioles in response to neural activity,[23] through activation of smooth muscle cell potassium inward rectifier channels, driving membrane potential hyperpolarization and vasodilation.[25,31] We have previously shown that this mechanism is sensitive to disruption at the level of the SMC K_{IR} channel.[19] Future studies will need to explore the role of vascular Kir channels in the ACD in more detail.

To further explore the time course and localization of vascular dysfunction during aging, we used hypercapnia by inhalation of CO_2, which induces nitric-oxide dependent vasodilation.[29,32,33] Examining the global increase of CBF after inhalation of 5% or 10% CO_2, we were not able to find any neurovascular dysfunction in mice up to an age of 12 months as previously published by Park *et al*.[13] However, visualization of pial microvessels by *in vivo*

© 2015 ISCBFM

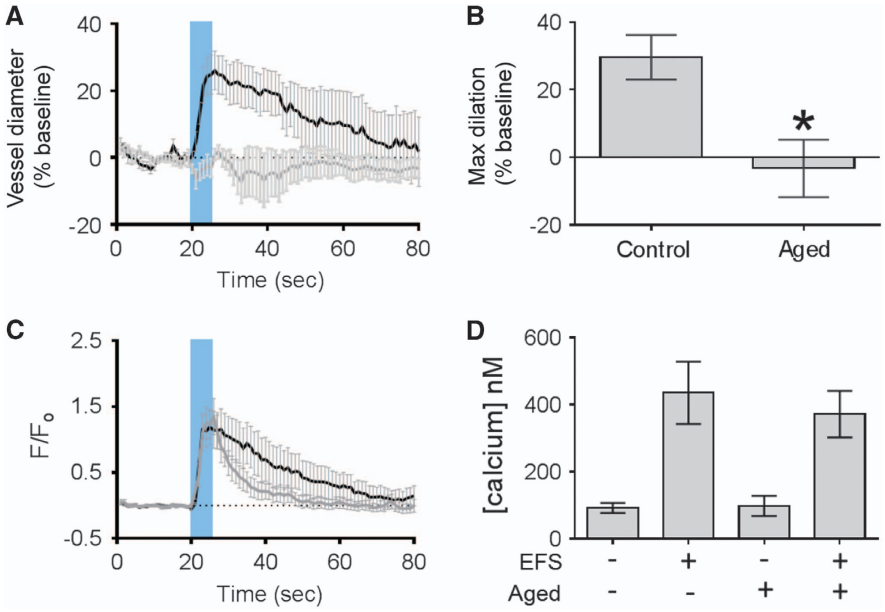

Figure 6. Neurovascular coupling in brain slices from young and old mice. (**A**) Electric field stimulation (EFS) evoked substantial vasodilations in arterioles in cortical brain slices taken from young (control) and old mice (black line, eight arterioles from four mice). In contrast, EFS evoked a small constriction in arterioles in slices from 18-month-old mice (gray line, 10 arterioles from five mice). Blue bar indicates the duration of EFS. (**B**) Summary data showing the maximal vasodilation evoked by EFS in both control and aged mice. (**C**) EFS evoked a substantial increase in astrocytic endfoot calcium in both control and aged mice, and we observed a trend for faster decay of calcium transients in aged (gray line, $n = 10$ aged endfeet, five mice) compared with control mice (black line, $n = 8$ control endfeet, four mice). (**D**) There was no difference in both resting or evoked endfoot calcium concentration between control ($n = 6$ endfeet, four mice) and aged mice ($n = 6$ endfeet, four mice). Data are shown as mean ± s.e.m. $^*P < 0.01$ vs. control.

microscopy allowed us to detect a significant lack of CO_2-induced vasodilation in pial arterioles already in 8-month-old mice. These findings suggest that AVD starts in pial arteries and precipitates down the neurovascular tree during aging. This is supported by published data showing that aging affects the global increase of CBF after inhalation of CO_2 only in mice older than 1.5 years[13] and by experiments showing accelerated aging of pial arteries in a mouse model small-vessel disease.[7] Furthermore, since CO_2-induced vasodilation is mediated by constitutively expressed endothelial and neuronal NO synthases, the current data also suggest that AVD may be caused by disturbed NO signaling.

Taken together, our results show that age impairs neurovascular coupling at an unexpectedly young age in mice (30% of the mouse's mean life span). This dysfunction starts in pial vessels and is not accompanied by any changes on the cellular composition of the NVU or by impaired astrocytic Ca^{2+} reactivity. The lack of vascular CO_2 reactivity suggests that defective constitutive NO signaling may represent a possible mechanism. The current study identified the onset and location of age-related neurovascular dysfunction and suggests a putative mechanism, thereby paving the way for the development of novel strategies to maintain neurovascular function during aging.

AUTHOR CONTRIBUTIONS

MB performed all *in vivo* experiments and wrote the manuscript. MG performed all immunohistochemical staining. TAL performed all *in vitro* experiments, contributed wiring, and edited the manuscript. MJV and BG analyzed data on neuronal firing. FH worked as a statistical consultant and edited the manuscript. AL worked as a statistical consultant. MTN edited the manuscript. NP designed the study, wrote, and edited the manuscript

DISCLOSURE/CONFLICT OF INTEREST

The authors declare no conflict of interest.

ACKNOWLEDGMENTS

The authors thank Dr Susanne Schwarzmaier for technical support and Dr Arthur Liesz for critical discussions and comments on the manuscript.

REFERENCES

1 Girouard H, Iadecola C. Neurovascular coupling in the normal brain and in hypertension, stroke, and Alzheimer disease. *J Appl Physiol (1985)* 2006; **100**: 328–335.
2 Farkas E, Luiten PG. Cerebral microvascular pathology in aging and Alzheimer's disease. *Prog Neurobiol* 2001; **64**: 575–611.
3 Mitchell GF, van Buchem MA, Sigurdsson S, Gotal JD, Jonsdottir MK, Kjartansson O *et al.* Arterial stiffness, pressure and flow pulsatility and brain structure and function: the Age, Gene/Environment Susceptibility—Reykjavik study. *Brain* 2011; **134**: 3398–3407.
4 Panczel G, Daffertshofer M, Ries S, Spiegel D, Hennerici M. Age and stimulus dependency of visually evoked cerebral blood flow responses. *Stroke* 1999; **30**: 619–623.
5 Fischer M, Dietmann A, Beer R, Broessner G, Helbok R, Pfausler B *et al.* Differential regulation of matrix-metalloproteinases and their tissue inhibitors in patients with aneurysmal subarachnoid hemorrhage. *PLoS One* 2013; **8**: e59952.
6 Jennings JR, Heim AF, Kuan DC, Gianaros PJ, Muldoon MF, Manuck SB. Use of total cerebral blood flow as an imaging biomarker of known cardiovascular risks. *Stroke* 2013; **44**: 2480–2485.
7 Joutel A, Monet-Lepretre M, Gosele C, Baron-Menguy C, Hammes A, Schmidt S *et al.* Cerebrovascular dysfunction and microcirculation rarefaction precede white matter lesions in a mouse genetic model of cerebral ischemic small vessel disease. *J Clin Invest* 2010; **120**: 433–445.
8 Thal SC, Plesnila N. Non-invasive intraoperative monitoring of blood pressure and arterial pCO2 during surgical anesthesia in mice. *J Neurosci Methods* 2007; **159**: 261–267.
9 Schwarzmaier SM, Terpolilli NA, Dienel A, Gallozzi M, Schinzel R, Tegtmeier F *et al.* Endothelial nitric oxide synthase mediates arteriolar vasodilatation after traumatic brain injury in mice. *J Neurotrauma* 2014; **32**: 731–738.
10 Schwarzmaier SM, Zimmermann R, McGarry NB, Trabold R, Kim SW, Plesnila N. In vivo temporal and spatial profile of leukocyte adhesion and migration after experimental traumatic brain injury in mice. *J Neuroinflammation* 2013; **10**: 32.

© 2015 ISCBFM

11 Schwarzmaier SM, Kim SW, Trabold R, Plesnila N. Temporal profile of thrombogenesis in the cerebral microcirculation after traumatic brain injury in mice. *J Neurotrauma* 2010; **27**: 121–130.
12 Menuet C, Kourdougli N, Hilaire G, Voituron N. Differences in serotoninergic metabolism possibly contribute to differences in breathing phenotype of FVB/N and C57BL/6 J mice. *J Appl Physiol (1985)* 2011; **110**: 1572–1581.
13 Park L, Anrather J, Girouard H, Zhou P, Iadecola C. Nox2-derived reactive oxygen species mediate neurovascular dysregulation in the aging mouse brain. *J Cereb Blood Flow Metab* 2007; **27**: 1908–1918.
14 Knot HJ, Zimmermann PA, Nelson MT. Extracellular K(+)-induced hyperpolarizations and dilatations of rat coronary and cerebral arteries involve inward rectifier K(+) channels. *J Physiol* 1996; **492**: 419–430.
15 Terpolilli NA, Kim SW, Thal SC, Kataoka H, Zeisig V, Nitzsche B *et al.* Inhalation of nitric oxide prevents ischemic brain damage in experimental stroke by selective dilatation of collateral arterioles. *Circ Res* 2012; **110**: 727–738.
16 Kataoka H, Kim SW, Plesnila N. Leukocyte-endothelium interactions during permanent focal cerebral ischemia in mice. *J Cereb Blood Flow Metab* 2004; **24**: 668–676.
17 Friedrich B, Muller F, Feiler S, Scholler K, Plesnila N. Experimental subarachnoid hemorrhage causes early and long-lasting microarterial constriction and microthrombosis: an in-vivo microscopy study. *J Cereb Blood Flow Metab* 2012; **32**: 447–455.
18 Friedrich B, Michalik R, Oniszczuk A, Abubaker K, Kozniewska E, Plesnila N. CO2 has no therapeutic effect on early microvasospasm after experimental subarachnoid hemorrhage. *J Cereb Blood Flow Metab* 2014; **34**: e1–e6.
19 Longden TA, Dabertrand F, Hill-Eubanks DC, Hammack SE, Nelson MT. Stress-induced glucocorticoid signaling remodels neurovascular coupling through impairment of cerebrovascular inwardly rectifying K+ channel function. *Proc Natl Acad Sci USA* 2014; **111**: 7462–7467.
20 Faraci FM, Heistad DD. Regulation of the cerebral circulation: role of endothelium and potassium channels. *Physiol Rev* 1998; **78**: 53–97.
21 Suckow MA, Danneman P, Brayton C. The laboratory animal pocket reference series: 8. *The Laboratory Mouse*. CRC Press: Boca Raton, FL, 2001.
22 Armulik A, Genove G, Mae M, Nisancioglu MH, Wallgard E, Niaudet C *et al.* Pericytes regulate the blood-brain barrier. *Nature* 2010; **468**: 557–561.
23 Filosa JA, Bonev AD, Straub SV, Meredith AL, Wilkerson MK, Aldrich RW *et al.* Local potassium signaling couples neuronal activity to vasodilation in the brain. *Nat Neurosci* 2006; **9**: 1397–1403.
24 Koide M, Bonev AD, Nelson MT, Wellman GC. Inversion of neurovascular coupling by subarachnoid blood depends on large-conductance Ca^{2+}-activated K^{+} (BK) channels. *Proc Natl Acad Sci USA* 2012; **109**: E1387–E1395.
25 Straub SV, Nelson MT. Astrocytic calcium signaling: the information currency coupling neuronal activity to the cerebral microcirculation. *Trends Cardiovasc Med* 2007; **17**: 183–190.
26 Kazama K, Anrather J, Zhou P, Girouard H, Frys K, Milner TA *et al.* Angiotensin II impairs neurovascular coupling in neocortex through NADPH oxidase-derived radicals. *Circ Res* 2004; **95**: 1019–1026.
27 Niwa K, Araki E, Morham SG, Ross ME, Iadecola C. Cyclooxygenase-2 contributes to functional hyperemia in whisker-barrel cortex. *J Neurosci* 2000; **20**: 763–770.
28 Mayhan WG, Faraci FM, Baumbach GL, Heistad DD. Effects of aging on responses of cerebral arterioles. *Am J Physiol* 1990; **258**: H1138–H1143.
29 Girouard H, Park L, Anrather J, Zhou P, Iadecola C. Cerebrovascular nitrosative stress mediates neurovascular and endothelial dysfunction induced by angiotensin II. *Arterioscler Thromb Vasc Biol* 2007; **27**: 303–309.
30 McCarron JG, Halpern W. Impaired potassium-induced dilation in hypertensive rat cerebral arteries does not reflect altered Na+, K(+)-ATPase dilation. *Circ Res* 1990; **67**: 1035–1039.
31 Girouard H, Bonev AD, Hannah RM, Meredith A, Aldrich RW, Nelson MT. Astrocytic endfoot Ca2+ and BK channels determine both arteriolar dilation and constriction. *Proc Natl Acad Sci USA* 2010; **107**: 3811–3816.
32 Lindauer U, Megow D, Matsuda H, Dirnagl U. Nitric oxide: a modulator, but not a mediator, of neurovascular coupling in rat somatosensory cortex. *Am J Physiol* 1999; **277**: H799–H811.
33 Lindauer U, Kunz A, Schuh-Hofer S, Vogt J, Dreier JP, Dirnagl U. Nitric oxide from perivascular nerves modulates cerebral arterial pH reactivity. *Am J Physiol Heart Circ Physiol* 2001; **281**: H1353–H1363.

Supplementary Information accompanies the paper on the Journal of Cerebral Blood Flow & Metabolism website (http://www.nature.com/jcbfm)

© 2015 ISCBFM

3 Acute changes in neurovascular reactivity after subarachnoid hemorrhage *in vivo*

3.1 Summary

Using the animal model for subarachnoid hemorrhage, I investigated the reactivity of pial and parenchymal arterioles to CO_2 and sensory stimulation using CBF measurements and two-photon microscopy. My investigation of SAH revealed for the first time that intraparenchymal vessels show severe functional impairments after SAH. Pial and parenchymal vessel dilated normally in response to inhalation of 10% CO_2 in sham operated mice, while no response was observed after SAH. Neurovascular coupling is not altered 3 hours after SAH. Artery dilation in response to a discrete electrical stimulation showed no difference between the experimental groups. CBF increase and artery dilation in response to continuous electrical stimulation showed no difference between sham-operated mice and mice subjected to SAH. Electrical field stimulation (EFS)-induced vasodilation was unaltered in brain slices 4 hours after SAH. These findings suggest that communication between neurons, astrocytes, and parenchymal arterioles is not affected in the first few hours after SAH, while CO_2 reactivity, which is dependent on NO signaling, is completely lost.

Acute changes in neurovascular reactivity after subarachnoid hemorrhage *in vivo*

Matilde Balbi[1,2], Masayo Koide[3], Susanne M. Schwarzmaier[1], George C. Wellman[3] and Nikolaus Plesnila[1,2,4]

[1]Institute for Stroke and Dementia Research (ISD), University of Munich Medical Center & [2]Graduate School of Systemic Neurosciences (GSN), Ludwig-Maximilians University (LMU), Munich, Germany; [3]Department of Pharmacology, University of Vermont, Burlington, VT, USA and [4]Munich Cluster for Systems Neurology, Munich, Germany. Correspondence: Professor, Dr Nikolaus Plesnila, Institute for Stroke and Dementia Research (ISD), University of Munich Medical Center, Feodor-Lynen Straße 17, Munich 81377, Germany. E-mail: nikolaus.plesnila@med.uni-muenchen.de

Subarachnoid hemorrhage (SAH) causes acute and long-lasting constrictions of pial arterioles. Whether these vessels dilate normally to neuronal activity is of great interest since a mismatch between delivery and consumption of glucose and oxygen may cause additional neuronal damage. Therefore, we investigated neuro-vascular reactivity of pial and parenchymal arterioles after experimental SAH. C57BL/6 mice were subjected to SAH by filament perforation or sham surgery. Neuro-vascular reactivity was assessed three hours later by forepaw stimulation or inhalation of 10% CO_2. Diameters of cerebral arterioles were assessed using two-photon microscopy. Neuro-vascular coupling (NVC) and astrocytic end-foot Ca^{2+} were measured in brain slices using two-photon and infrared-differential interference contrast (IR-DIC) microscopy. Vessels of sham operated mice dilated normally to CO_2 and forepaw stimulation. Three hours after SAH, CO_2 reactivity was completely lost in both pial and parenchymal arterioles while NVC was not affected. Brain slices studies also showed normal NVC and a normal increase in astrocytic end-foot Ca^{2+} acutely after SAH. These findings suggest that communication between neurons, astrocytes, and parenchymal arterioles is not affected in the first few hours after SAH, while CO2 reactivity, which is dependent on NO signaling, is completely lost.

Journal of Cerebral Blood Flow & Metabolism, accepted for publication

Key words: Subarachnoid hemorrhage, neurovascular coupling, CO2, parenchymal vessels, in vivo

INTRODUCTION

Activation of specific regions of the brain induces a focal increase in cerebral blood flow (CBF) in order to match the delivery of oxygen and glucose to the increased metabolic demand of depolarized neurons.[1] This process is called "neurovascular coupling" (NVC) and is mediated through a still not completely understood interplay between neurons, astrocytes, and cerebral vessels.[2, 3] Disturbances of NVC, as observed after cerebral ischemia or brain trauma, may compromise the metabolic status of neurons and further aggravate brain damage. Accordingly, it is of great scientific and clinical interest to understand the mechanisms of NVC in the healthy and diseased brain.

Subarachnoid hemorrhage (SAH) is a subtype of stoke which accounts for 5% of all first-ever strokes.[4] Despite its relatively low incidence SAH is responsible for 20% of all cerebrovascular related deaths[5] and only 10% of all SAH patients recover completely. In most cases, SAH is caused by the rupture of a cerebral aneurysm located at the base of the skull. Experimental data show that immediately after vessel rupture the subarachnoid space fills with blood and intracranial pressure (ICP) increases to levels that blunt cerebral perfusion pressure (CPP) and cause global cerebral ischemia. If patients survive this acute spike in ICP, lasting approximately five minutes, ICP decreases and CPP normalizes. Despite normal CPP, however, many SAH patients still suffer from severe and wide spread reductions in CBF.[6] Since large brain surface arteries become spastic only after several days of exposure to subarachnoid blood, these early reductions in CBF are most likely caused by disturbances at the level of the cerebral microcirculation. Direct visualization of cerebral microvessels within the first few hours after SAH in patients and experimental animals indeed demonstrated microvasospasms of pial arterioles that reduced cerebral perfusion by 60-80%.[7-9] These reductions in CBF trigger a cascade of events resulting in brain edema formation, neuronal cell death, and unfavorable neurological outcome referred to as “early brain injury”.[10-12]

Despite the importance of cerebral microvessels in the pathophysiology of SAH relatively little is known about the consequences of SAH on neurovascular function *in vivo*. Recently, we demonstrated that NVC is impaired 96 hours after SAH in rat brain slice preparations.[13] This suggests that neuron activation may not dilate cerebral vessels after SAH to elicit an adequate increase in CBF, thereby significantly increasing the risk for further neuronal damage and loss of function. However, it is not known if NVC is impaired immediately after SAH *in vivo*. Therefore the aim of the current study was to subject mice to experimental SAH for three hours and use two-photon microscopy to investigate the reactivity of pial and parenchymal arterioles to sensory stimulation and CO_2, two well established *in vivo* paradigms of neuro-vascular communication.

MATERIALS AND METHODS

Animal breeding, housing and all experimental procedures were conducted according to institutional guidelines and were approved by the Ethical Review Board of the Government of Upper Bavaria (protocol number 220-13) and the Institutional Animal Care and Use Committee at the University of Vermont.

Male C57BL/6 mice (20 to 23 g body weight Charles River Laboratory, Sulzfeld, Germany and Charles River Laboratory, Saint Constant, Quebec, Canada) were used for this study. Experiments were planned, carried out, and reported according to the ARRIVE guidelines.[14]

Animal preparation and monitoring

Experimental animals had free access to food and water prior and after surgery. For induction of SAH, anesthesia was induced by intraperitoneal injection of midazolam (5 mg/kg; Braun, Melsungen, Germany), fentanyl (0.05 mg/kg; Jansen-Cilag, Neuss, Germany), and medetomidine (0.5 mg/kg; Pfizer, Karlsruhe, Germany) as previously described.[15, 16] Mice were orotrachealy intubated and mechanically ventilated (Minivent, Hugo Sachs, Hugstetten, Germany). End-tidal pCO_2 was measured with a microcapnometer (Capnograph, Hugo Sachs, Hugstetten, Germany) and kept constant between 30 and 40 mmHg by respective adjustments to the ventilation.[16] A thermostatically regulated, feedback-controlled heating pad (FHC, Bowdoin, ME, USA) was used to maintain body temperature at 37°C. Intracranial pressure (ICP) was measured in each animal for 15 minutes after SAH using a microsensor based ICP probe (Codman & Shurteff Inc, Raynham, MA) to prove successful induction of SAH as described before.[17] For continuous monitoring of regional cerebral blood flow (rCBF) a flexible laser-Doppler probe (Periflux 4001 Master, Perimed, Stockholm, Sweden) was glued onto the skull above the territory of the left middle cerebral artery (MCA). Blood gases and electrolytes were determined at the end of each experiment.

For experiments on neurovascular reactivity mice were initially anesthetized with 2% isoflurane in 70% N_2O and 30% O_2. Later on, isoflurane was gradually reduced over the course of 10 minutes to a range of 0.5 to 0.9% in 70% room air and 30% O_2. At the same time, a continuous intra-arterial infusion of ketamine (30 mg/kg/h, Inresa, Freiburg, Germany) was administrated.[18]

Induction of subarachnoid hemorrhage

SAH was induced using the filament perforation model as previously described.[17, 19, 20] Briefly, a 5-0 monofilament was introduced via the left external carotid artery into the internal carotid artery and advanced intracranially. SAH induction was indicated by a sudden increase of ICP. Immediately after, the filament was withdrawn and the external carotid artery was ligated. Sham operated mice were treated at the same way with the only exception that the filament was not advanced far enough to induce hemorrhage. Anesthesia was terminated by intraperitoneal injection of atipamezole (2.5 mg/kg; Pfizer) naloxone (1.2 mg/kg; Inresa, Freiburg, Germany), and flumazenil (0.5mg/kg; Hoffmann-La-Roche, Grenzach-Wyhlen,Germany). Thereafter, mice were kept in an incubator at 33°C for 2.5 hours.

Forepaw-evoked neurovascular coupling

Mice were re-anesthetized 2.5 hours after SAH and the CBF response after neurovascular coupling was evaluated as previously described.[18] Briefly, the left forepaw was stimulated with two subdermally inserted needle electrodes with a diameter of 0.2 mm (Hwato, Suzhou, China) at an intensity of 2 mA for 0.3 ms (Digitimer Ltd, Hertfordshire, England). One stimulation cycle contained 96 stimulations and lasted for 16 seconds (6 Hz). The interval between two stimulation cycles was 40 seconds. CBF was assessed at five different locations covering the whole somatosensory cortex. The region with the strongest CBF response was also continuously stimulated (2 mA) for one minute in order to evaluate the response to a tonic stimulus. This region was then considered for analysis and further for assessment of the microvascular response by two-photon microscopy. A graphical representation of the experimental protocol is shown in figure 1A.

Two-photon microscopy

After assessing the CBF response to forepaw stimulation, i.e. fours after SAH, a cranial window (2 x 1 mm) was drilled under constant cooling above the area of the somatosensory cortex associated to the fore paw leaving the dura mater intact as previously described.[21] Mice were placed under a two-photon microscope (Zeiss LSM-7 MP, Oberkochen, Germany) equipped with a Li:Ti laser (Chameleon, Coherent, USA) as described previously,[22] and the exposed dura mater was kept wet with isotonic saline. The fluorescent plasma dye, fluorescein isothiocyanate (FITC-dextran; molecular weight 150 kDa) was given systematically via femoral artery injection (0.05 ml of a 0.5% solution; Sigma, Deisenhofen, Germany) and all parenchymal (diameter: 5 - 20 µm; depth: 100 µm) and pial arterioles (diameter: 20 to 40 µm) in the region previously selected (see above) were visualized using 2-photon fluorescence microscopy and a 10x Zeiss EC Plan-NeoFluar objective. Pial arterioles were followed into the parenchyma along an axis normal to the brain surface. Arterioles were distinguished from venules on the basis of velocity and direction of the blood flow.

Neurovascular reactivity to CO2

Diameters of both parenchymal and pial arterioles were examined under physiological conditions in order to obtain baseline values. Thereafter, arteriolar diameter was observed during inhalation of 10% CO_2 for 10 minutes. The amount of inhaled CO_2 was measured by microcapnometry (Hugo-Sachs Elektronik, March-Hugstetten, Germany). Arteriolar diameters were quantified with a calibrated image analysis software (Zen, Zeiss, Oberkochen, Germany) and expressed in percentage of baseline as previously described.[18]

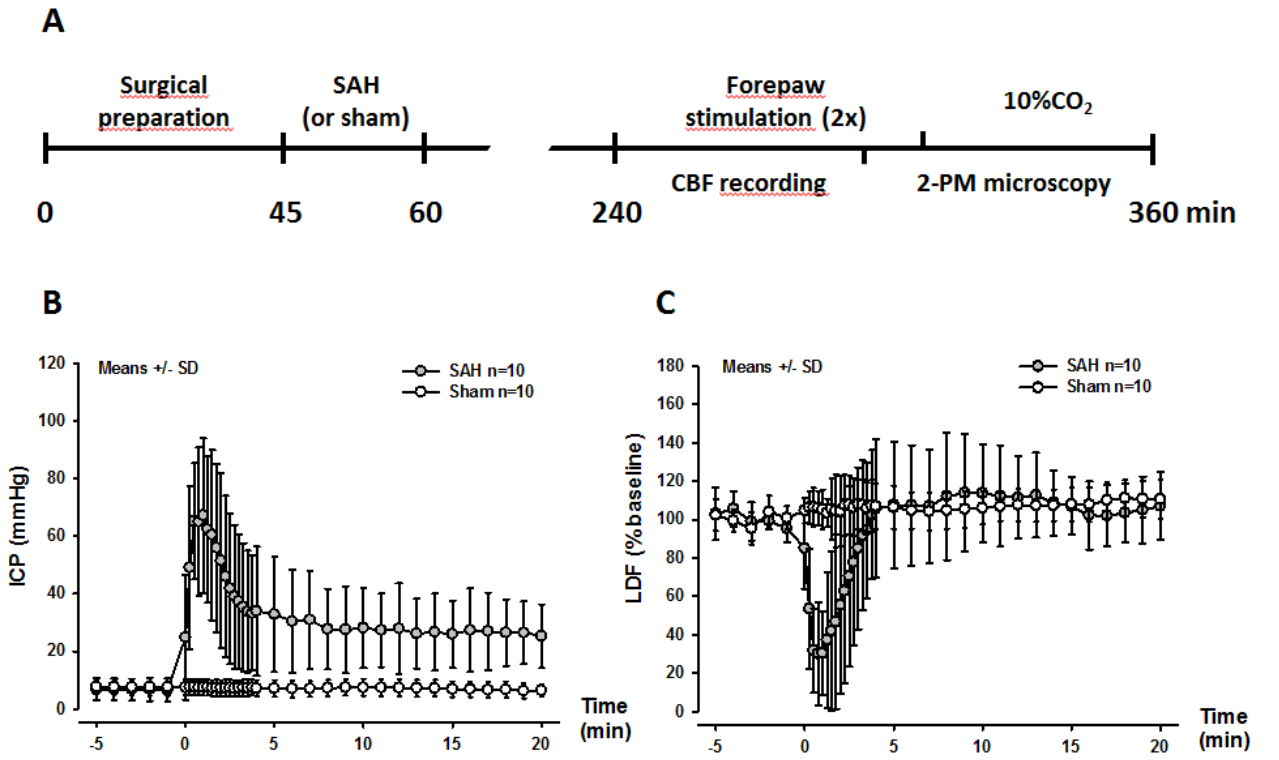

Figure 1. SAH induction and experimental design. **(A)** Schematic representation of the experimental design for SAH (or sham) surgery and forepaw stimulation followed by 10% CO_2 inhalation. **(B)** Intracranial pressure and **(C)** cerebral blood flow over time, starting five minutes before SAH induction until 20 minutes thereafter. A sudden increase in ICP and drop in CBF confirm vessel perforation. Mean +/- SD, n=10 each.

Vessel diameter during forepaw-evoked neurovascular coupling

For evaluation of changes in vessel diameter after forepaw stimulation the same protocol as for assessment of CBF was used. Briefly, the region yielding the most pronounced CBF response was stimulated with one stimulation cycle contained 96 stimulations and lasted for 16 seconds (6 Hz). The interval between two stimulation cycles was 40 seconds. Thereafter the same region was also continuously stimulated (2 mA) for one minute in order to evaluate the response to a tonic stimulus.

Ex vivo neurovascular coupling in freshly prepared brain slices

To examine neurovascular coupling ex vivo, parenchymal arteriolar diameter and astrocytic endfoot Ca^{2+} were simultaneously measured in freshly prepared cortical brain slices using a combination of two-photon and infrared-differential interference contrast (IR-DIC) microscopy as described previously.[13] Four hours after SAH induction mice were euthanized by decapitation under deep pentobarbital anesthesia (60 mg/kg). Coronal sections of somatosensory cortex (160 µm thick), prepared from the middle cerebral artery region using a vibratome (Leica VT1000S), were loaded with the Ca^{2+} indicator dye, fluo-4 (Invitrogen), for 1.5 hours at 29°C. Throughout the experiment, brain slices were superfused with artificial cerebral spinal fluid (aCSF; 125 mM NaCl, 3 mM KCl, 18 mM $NaHCO_3$, 1.25 mM NaH_2PO_4, 1 mM $MgCl_2$, 2 mM $CaCl_2$, and 5 mM glucose , aerated with 5% CO_2/20% O_2/75% N_2, pH ~7.35, 35-37°C) containing 125 Nm U46619 (a thromboxane A2 analog, Calbiochem) and 0.4 Mm ascorbic acid. U46619 was added to establish a physiological level of arteriolar tone and ascorbic acid was used as a supplement to prevent swelling of brain slices[13, 23] The following criteria was used to a elect the recording region within brain slices for neurovascular coupling: 1) brain parenchymal arterioles encased by astrocyte endfeet (i.e. arterioles past the end of Virchow-Robin space, or at least 50 µm from the brain surface), 2) Arterioles that are no greater than 300 µm from brain surface, and 3) Arterioles with adjacent astrocyte endfeet with detectable fluorescent Ca^{2+} indicator. Neurovascular coupling was initiated using electrical field stimulation (EFS, 50 Hz, 0.3-msec alternating square pulse, 3 sec duration). IR-DIC and fluorescent (Ex 820 nm, Em 525/50 nm) images were simultaneously acquired at ~ 1 Hz using a Zeiss LSM-7 multiphoton imaging system. Custom software SparkAn (written by Dr. Bonev, Univeristy of Vermont) was used to measure arteriolar diameter at 3 points along the segment (~10 µm) of the arteriole exhibiting the largest response to EFS, and are expressed as percent diameter change compared to the first image of the recording (prior to EFS). Estimated Ca^{2+} concentration in the astrocyte endfoot adjacent to the arteriolar segment of interest was obtained using the maximal fluorescent method.[23]

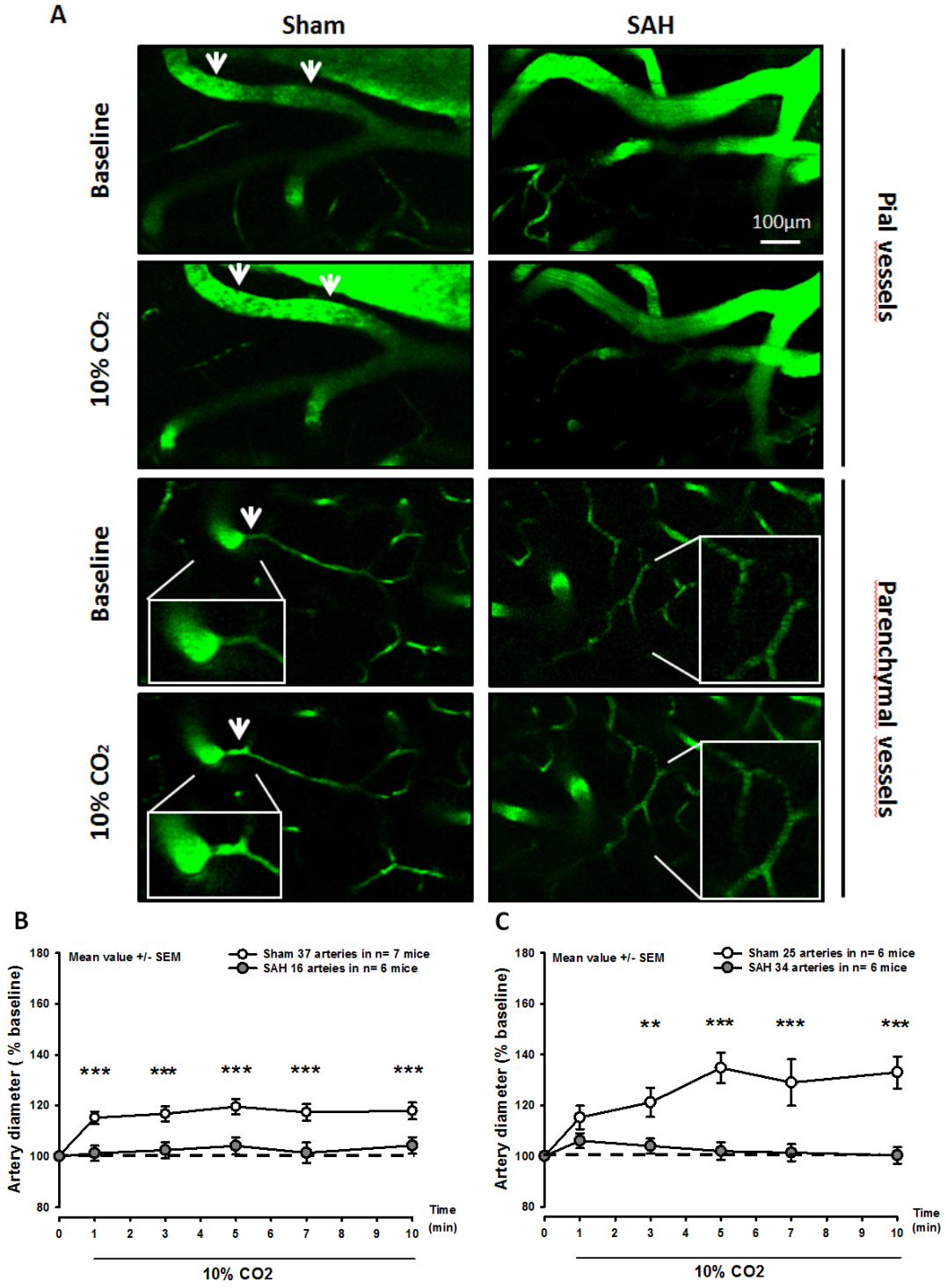

Figure 2. Pial and parenchymal arteries do not dilate in response to hypercapnia after SAH. **(A)** Representative two-photon microscopy images of pial (top) and parenchymal arteries (bottom) of SAH (left) and sham operated (right) mice before and during 10% CO_2 inhalation. **(B)** Surface and **(C)** parenchymal artery diameter during hypercapnia of mice subjected to sham surgery (white symbols) or SAH (gray symbols). Pial and parenchymal vessel dilated normally in response to inhalation of 10% CO_2 in sham operated mice (white symbols), while no response was observed after SAH (gray symbols). Mean +/- SEM; Mann-Whitney Rank Sum test; 16 to 37 arteries **(B)** and 25 to 34 arteries **(C)** in n=6-7 mice per group. ** P < 0.01 *** P < 0.001

Statistical Analysis

For the *in vivo* study, statistical analysis was performed with a standard statistical software package (Sigma Plot 12.5; Systat Software, Erkrath, Germany). Results for CO_2 reactivity experiments are presented as mean ± standard error of the mean (SEM). Results for somatosensory stimulation are presented as median ± 75/25 percentile. Differences across groups were evaluated using the Mann- Whitney Rank Sum test with the Bonferroni correction.

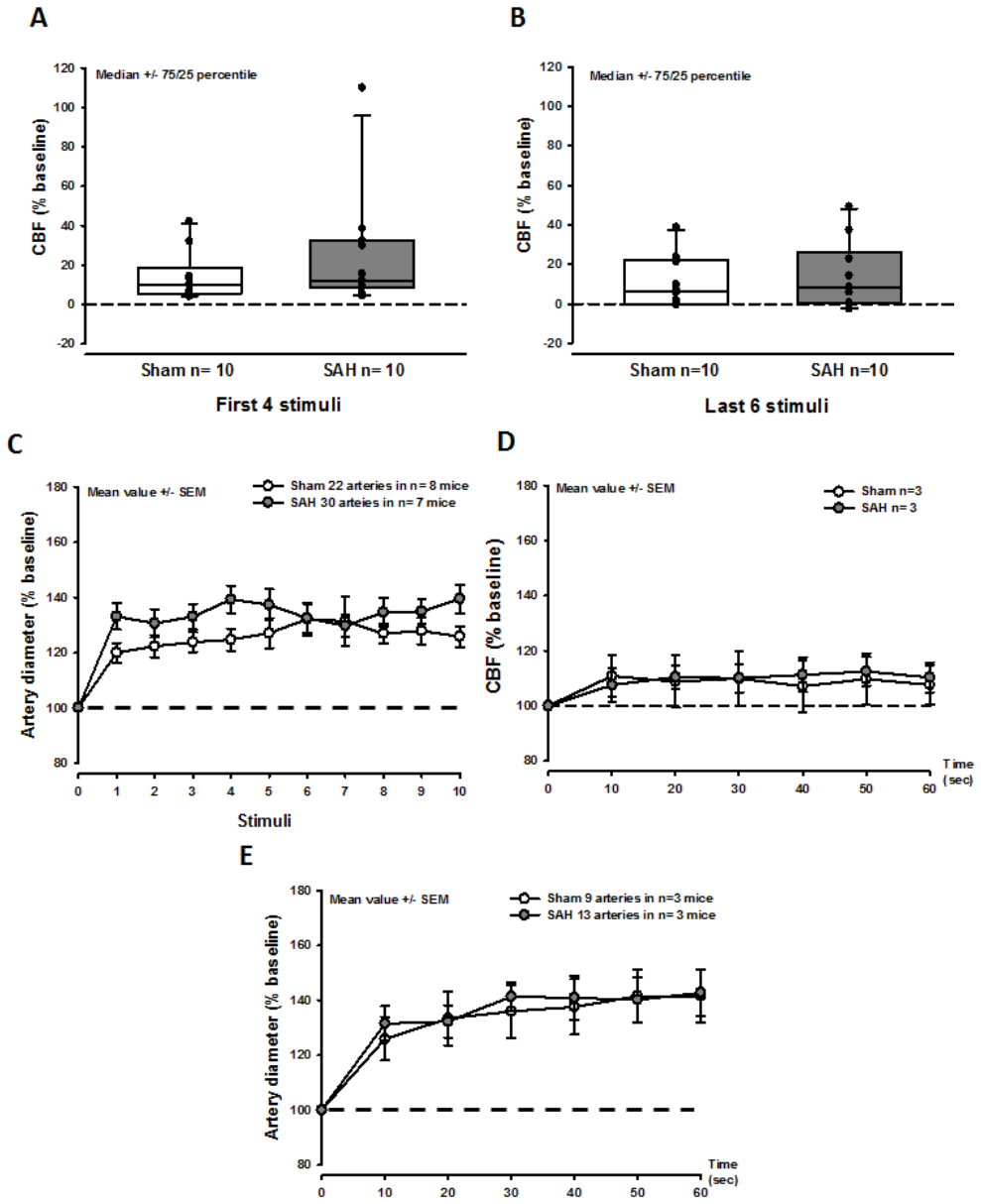

Figure 3. Neurovascular coupling is not altered 3 hours after SAH. **(A-B)** Box plots showing CBF increase in response to the first four (A) and last six (B) discrete electrical stimuli to the forepaw, in sham operated mice (white symbols) and after SAH (gray symbols). No significant effect was found between the experimental groups. Median +/- 75/25, n=10 each. **(C)** Artery dilation in response to a discrete electrical stimulation shows no difference between the experimental groups. Mean +/- SEM; 22 to 30 arteries from n=7-8 mice. **(D)** CBF increase in response to continuous electrical stimulation shows no difference between sham operated mice and mice subjected to SAH. Mean +/- SEM; Mann-Whitney Rank Sum test n=3 mice each. **(E)** Artery dilation in response to a continuous electrical stimulation shows no difference between SAH or sham operated mice. Mean +/- SEM; Mann-Whitney Rank Sum test; 9 to 13 arteries from n=3 mice each

For the ex vivo study, Origin 9.1 software (Origin Lab, Northampton, MA, USA) was used for statistical analysis. EFS-induced dilations (control vs SAH) were compared by unpaired t-test. Ca^{2+} concentrations in astrocyte endfoot (control vs SAH, before and after EFS) were analyzed by one-way ANOVA followed by post hoc comparison of means using the Tukey test. Data, in this case, are presented as mean ± SEM.

Randomization and Blinding

All animals were randomly assigned to the procedures; the surgical preparation and data analysis were performed by a researcher blinded towards the treatment of the animals.

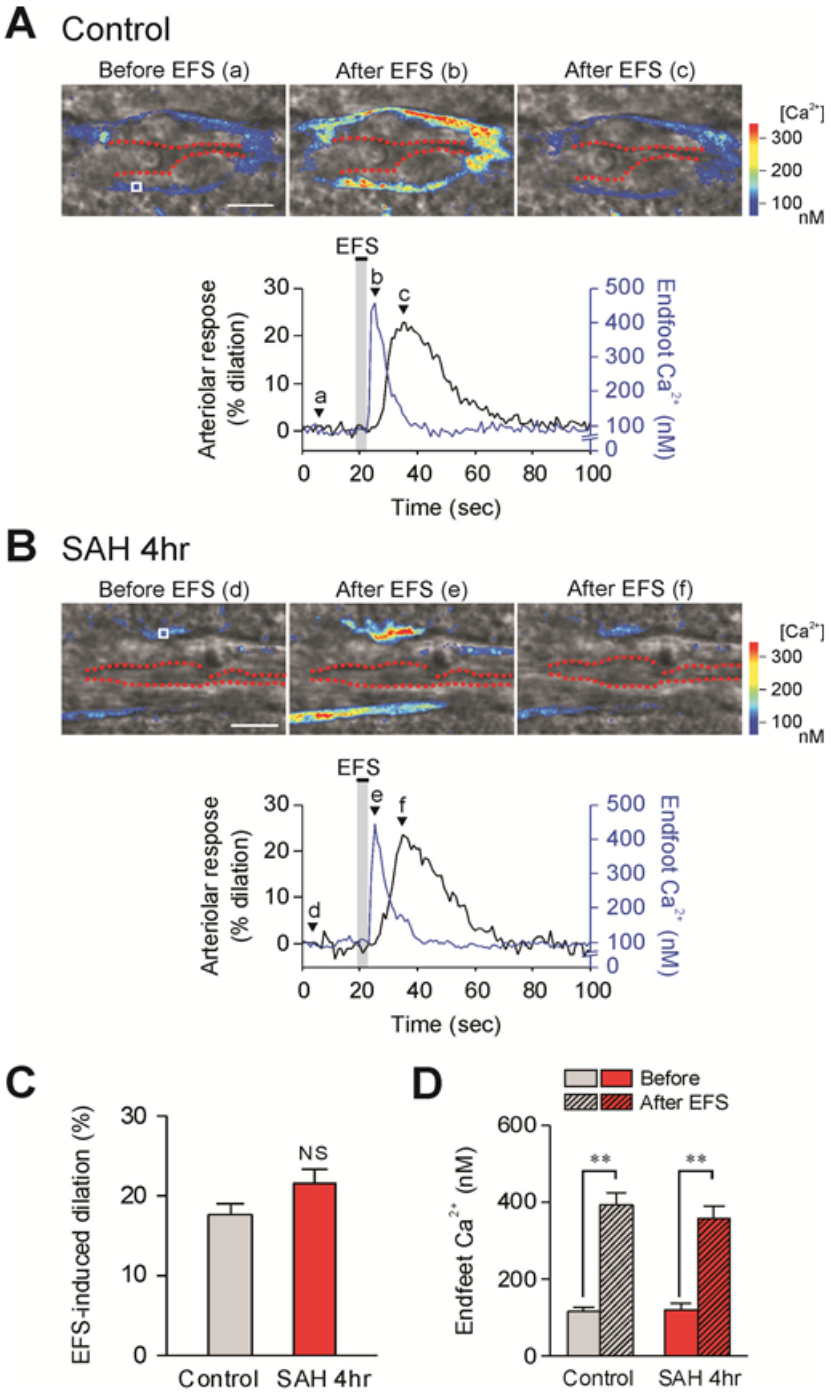

Figure 4. EFS-induced vasodilation is unaltered in brain slices 4 hours after SAH. **(A-B** upper panels**)** Infrared-differential interference contrast (IR-DIC) images of cortical brain slices from control and 4 hr SAH mice. The time points corresponding to IR-DIC images (a-f) are indicated by alphabetically labeled arrows in the lower panels. Red dashes outline the intraluminal diameter of parenchymal arterioles. Pseudocolor regions overlapping IR-DIC images depict estimated Ca^{2+} levels in astrocyte endfeet, which were imaged simultaneously with arteriolar diameter using the fluorescent Ca^{2+} indicator Fluo-4 and two-photon imaging. Scale bars, 10 µm. (A-B lower panels) EFS-induced changes in arteriolar diameter (black lines) and endfoot Ca^{2+} concentration (blue lines) obtained from brain slices depicted in upper images. Regions of interest (ROI) used for endfoot Ca^{2+} calculation are shown in images **A** and **D** labeled "Before EFS". **(C-D)** Summary of EFS-evoked changes in arteriolar diameter **(C)** and astrocytic endfoot Ca^{2+} **(D)** in control and 4hr SAH animals (n=5 each). Average diameters before EFS were 4.08 ± 0.44 µm (control) and 3.84 ± 0.50 µm (SAH 4hr), and were not significantly different between groups. NS: not significant. ** $P < 0.01$ vs endfoot Ca^{2+} before EFS in each group.

RESULTS

In vivo physiological parameters and mortality

Body temperature, systemic blood pressure, blood pH, pCO_2 and pO_2 – factors shown to have strong effects on CBF[24] – were carefully monitored in all investigated mice. Parameters did not differ between groups with the exception of the blood pressure which, as expected, was significantly increased in the SAH group (P=0.03) as a consequence of the Cushing reflex due to high ICP that results from the induction of SAH[25] (**Figure 1B** and **Supplementary Table S1**). Despite this increase in systemic blood pressure the high ICP observed immediately after SAH caused a reduction in cerebral perfusion pressure that resulted in reduction of cerebral blood flow by almost 80%. After ICP decreased to values around 30 mmHg CBF normalized and remained at this level for the remaining observation period (**Figure 1C**). After SAH animals show reduced motor activity. Two mice from each group (4/24) died before imaging could be performed, i.e. within three hours after SAH.

In vivo CO2 reactivity in cerebral pial arteries and parenchymal arterioles is abolished after SAH

In sham-operated mice, pial arterioles dilated by 17-20% upon inhalation of 10% CO_2 (**Figure 2A and 2B white symbols**). A similar, though stronger response was observed in parenchymal arterioles (**Figure 2A and 2C white symbols**). Following SAH pial vessels of a diameter of 20 to 40 µm were non-reactive to the increase in pCO_2 as compared to the sham group (**Figure 2A** and **Figure 2B, gray symbols**). Given this lack of pial microvascular CO_2 reactivity three hours after SAH, we also investigated the response of parenchymal arterioles. Following SAH parenchymal arterioles were also non-reactive to CO_2 (**Figure 2A** and **Figure 2C, gray symbols**). These results demonstrate that exposure to CO_2, which results in vasodilation in healthy mice is dramatically abolished in pial and parenchymal arterioles after SAH.

In vivo neurovascular coupling is maintained in acute SAH animals

Three hours after hemorrhage sensory stimulation of the forepaw resulted in a comparable increase of CBF and vessel diameter in both sham-operated and SAH mice (**Figure 3A-C**). In response to the stimulation the increase in artery diameter of parenchymal vessels reached values of 20-25% in the sham-operated group (**Figure 3C, white symbols**) while after SAH arterioles dilated by 30-40% (**Figure 3C, gray symbols**). Continuous sensory stimulation of the forepaw for one minute increased CBF by 15% (**Figure 3D, white** and **gray symbols**) and the diameter of parenchymal arteries by approximately 40% in sham and SAH mice (**Figure 3E**). These results point to a preserved neurovascular coupling early after SAH *in vivo*.

Preserved *ex vivo* neurovascular coupling in brain slices from four hours SAH animals

To examine the acute effects of SAH on ex vivo neurovascular coupling, two-photon imaging was performed on cortical brain slices prepared from mice four hours after induction of SAH via endovascular perforation. In brain slices from un-operated control animals, local neuronal activation by EFS caused the anticipated increase in astrocytic end-foot Ca^{2+} followed by vasodilation of the adjoining parenchymal arteriole (18 ± 1% increase in diameter, n=5; **Figure 4A-C**). EFS also induced vasodilation in brain slices obtained four hours after SAH (22 ± 2% increase in diameter, n=5; **Figure 4B and C**), similar to that observed in brain slices from control mice. Further, basal end-foot Ca^{2+} concentration (control: 118 ± 11 nM, SAH 121 ± 16 nM, n=5 each; **Figure 4D**) and end-foot Ca^{2+} concentration after EFS (control: 394 ± 32 nM, SAH 360 ± 29 nM n=5 each) were not significantly different between groups. These results demonstrate preserved neurovascular coupling in cortical brain slices four hours after SAH.

DISCUSSION

In this study, we have examined the acute effects, within the first 3-4 hours, of SAH on *in vivo* CO_2 reactivity and *in vivo* and *ex vivo* neurovascular coupling using endovascular perforation of mouse SAH model. Our data show that within three hours after SAH pial as well as intraparenchymal arterioles show a complete loss of reactivity to CO_2, a specific cerebral vasodilator while neurovascular coupling, that is the dilatation of cerebral vessels upon neuronal activation, was completely preserved. Thus our data demonstrate that 1) after SAH not only pial vessels but also intraparenchymal vessels lost in vivo CO_2 reactivity and 2) *in vivo* and *ex vivo* NVC remains unaffected in the acute phase of SAH. nce CO_2 reactivity depends, among others, on proper function of constitutive nitric oxide synthases (NOS)[26, 27] our data suggest that SAH may cause a rapid dysfunction of NO signaling throughout brain pial and parenchymal arterioles**.**

Disturbances of the cerebral microcirculation after SAH were described for the first time in 1975 by Herz et al., when they observed acute vasoconstriction of pial vessels after vascular micropuncture in guinea pigs.[28] Since then, little research has been done to understand the role of the cerebral microcirculation after SAH. The majority of studies investigating pial and parenchymal arterioles used *in vitro* systems[29-35] which require experimental conditions not necessarily reflecting microvascular function *in vivo*. The few published *in vivo* studies investigating the cerebral microcirculation after SAH used conventional epi-fluorescence microscopy and were due to the limited penetration depth of this technology limited to pial vessels.[36-38] These vessels were of specific interest in the context of SAH since these are the only cerebral microvessels coming in direct contact with extravasated blood after subarachnoid bleeding. Indeed, pial vessels were shown to constrict after SAH in experimental animals models and in SAH patients thereby suggesting that spasms of cerebral microvessels are one of the main reasons for the cerebral ischemia observed after SAH.[7-9] Pial microvessels, however, are morphologically distinct from parenchymal

arterioles in that pial vessels have perivascular innervation and lack of astrocytic endfeet coverage.[39] Most importantly, parenchymal, not pial, arterioles are in direct contact with the brain parenchyma, directly communicate with astrocytes and neurons, and increase their diameter upon neuronal activation. However, parenchymal arterioles within the brain beyond the range of conventional epi-fluorescence microscopy. Here, we applied the novel technology, i.e. two-photon microscopy in combination with neuronal stimulation paradigms, to provide the first measurements of parenchymal arteriolar functionality acutely after SAH.

Using this approach our results show that SAH results in the loss of CO_2 reactivity inparenchymal arterioles in addition to pial arteries at 3 hours after SAH, confirming our previous results on the lack of CO_2 reactivity in pial arterioles at 3 and 24 hours after SAH.[37] Our results show that not only microvessels located in the subarachnoid space and coming in direct contact with blood, but also arterioles in the parenchyma where blood is not present lose their ability to dilate in the face of increased levels of CO_2. Thus the brain as a whole seems to lose its ability to regulate blood flow in response to metabolic stress and may thus become increasingly vulnerable to additional damage. Since CO_2 reactivity is at least partly mediated through the activation of constitutive NO synthases,[26, 27] our results point towards a possible lack of proper NO signaling in this process in the acute phase of SAH. Further experiments need to clarify if targeting NO signaling or other signaling pathways downstream of CO_2 have the potential to restore microvascular function and to improve outcome after SAH.

Interestingly, neurovascular coupling, the process coupling neuronal activation to vasodilatation of neighboring vessels, was not affected in the first few hours after SAH, a time point associated with pial microvasospasms, pial microthrombosis, and decrease of cerebral blood flow in experimental SAH and in SAH patients.[6, 7] Mechanistically this suggests that CO_2 reactivity and NVC are at least partly mediated by different signaling pathways and that these pathways are differentially affected by SAH. Another important point is that SAH seems to affect *in vivo* CO_2 reactivity much earlier than NVC since *ex vivo* studies report a paradoxical inversion of NVC from dilation to constriction that emerges 24 to 96 hours after SAH.[40] In the current study our *in vivo* and *ex vivo* data univocally demonstrate that NVC coupling is not impaired within the first few hours after SAH. Thus, targeting SAH-induced impairment of NVC, that develops with a delayed onset (i.e. longer therapeutic window), may also have clinical potential. The mechanisms underlying SAH-induced inversion of NVC are not fully understood but are likely to involve an increase in the amplitude of spontaneous Ca^{2+} release events in astrocyte endfeet leading to elevation of K^+ in the restricted perivascular space around parenchymal arterioles[13, 37].

Taken together, the current study investigated for the first time the consequences of SAH on the functional integrity of parenchymal microvessels. Pial and parenchymal microvessels show a very early loss of CO_2-induced vasodilation *in vivo* but display normal *in vivo* and *ex vivo* NVC within the first few hours after SAH. These results suggest an early dysfunction of NO signaling in cerebral vessels after SAH. Together with our previous results on delayed dysfunction of NVC later than 24 hours after SAH we conclude that multiple molecular pathways seem to be involved in microvascular dysfunction after SAH. Thus multiple molecular pathways seem to be involved in microvascular dysfunction after SAH. Further research is needed to decipher these mechanisms thereby paving the way for novel therapeutic strategies for SAH patients who suffer from early and delayed cerebral ischemia.

ACKNOWLEDGEMENTS

This work was supported by the Solorz-Żak foundation, by the American Heart Association (14SDG20150027), National Institutes of Health (P01 HL095488, P30 RR032135, P30 GM103498 and S10 OD10583), Totman Medical Research Trust Fund, the Peter Martin Brain Aneurysm Endowment, and the Deutsche Forschungsgemeinschaft through the Munich Cluster of Systems Neurology (Synergy).

AUTHOR CONTRIBUTIONS

MB: performed all *in vivo* experiments and wrote the manuscript. MK: performed all ex vivo experiments and wrote the manuscript. SMS: provided technical input. GCW: designed the study and edited the manuscript. NP: designed the study, wrote and edited the manuscript

DISCLOSURE/CONFLICT OF INTEREST

No competing financial interests exist.

REFERENCES

1. Moore CI, Cao R. The hemo-neural hypothesis: on the role of blood flow in information processing. *Journal of neurophysiology* 2008; 99(5)**:** 2035-47.
2. Iadecola C, Nedergaard M. Glial regulation of the cerebral microvasculature. *Nature neuroscience* 2007; 10(11)**:** 1369-76.
3. Attwell D, Buchan AM, Charpak S, Lauritzen M, Macvicar BA, Newman EA. Glial and neuronal control of brain blood flow. *Nature* 2010; 468(7321)**:** 232-43.
4. Cahill J, Zhang JH. Subarachnoid hemorrhage: is it time for a new direction? *Stroke; a journal of cerebral circulation* 2009; 40(3 Suppl)**:** S86-7.
5. Weaver JP, Fisher M. Subarachnoid hemorrhage: an update of pathogenesis, diagnosis and management. *Journal of the neurological sciences* 1994; 125(2)**:** 119-31.
6. Schubert GA, Seiz M, Hegewald AA, Manville J, Thome C. Acute hypoperfusion immediately after subarachnoid hemorrhage: a xenon contrast-enhanced CT study. *Journal of neurotrauma* 2009; 26(12)**:** 2225-31.
7. Friedrich B, Muller F, Feiler S, Scholler K, Plesnila N. Experimental subarachnoid hemorrhage causes early and

long-lasting microarterial constriction and microthrombosis: an in-vivo microscopy study. *Journal of cerebral blood flow and metabolism : official journal of the International Society of Cerebral Blood Flow and Metabolism* 2012; 32(3)**:** 447-55.

8. Pennings FA, Bouma GJ, Ince C. Direct observation of the human cerebral microcirculation during aneurysm surgery reveals increased arteriolar contractility. *Stroke; a journal of cerebral circulation* 2004; 35(6)**:** 1284-8.
9. Uhl E, Lehmberg J, Steiger HJ, Messmer K. Intraoperative detection of early microvasospasm in patients with subarachnoid hemorrhage by using orthogonal polarization spectral imaging. *Neurosurgery* 2003; 52(6)**:** 1307-15; disacussion 1315-7.
10. Zhang JH. Molecular neurosciences. *Neurological research* 2009; 31(2)**:** 113.
11. Sehba FA, Hou J, Pluta RM, Zhang JH. The importance of early brain injury after subarachnoid hemorrhage. *Progress in neurobiology* 2012; 97(1)**:** 14-37.
12. Hockel K, Scholler K, Trabold R, Nussberger J, Plesnila N. Vasopressin V(1a) receptors mediate posthemorrhagic systemic hypertension thereby determining rebleeding rate and outcome after experimental subarachnoid hemorrhage. *Stroke; a journal of cerebral circulation* 2012; 43(1)**:** 227-32.
13. Koide M, Bonev AD, Nelson MT, Wellman GC. Inversion of neurovascular coupling by subarachnoid blood depends on large-conductance Ca2+-activated K+ (BK) channels. *Proceedings of the National Academy of Sciences of the United States of America* 2012; 109(21)**:** E1387-95.
14. Kilkenny C, Browne W, Cuthill IC, Emerson M, Altman DG. Animal research: reporting in vivo experiments: the ARRIVE guidelines. *British journal of pharmacology* 2010; 160(7)**:** 1577-9.
15. Thal SC, Plesnila N. Non-invasive intraoperative monitoring of blood pressure and arterial pCO2 during surgical anesthesia in mice. *Journal of neuroscience*
16. Schwarzmaier SM, Plesnila N. Contributions of the immune system to the pathophysiology of traumatic brain injury - evidence by intravital microscopy. *Frontiers in cellular neuroscience* 2014; 8**:** 358.
17. Feiler S, Friedrich B, Scholler K, Thal SC, Plesnila N. Standardized induction of subarachnoid hemorrhage in mice by intracranial pressure monitoring. *Journal of neuroscience methods* 2010; 190(2)**:** 164-70.
18. Balbi M, Ghosh M, Longden TA, Jativa Vega M, Gesierich B, Hellal F *et al.* Dysfunction of mouse cerebral arteries during early aging. *Journal of cerebral blood flow and metabolism : official journal of the International Society of Cerebral Blood Flow and Metabolism* 2015.
19. Scholler K, Feiler S, Anetsberger S, Kim SW, Plesnila N. Contribution of bradykinin receptors to the development of secondary brain damage after experimental subarachnoid hemorrhage. *Neurosurgery* 2011; 68(4)**:** 1118-23.
20. Buhler D, Schuller K, Plesnila N. Protocol for the induction of subarachnoid hemorrhage in mice by perforation of the Circle of Willis with an endovascular filament. *Translational stroke research* 2014; 5(6)**:** 653-9.
21. Terpolilli NA, Kim SW, Thal SC, Kataoka H, Zeisig V, Nitzsche B *et al.* Inhalation of nitric oxide prevents ischemic brain damage in experimental stroke by selective dilatation of collateral arterioles. *Circulation research* 2012; 110(5)**:** 727-38.
22. Schwarzmaier SM, Zimmermann R, McGarry NB, Trabold R, Kim SW, Plesnila N. In vivo temporal and spatial profile of leukocyte adhesion and migration after experimental traumatic brain injury in mice. *Journal of neuroinflammation* 2013; 10**:** 32.
23. Girouard H, Bonev AD, Hannah RM, Meredith A, Aldrich RW, Nelson MT. Astrocytic endfoot Ca2+ and BK channels determine both arteriolar dilation and constriction. *Proceedings of the National Academy of Sciences of the United States of America* 2010; 107(8)**:** 3811-6.
24. Faraci FM, Heistad DD. Regulation of the cerebral circulation: role of endothelium and potassium channels. *Physiological reviews* 1998; 78(1)**:** 53-97.
25. Ayling J. Managing head injuries. *Emergency medical services* 2002; 31(8)**:** 42.
26. Iadecola C. Does nitric oxide mediate the increases in cerebral blood flow elicited by hypercapnia? *Proceedings of the National Academy of Sciences of the United States of America* 1992; 89(9)**:** 3913-6.
27. Iadecola C, Zhang F. Nitric oxide-dependent and -independent components of cerebrovasodilation elicited by hypercapnia. *The American journal of physiology* 1994; 266(2 Pt 2)**:** R546-52.
28. Herz DA, Baez S, Shulman K. Pial microcirculation in subarachnoid hemorrhage. *Stroke; a journal of cerebral circulation* 1975; 6(4)**:** 417-24.
29. Kajita Y, Dietrich HH, Dacey RG, Jr. Effects of oxyhemoglobin on local and propagated vasodilatory responses induced by adenosine, adenosine diphosphate, and adenosine triphosphate in rat cerebral arterioles. *Journal of neurosurgery* 1996; 85(5)**:** 908-16.
30. Park KW, Metais C, Dai HB, Comunale ME, Sellke FW. Microvascular endothelial dysfunction and its mechanism in a rat model of subarachnoid hemorrhage. *Anesthesia and analgesia* 2001; 92(4)**:** 990-6.
31. Park KW, Dai HB, Metais C, Comunale ME, Sellke FW. Isoflurane does not further impair microvascular vasomotion in a rat model of subarachnoid hemorrhage. *Canadian journal of anaesthesia = Journal canadien d'anesthesie* 2002; 49(4)**:** 427-33.
32. Katusic ZS, Milde JH, Cosentino F, Mitrovic BS. Subarachnoid hemorrhage and endothelial L-arginine pathway in small brain stem arteries in dogs. *Stroke; a journal of cerebral circulation* 1993; 24(3)**:** 392-9.
33. Nystoriak MA, O'Connor KP, Sonkusare SK, Brayden JE, Nelson MT, Wellman GC. Fundamental increase in pressure-dependent constriction of brain parenchymal arterioles from

subarachnoid hemorrhage model rats due to membrane depolarization. *American journal of physiology. Heart and circulatory physiology* 2011; 300(3)**:** H803-12.

34. Koide M, Wellman GC. SAH-induced suppression of voltage-gated K(+) (K (V)) channel currents in parenchymal arteriolar myocytes involves activation of the HB-EGF/EGFR pathway. *Acta neurochirurgica. Supplement* 2013; 115**:** 179-84.
35. Ishiguro M, Puryear CB, Bisson E, Saundry CM, Nathan DJ, Russell SR *et al.* Enhanced myogenic tone in cerebral arteries from a rabbit model of subarachnoid hemorrhage. *American journal of physiology. Heart and circulatory physiology* 2002; 283(6)**:** H2217-25.
36. Sun BL, Zheng CB, Yang MF, Yuan H, Zhang SM, Wang LX. Dynamic alterations of cerebral pial microcirculation during experimental subarachnoid hemorrhage. *Cellular and molecular neurobiology* 2009; 29(2)**:** 235-41.
37. Friedrich B, Michalik R, Oniszczuk A, Abubaker K, Kozniewska E, Plesnila N. CO2 has no therapeutic effect on early microvasospasm after experimental subarachnoid hemorrhage. *Journal of cerebral blood flow and metabolism : official journal of the International Society of Cerebral Blood Flow and Metabolism* 2014; 34(8)**:** e1-6.
38. Ishikawa M, Kusaka G, Yamaguchi N, Sekizuka E, Nakadate H, Minamitani H *et al.* Platelet and leukocyte adhesion in the microvasculature at the cerebral surface immediately after subarachnoid hemorrhage. *Neurosurgery* 2009; 64(3)**:** 546-53; discussion 553-4.
39. Cipolla MJ. In: *The Cerebral Circulation*: San Rafael (CA), 2009.
40. Koide M DK, Bulkeley EA, Nelson MT, Wellman GC. In vivo and ex vivo dysfunction of neurovascular coupling in a mouse model of subarachnoid hemorrhage. *FASEB* 2014; 28 (1 Supplement), 676.3.

Supplementary Information accompanies the paper on the Journal of Cerebral Blood Flow & Metabolism website (http://www.nature.com/jcbfm)

4 Pericytes are involved in the pathogenesis of CADASIL

4.1 Summary

As a next step I decided to analyze the burden of a chronic pathology such as small vessel disease on neurovascular reactivity. CADASIL is one of two animal models to study small vessel disease. Histological analysis to understand the role of pericytes in the progress of the disease revealed a decrease in number of pericytes and in their coverage of blood vessels. I took advantage of the classical CO_2 challenge to analyze the effects of CADASIL on CBF regulation and vascular endothelial reactivity, and I was able to detect impairment in CBF in response to 10% CO_2 challenge in 12-month-old CADASIL mice. I decided to analyze the consequences of this impairment on neurovascular coupling using the forepaw stimulation paradigm. However, the reduction I found in neurovascular coupling was not due to the mutation, but the age of the mice. These data suggest that morphological changes to the cerebral microvasculature occur earlier than functional changes, and that NO-dependent vasodilatation is impaired at later stages in CADASIL mice. Therefore, targeting either pericytes or the NOS system could represent novel therapeutic strategies for CADASIL and small vessel disease.

Pericytes are involved in the pathogenesis of CADASIL

Mitrajit Ghosh, PhD[1,2,5,6], Matilde Balbi, MSc[1,3,6], Farida Hellal, PhD[1,5], Martin Dichgans, MD, PhD[1,5], Ute Lindauer, MD, PhD[2,4,5,7], and Nikolaus Plesnila, MD, PhD[1,4,5,7,8]

[1]Institute for Stroke and Dementia Research (ISD), University of Munich Medical Center, Ludwig-Maximilians-University, 81377 Munich, Germany. [2]Experimental Neurosurgery, Department of Neurosurgery, Klinikum recht der Isar, Technical University Munich, 81675 Munich, Germany.[3]Graduate School of Systemic Neurosciences (GSN), Ludwig-Maximilians University (LMU). [4]Translational Neurosurgery and Neurobiology, Department of Neurosurgery, Medical Faculty, RWTH Aachen University, 52074 Aachen, Germany, [5]Munich Cluster for Systems Neurology (SyNergy), Munich, Germany, [6]Co-first author; [7]Co-senior author, [8]Corresponding author: Prof. Dr. med. Nikolaus Plesnila, Institut für Schlaganfall- und Demenzforschung, Klinikum der Universität München, Feodor-Lynen-Straße 17, D-81377 München, Germany. Tel.: +49 (0) 89 4400 46 219 or 220, Email: nikolaus.plesnila@med.uni-muenchen.de, Internet: www.isd.klinikum.uni-muenchen.de

Objective: Cerebral autosomal dominant arteriopathy with subcortical infarcts and leukoencephalopathy (CADASIL), the most common inherited small-vessel disease, is associated with vascular aggregation of mutant Notch3 protein, dysfunction of cerebral vessels, and dementia. Pericyte, perivascular cells involved in microvascular function, express Notch3. Therefore we hypothesize that these cells may play a role in the pathogenesis of CADASIL. **Methods:** Two, seven, and 12 month old CADASIL mutant mice (TgNotch3R169C) and wild-type controls were examined regarding Notch3 aggregation in pericytes, the coverage of cerebral vessels by pericytes, pericyte numbers, capillary density, BBB integrity, astrocytic end-feet and the expression of astrocytic gap-junction and endothelial adherens-junction protein using immunostaining and western blot analysis. In addition, we examined cerebrovascular CO2 reactivity using laser Doppler fluxmetry and in vivo microscopy. **Results:** With increasing age, mutated Notch3 aggregated around pericytes and smooth muscle cells. Notch3 aggregation caused significant reduction of pericyte number and coverage of capillaries by pericyte processes ($p<0.01$). These changes were associated with detachment of astrocytic end-feet from cerebral microvessels, leakage of plasma proteins, reduction in expression of endothelial adherens-junction protein, and reduced microvascular reactivity to CO2. Smooth muscle cells were not affected by Notch3 accumulation. **Interpretation:** Our results show that pericytes are the first cells affected by Notch3 aggregation in CADASIL mice. Pericyte pathology causes opening of the BBB and microvascular dysfunction. Therefore, protecting pericytes may represent a novel therapeutic strategy for vascular dementia.

INTRODUCTION

Cerebral autosomal dominant arteriopathy with subcortical infarcts and leukoencephalopathy (CADASIL) is the most common cause of monogenic stroke and vascular dementia.[1,2,3] CADASIL is caused by mutations in the Notch3 gene that encodes a cell surface receptor on smooth muscle cells and pericytes.[4] The mutated Notch3 receptor ($Notch3^{ECD}$) accumulates in blood vessels of CADASIL patients and CADASIL mutant mice. These aggregates are associated with fibrosis of the arteries and arterioles, reduced blood flow, and ultimately white matter lesions, thinning of the cortex, and dementia.[5-8]

At the cellular level, CADASIL is believed to arise from the damage and death of smooth muscle cells (SMCs) in the wall of cerebral vessels due to the accumulation of mutant $Notch3^{ECD}$ aggregates.[3] However, it was previously shown that SMC viability was not affected in a CADASIL mouse model.[5] Thus, the cell type which ultimately drives CADASIL pathology remains unclear.

We and others revealed an important role for cerebral pericytes (perivascular cells located between the capillary endothelium and astrocytic end-feet) in the regulation of microvascular function and in maintaining the integrity of the blood-brain barrier (BBB).[9-14] Because pericytes contain contractile elements, they may be an important regulator of cerebral blood flow at the capillary level under both physiological and pathological conditions.[14,15] Pericytes express the PDGF receptor β (PDGFRβ) and are responsible for the function and survival of endothelial cells and for sufficient expression of tight junction proteins.[16] Thus, pericytes play a central role in maintaining microvascular perfusion and in the proper functioning of the BBB.

The Notch3 receptor is also expressed in capillary pericytes and recent electron microscopy studies found altered pericyte morphology in CADASIL mice.[17,18] However, the functional relevance of these findings is unclear, and the role of pericytes in the initiation and progression of CADASIL is currently unknown. Therefore, the aim of this study was to examine whether pericytes play a role in the pathogenesis of CADASIL.

MATERIALS AND METHODS

Ethics statement

Mice were bred at the Zentrum für Neuropathologie und Prionforschung animal facility (Munich, Germany) and experiments were approved by the Government of Upper Bavaria (protocol no. 220/30).

Randomization and blinding

All experiments were performed using a randomized and blinded protocol and data were analyzed by a researcher who was blinded with respect to the genotype of the mice.

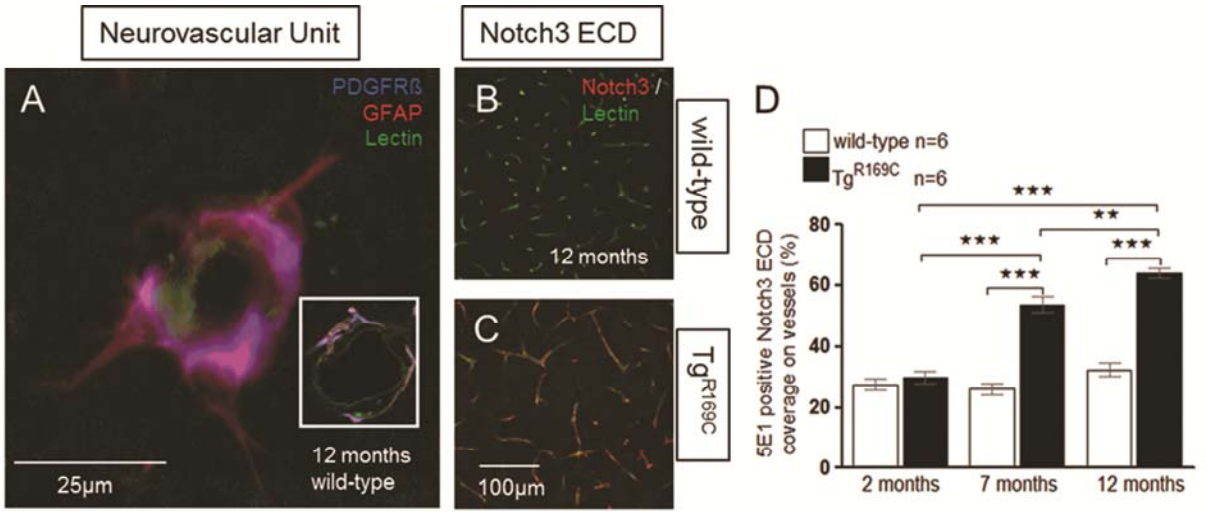

Figure 1. Increased Notch3 aggregation in CADASIL mouse. **(A)** Confocal microscopy image of the neurovascular unit in a wild-type mouse cerebral cortex. PDGFRβ-positive pericytes on brain capillaries are shown in blue, glial-fibrillar acidic protein (GFAP)-positive astrocytes are shown in red, and lectin-positive endothelial cells are shown in green. *Inset*: cross-section of a capillary, showing co-localization of pericytes with capillary endothelial cells. **(B-C)**. Increased Notch3 aggregation in the cortex of 12-month-old TgNotch3^{R169C} mice compared to age-matched wild-type controls. Notch3 was stained using the 5E1 antibody (which recognizes an extracellular domain in Notch3; shown in red), and lectin-positive capillaries are shown in green. **(D)**. Quantification of Notch3 coverage on vessels in TgNotch3^{R169C} and wild-type mice at the indicated ages. Scale in A = 25µm, B&C = 100µm. D is presented as mean ± SEM (n = 6 mice/group). ***P≤0.001.

Subjects

CO_2 reactivity was measured using 7-month-old and 12-month-old FVB/N mice (n = 21 and 22 mice, respectively). The immunofluorescence staining and western blot experiments were performed using 2-month-old, 7-month-old, and 12-month-old FVB/N mice (n=6 mice/group, for a total of 54 mice).

The following lines of mice used for this study: wild-type (non-transgenic); TgNotch3^{WT} mice, which overexpress the wild-type rat Notch3 protein; and TgNotch3^{R169C} mice, which overexpress rat Notch3 with the R169C mutation. The TgNotch3^{R169C} line is an established mouse model for CADASIL.[5]

Surgical procedure for investigating in vivo microvascular reactivity

The mice had free access to food and water before surgery. The surgical procedure was performed as previously described.[19,20] In brief, animals were anesthetized with an intraperitoneal injection of midazolam (5 mg/kg; Braun, Melsungen, Germany), fentanyl (0.05 mg/kg; Jansen-Cilag, Neuss, Germany), and medetomidine (0.5 mg/kg; Pfizer, Karlsruhe, Germany), after which the mice were intubated with an endotracheal tube and mechanically ventilated. Body temperature and end-tidal pCO2 were monitored continuously. A cannula was placed in the left femoral artery and used to monitor blood pressure and measure blood gases; all values were within their respective normal range throughout the experiments.

Intravital microscopy

Intravital microscopy was performed as previously described.[21] In brief, a 4 mm x 4 mm cranial window was drilled above the right parietal cortex, leaving the dura mater intact. The exposed dura mater was rinsed periodically with saline. The pial vessels were visualized by an arterial injection of fluorescein isothiocyanate (FITC-dextran) prior to the first measurement. Four regions of interest (ROIs) containing pial arterioles, venules, and capillaries were investigated. Cerebral blood flow (CBF) was measured using a laser Doppler probe positioned over the territory of the middle cerebral artery.

Baseline values were measured after the physiological parameters were stable. CBF and vessel diameter were measured after fixing CO_2 at 10% in the ventilator in order to increase arterial pCO_2 for 15 minutes. After this time, pCO_2 was returned to normal levels, and CBF and vessel diameter were recorded for an additional 15 minutes (i.e., 30 minutes in total). The response of pial arterioles to CO2 and the CBF response to CO2 were both integrated only during the time of CO2 inhalation, which is for 15 min. Images were recorded and analyzed at 10X magnification. Arterial blood pressure was monitored throughout the experiment to ensure that any changes in CBF were not due to a change in systemic blood pressure.

Analysis of the pial microvasculature

Vessel diameter was quantified using image analysis software (Zeiss). For graphical and statistical representations, the vessels

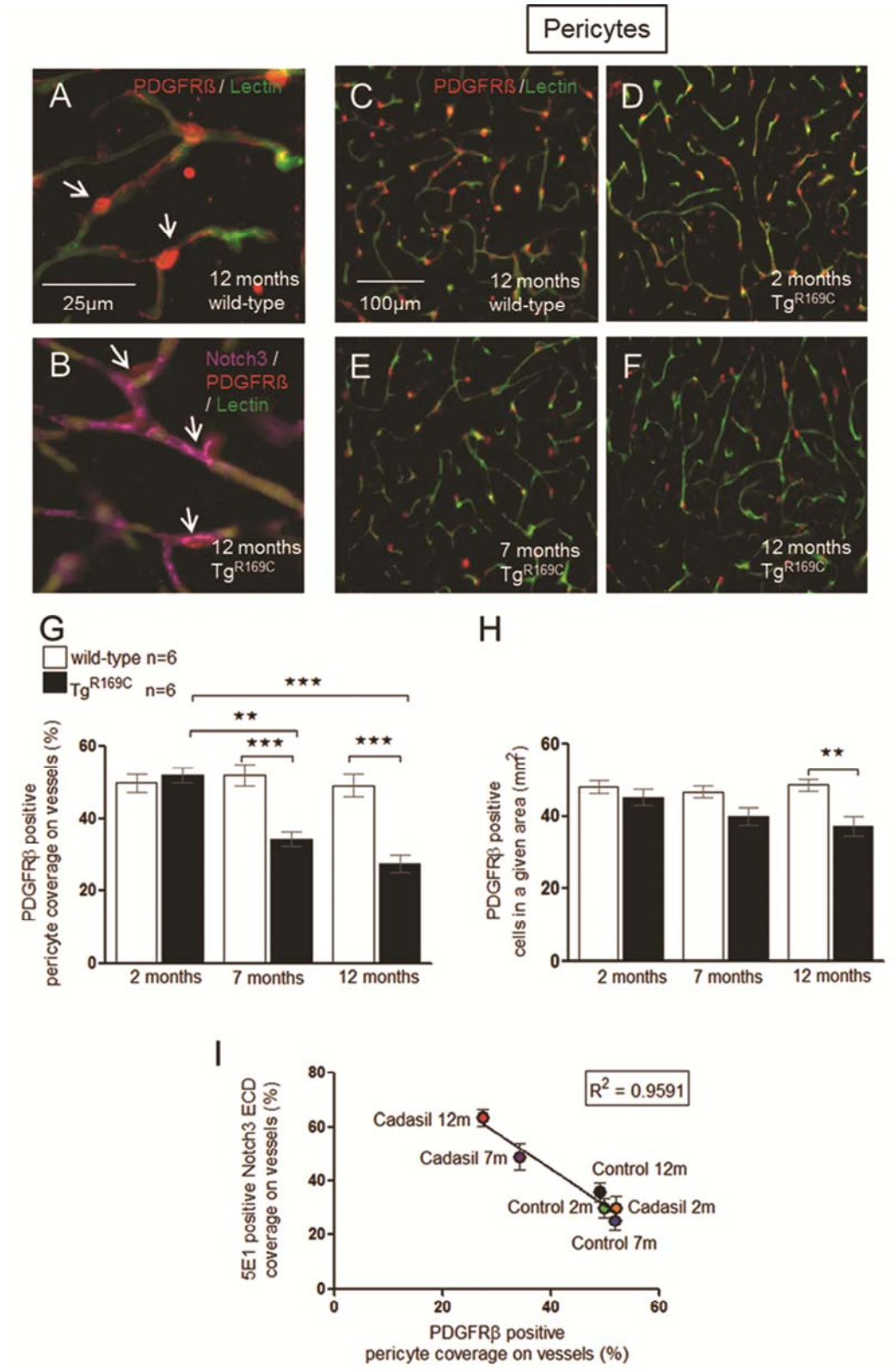

Figure 2. Pericyte coverage and the number on cerebral capillaries in the cortex are reduced in CADASIL mice. **(A)** Representative confocal microscopy image of a 12-month-old wild-type mouse cortex, showing PDGFRβ-positive pericytes (red) with cell bodies and processes extended over lectin-positive capillaries (green). *White arrows* indicate the pericytes cell body and processes on the capillaries. **(B)** Confocal microscopy image of Notch3 aggregates (magenta) in the proximity of PDGFRβ-positive pericytes (red) on lectin-positive capillaries (green) in a 12-month-old TgNotch3^{R169C}mouse. *White arrows* indicate the pericytes cell body and processes

with Notch3 aggregates on the capillaries. **(C)** Representative confocal microscopy image of a 12-month-old wild-type mouse cortex. PDGFRβ-positive pericytes are shown in red, and lectin-positive capillaries are shown in green. **(D-F)** Confocal microscopy of pericyte coverage in TgNotch3^{R169C} mice at 2, 7, and 12 months of age, respectively. **(G)** Quantification of PDGFRβ-positive pericyte coverage on lectin-positive capillaries in TgNotch3^{R169C} and wild-type mice at the indicated ages. **(H)** Quantification of PDGFRβ-positive pericytes in a 0.4-mm^2 area in TgNotch3^{R169C} and wild-type mice at the indicated ages. **(I)** Notch3 aggregation is negatively correlated with pericyte coverage of brain capillaries in the cerebral cortex. The dots represent mean of six mice in each group. Scale in **(A)** and **(B)** = 25μm, C-F = 100μm. The data in panels **(G)** and **(H)** are presented as mean ± SEM (n = 6 mice/group). **P≤0.01; ***P≤0.001. R^2 = pearson coefficient of determination.

were categorized by diameter as follows: <10μm; 10-20μm; 20 - 30 μm; 30-50μm; and >50μm). The average vessel diameter (expressed as a percentage of baseline) in each category was compared between groups of animals. Vessels 20-30μm in diameter were used for further analysis.

Vibratome sectioning and immunofluorescence staining (Fluorescent lectin staining and tissue immunofluorescence staining)

Mice were anesthetized and arterially perfused with lectin, after which they were sacrificed by transcardial perfusion with 0.9% sodium chloride (NaCl) and 4% paraformaldehyde (PFA). The brains were removed and post-fixed overnight in PFA. Coronal sections of the cerebral cortex (50-μm thick) were prepared using a VS1200vibratome (Leica). The free-floating sections were collected either in phosphate-buffered saline (PBS) for immediate use or in a cryoprotectant solution (for later use). The sections were then processed for immunostaining. Three sections per brain were used for immunostaining. Sections were blocked with 3% BSA (w/v) for 60min, and then incubated with primary antibody diluted in blocking solution overnight at 4°C. The sections were then washed in PBS and were incubated in fluorophore-conjugated secondary antibodies for 2 hrs at room temperature. The sections were then washed and mounted using Fluoromount mounting medium (Sigma). The following primary antibodies were used: for smooth muscle cells: Cy3-conjugated anti-alpha smooth muscle actin (α-SMA;1:100, Sigma, C6198); for pericytes: goat anti-PDGFRβ (1:100, R&D Systems, AF1042), rabbit anti-desmin (1:100, Millipore, MAB3430), and rabbit anti-aminopeptidase N (1:100, Antibodies Online, ABIN359551); for astrocytes: mouse anti-GFAP (1:100, Sigma, G3893) and rabbit anti-aquaporin-4 (1:100, Millipore, AB2218); for plasma protein: mouse anti-albumin (1:100, Sigma, A6684) and rabbit anti-fibrinogen (1:100, Dako, A0080). To visualize PGDFRβ-positive pericytes, sections were incubated in secondary Cy3-conjugated donkey anti-goat antibody (1:100, Jackson Immuno Research, 705165147). To visualize desmin-positive pericytes, fibrinogen extravasation, and aquaporin-4-positive astrocytes, sections were incubated in secondary Cy3-conjugated donkey anti-rabbit antibody (1:100, Jackson Immuno Research, 711165152). To visualize GFAP-positive astrocytes and albumin, sections were incubated in secondary Cy3-conjugated donkey anti-mouse antibody (1:100, Jackson Immuno Research, 715165150). For triple fluorescence measurements, the following secondary antibodies were also used: Alexa Fluor 680 goat anti-rabbit IgG (1:100, Invitrogen, A21109) or Alexa Fluor 680 goat anti-mouse IgG (1:100, Invitrogen, A21057).

Fluorescence and confocal microscopy

All tissue sections were imaged using a Zeiss Axiovert 200M inverted fluorescence microscope and a Leica TCS SP5 II confocal microscope. Quantitative image analysis was performed by an investigator who was blinded with respect to the genotype and treatment group (ImageJ software).

a) Capillary density in the cortex

To quantify capillary density, maximum projection *z*-stacks were reconstructed. The lectin-positive signal in the blood vessels was subjected to automated threshold processing after background correction, and the signal was quantified using the Area Measurement analysis tool in ImageJ. In each mouse, four regions of interests (ROIs) in the cortex were analyzed by randomly selecting four fields. These fields were analyzed in three nonadjacent sections (at ~100-μm intervals). Six animals per group were analyzed.

b) Notch3 coverage, Smooth muscle cell coverage, Pericyte coverage and astrocytes endfeet coverage in the cortex

For analysing coverage, maximum projection *z*-stacks were reconstructed. The Notch3 5E1, α-SMA, PDGFRβ, GFAP and lectin signals in the capillaries were subjected to automated threshold processing after background correction. The areas occupied by their respective signals were analyzed using the Area Measurement tool in ImageJ. Notch3, SMC, pericyte and astrocytes endfeet coverage was determined as the percentage of Notch3 5E1, α-SMA, PDGFRβ, GFAP -positive surface area covering lectin-positive capillary surface area per field (410 μm x 410 μm) respectively. In each mouse, four ROIs in the cortex were analyzed by randomly selecting four fields. These fields were analyzed in three nonadjacent sections (at ~100-μm intervals). Six animals per group were analyzed.

c) Pericyte numbers in the cortex

The number of PDGFRβ-positive pericytes per mm^2 of selected field area (410 μm x 410 μm) was analyzed. In each mouse, four ROIs in the cortex were analyzed by randomly selecting four

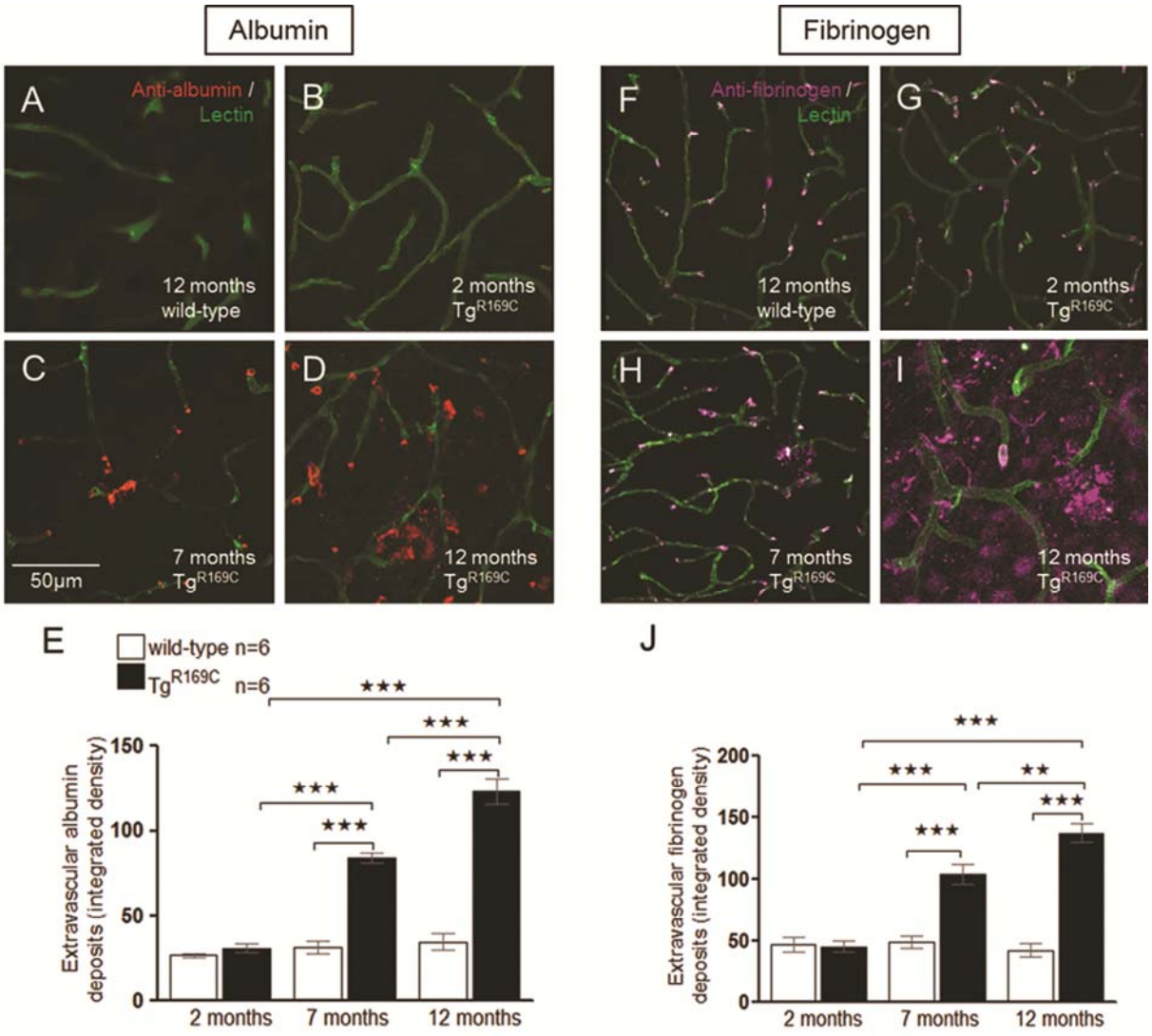

Figure 3. Blood-brain barrier breakdown in CADASIL mice. **(A)** Representative confocal microscopy image of a 12-month-old wild-type mouse, showing a lack of extravascular albumin (red) leakage through lectin-positive capillaries (green). **(B-D)**. Age-dependent increase in extravascular albumin (red) through lectin-positive capillaries (green) in the cortex of 2-, 7-, and 12–month-old TgNotch3^{R169C} mice, respectively. **(E)** Quantification of extravascular albumin in TgNotch3^{R169C} and wild-type mice at the indicated ages. **(F)** Representative confocal microscopy image of a 12-month-old wild-type mouse, showing a small amount of extravascular fibrinogen (magenta) leakage through lectin-positive capillaries (green). **(G-I)** Age-dependent increase in extravascular fibrinogen (magenta) through lectin-positive capillaries (green) in the cortex of 2-, 7-, and 12-month-old TgNotch3^{R169C} mice, respectively. **(J)** Quantification of extravascular fibrinogen in TgNotch3^{R169C} and wild-type mice at the indicated ages. Scale in **(A-D)** and **(F-I)** = 50µm. The data in **(E)** and **(J)** are presented as mean ± SEM (n = 6 mice/group). **P≤0.01; ***P≤0.001

fields. These fields were analyzed in three nonadjacent sections (at ~100-µm intervals). Six animals per group were analyzed.

d) Fluorescence intensity analysis of extravascular albumin and fibrinogen deposits

Endogenous mouse albumin and fibrinogen were detected using the fluorescent anti-albumin signal and the fluorescent anti-fibrinogen signal respectively. To quantify extravascular albumin and fibrinogen accumulation, maximum projection *z*-stacks were reconstructed. The albumin and fibrinogen positive signal outside of the blood vessels was subjected to threshold processing after background correction, and the signal was quantified using the Integrated Density analysis tool in ImageJ. In each mouse, four ROIs in the cortex were analyzed by randomly selecting four fields. These fields were analyzed in three nonadjacent sections (at ~100-µm intervals). Six animals per group were analyzed.

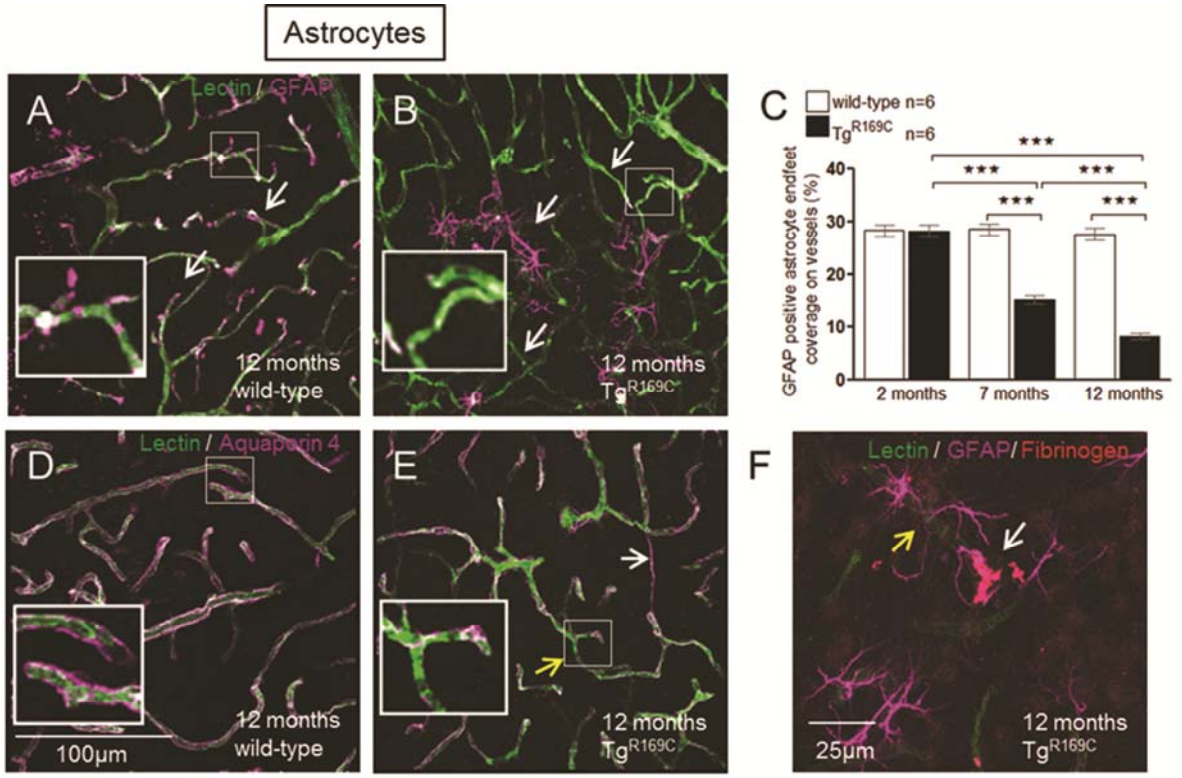

Figure 4. Astrocytic end-foot coverage is reduced and polarization defects appear in the astrocytic end-feet in the cortex of CADASIL mice. **(A)** Representative confocal microscopy image of a 12-month-old wild-type mouse, showing GFAP-positive astrocytic end-feet (magenta) on lectin-positive capillaries (green). *White arrows* indicate the astrocytic end-feet on the vessels.*Inset:* high magnification of the vessel with end feet. **(B)** Confocal microscopy image of a 12-month-old TgNotch3^{R169C} mouse, showing GFAP-positive retracting astrocytes (magenta) on lectin-positive capillaries (green). *White arrows* indicate the retracting astrocytes and vessels without astrocytic end-feet. *Inset:* high magnification of the vessel devoid of end feet. **(C)** Quantification of GFAP-positive astrocytic end-foot coverage in the cortex of TgNotch3^{R169C} and wild-type mice at the indicated ages. **(D)** Representative confocal microscopy image of a 12-month-old wild-type mouse, showing aquaporin-4-positive astrocytic end-feet (magenta) around lectin-positive capillaries (green). *Inset:* high magnification of the vessel with uniform end feet. **(E)** Aquaporin-4 staining of cortical vessels reveals irregular, hazy staining (indicated by *yellow arrow*) and characteristic bridge-like projections (indicated by *white arrow*) to adjacent vessels in the cortex of a TgNotch3^{R169C} mouse. *Inset:* high magnification of the vessel with non uniform end feet. **(F)** Representative confocal microscopy image of a 12-month-old TgNotch3^{R169C} mouse cortex, showing GFAP-positive retracting astrocytes (magenta) (indicated by *yellow arrow*) in the proximity of extravascular fibrinogen extravasation (red) (indicated by *white arrow*) around lectin-positive capillaries (green). *Small boxes*: in **(A,B,D** and **E**) show the part maginified in the respective insets. Scale in **(A-D)** = 100µm and F= 25µm. The data in **(C)** are presented as mean ± SEM (n = 6 mice/group). ***P≤0.001.

Western blot analysis

The cerebral cortex was homogenized and lysed in RIPA buffer containing 50mM Tris (pH 8.0), 150mM NaCl, 0.1% SDS, 1.0% NP-40, 0.5% sodium deoxycholate, and protease inhibitor cocktail (Roche). The lysates were then separated using SDS-PAGE and transferred to a nitrocellulose membrane. The membranes were blocked with 4% powdered milk (w/v). The membranes were then incubated in the primary antibody, followed by the appropriate HRP-conjugated secondary antibody. Bands were detected using the Immobilon Western ECL detection reagent (Millipore), exposed to a Fusion Fx7 imager equipped with 4.2/10 mio pixel CCD camera (Peqlab), and imaged using Fusion software (Peqlab).

The following primary antibodies were used for the western blot analysis: rabbit anti-VE-cadherin antibody (1:1000, Abcam, ab33168) and rabbit anti-connexin43/GJA1 antibody (1:1000, Abcam, ab11370).The mouse anti-β-tubulin antibody (1:1000, Sigma, T8328) was used as a loading control. The following secondary antibodies were used: HRP-conjugated goat anti-rabbit antibody (1:10000, Pierce, 31464) and HRP-conjugated goat anti-mouse (1:10000, Pierce, 31432).

Relative protein abundance: The protein bands were analyzed for densitometry using the Gel Analysis tool in ImageJ. The signal intensity of each protein band was normalized to the respective β-actin band to adjust for any minor differences in total protein loading.

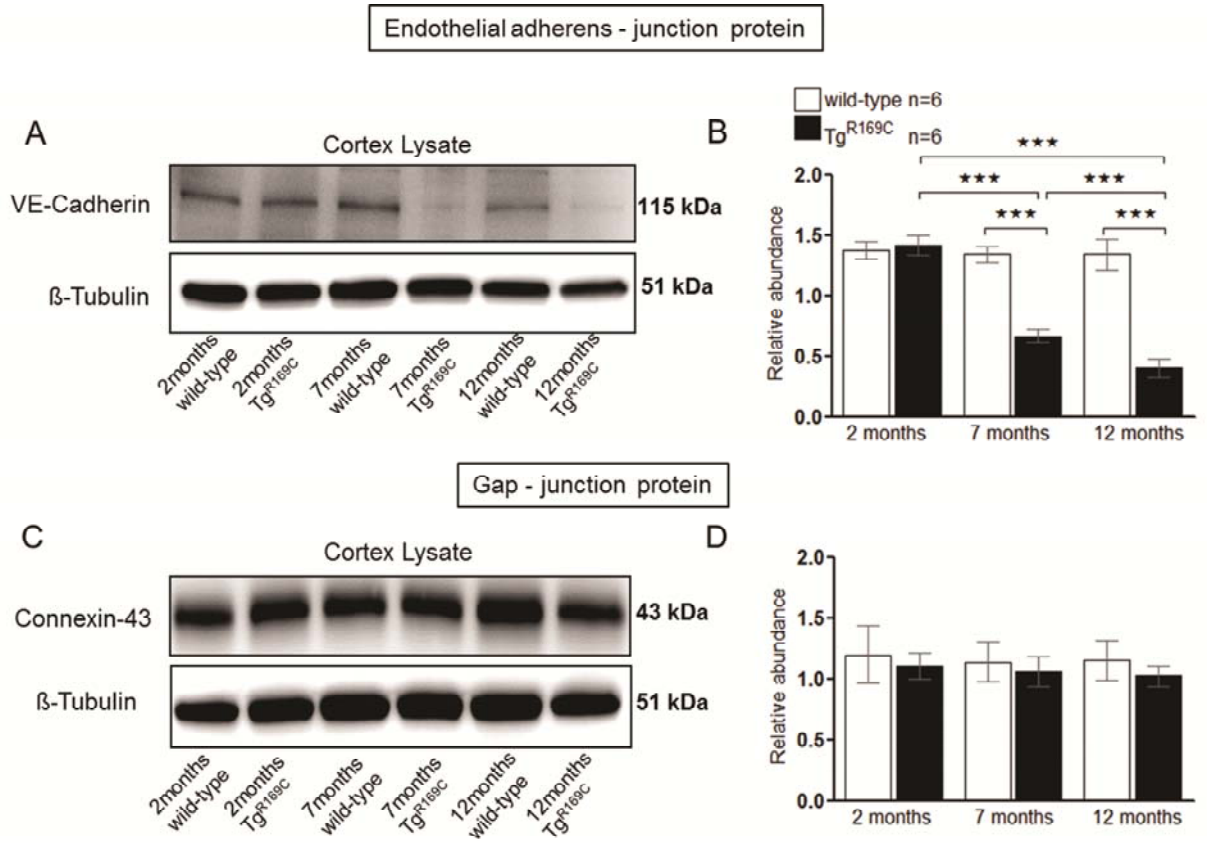

Figure 5. Endothelial adherens-junction protein levels decrease in the cortex of CADASIL mice. **(A)** Western blot analysis of lysates prepared from the cortex of TgNotch3^{R169C} and wild-type mice at the indicated ages. **(B)** Quantification of relative VE-cadherin levels in TgNotch3^{R169C} and wild-type mice at the indicated ages. **(C)** Western blot analysis of lysates prepared from the cortex of TgNotch3^{R169C} and wild-type mice at the indicated ages. **(D)** Quantification of connexin-43 levels in TgNotch3^{R169C} and wild-type mice at the indicated ages. The data in **(B)** and **(D)** are presented as mean ± SEM (n = 6 mice/group). ***P≤0.001.

Statistical analysis

For the *in vivo* study, the data were analyzed using Sigma Plot 12.5 (Systat Software, Erkrath, Germany). The results for the CO_2 reactivity experiments are presented as the mean ± SEM or as the median r the soth/25th percentiles. Differences between groups were analyzed using the Mann-Whitney rank-sum test with Bonferroni correction. Differences with a p-value <0.05 were considered statistically significant.

All other analyses were performed using GraphPad Prism 4 (GraphPad Software Inc., La Jolla, CA). All data were analyzed using the D'Agostino-Pearson omnibus test for normality and were found to be distributed normally. Accordingly, multiple group comparisons were analyzed using a one-way ANOVA followed by a Tukey´s post hoc analysis. Correlation was tested using Pearson´s correlation analysis. Two-group comparisons were analyzed using the Student´s *t*-test. Data are reported as the mean ± SEM. Differences with a p-value <0.05 were considered statistically significant.

RESULTS

Increased Notch3 aggregation in CADASIL mice

To study the location of pericytes within the neurovascular unit, we first examined the intimate relationship between glial-fibrillar acidic protein (GFAP)-positive astrocytes (labeled in red), PDGFRβ-positive pericytes (labeled in blue), and lectin-positive brain endothelial cells (labeled in green) in the mouse cortex (Figure 1A). As shown in the figure *inset*, in wild-type mice, pericyte processes cover most of the abluminal side of the brain capillary endothelial cells, and astrocytic end-foot processes sheath the microvessel wall (composed of endothelial cells and pericytes).

We next investigated the vascular changes in transgenic CADASIL mice (TgNotch3^{R169C}) at 2, 7, and 12 months of age; these changes were compared with age-matched wild-type (non-transgenic) mice. The accumulation of Notch3 protein is a hallmark feature of CADASIL; consistent with this feature, we found an age-dependent increase in the accumulation of mutant Notch3 proteins in the cortical vessels of TgNotch3^{R169C} mice (representative brain sections at 12 months of age are shown in Figure 1B & 1C). Age-dependent quantification of Notch3

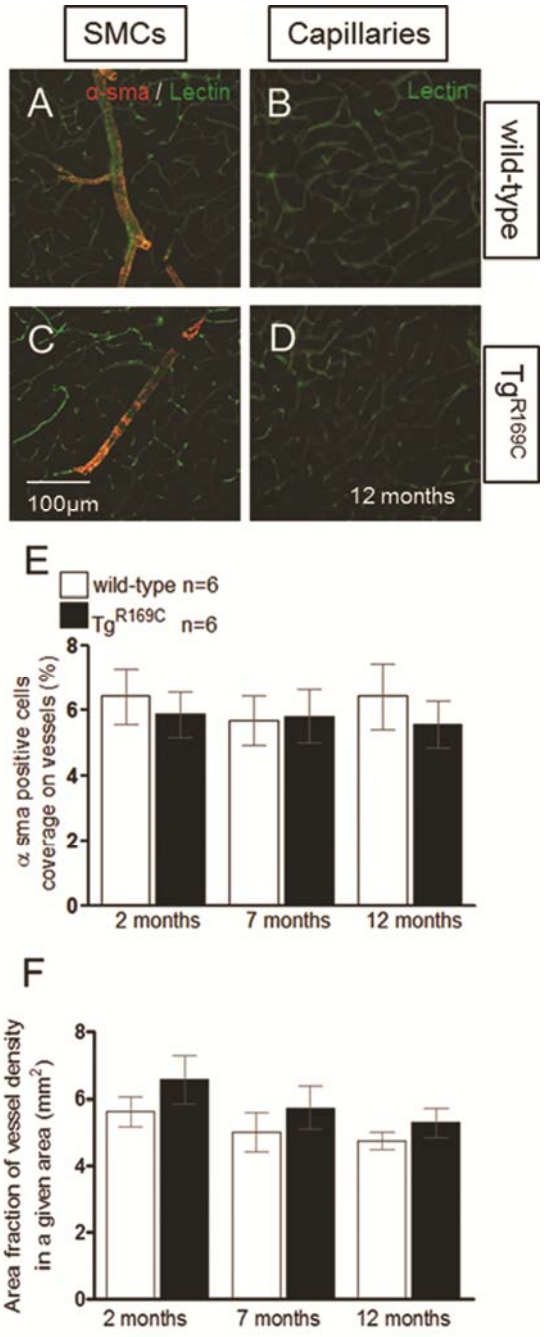

Figure 6. No change in smooth muscle cells coverage and capillary density in CADASIL mice. **(A-B)** SMC coverage in the cortex of 12-month-old TgNotch3^{R169C} and wild-type mice; alpha smooth muscle actin (α-SMA) is shown in red, and lectin-positive capillaries are shown in green. **(C-D)**. Capillary morphology and density was measured in 12-month-old TgNotch3^{R169C} and wild-type mice; lectin-positive capillaries are shown in green. **(E)** Quantification of smooth muscle cell coverage on vessels TgNotch3^{R169C} and wild-type mice at the indicated ages. **(F)** Quantification of capillary density in TgNotch3^{R169C} and wild-type mice in given area of 0.4 mm^2 at the indicated ages. Scale in **A-D** = 100µm. **E-F** are presented as mean ± SEM (n = 6 mice/group).

agregation in TgNotch3^{R169C} mice compared to age-matched wild-type littermates show a 2-fold and 3-fold increase at 7 and 12 months of age, respectively (Figure 1D).

Decreased pericyte coverage and pericyte number in CADASIL mice

As Notch3 is also expressed in pericytes we examined the microvasculature at the capillary level. Using dual immunostaining for PDGFRβ (to label pericytes) and FITC-labeled tomato lectin (to stain endothelial cells), we examined the morphology and profile of pericytes in the TgNotch3^{R169C}and wild-type mice. Consistent with previous reports,[15,22] at 7 months of age wild-type pericytes had typical fusiform and protruding cell bodies with extended, finger-tip like processes on the vessel (Figure 2A). Pericytes were also identified on the basis of their expression of the marker proteins aminopeptidase-N and desmin (data not shown) by immunostaining. We then examined the proximity of the Notch3 deposits to the pericytes by performing triple immunostaining in 12-month-old TgNotch3^{R169C} mice. Our analysis shows that the Notch3 aggregates co-localize with the pericyte's cell body and processes on the capillaries (Figure 2B). We also found an age-dependent progressive loss of pericyte coverage in the capillaries of TgNotch3^{R169C} mice compared with age-matched wild-type littermates (Figure 2C-F). Age-dependent quantification of pericyte coverage in TgNotch3^{R169C} mice compared to age-matched wild-type littermates show a loss of 30% and 50% at 7 and 12 months of age, respectively (Figure 2G). This observation was also reconfirmed by age-dependent quantification of desmin-positive pericyte coverage in TgNotch3^{R169C} mice (data not shown). While counting PDGFRß-positive cell bodies of pericytes, we also found a significant and age-dependent decrease in TgNotch3^{R169C} mice compared with age-matched wild-type littermates in 12 month old mice (around 15%) (Figure 2H). Interestingly, the reduction of pericyte cell numbers was smaller than the overall loss of pericyte coverage of microvessels over time, which may indicate a stronger and early adverse effect of Notch3 aggregation on pericyte processes than on the cell survival itself. In addition, there was a negative correlation between age-dependent loss in pericyte coverage and Notch3 aggregation, indicating that progressive pericyte degeneration is associated with progressive age-dependent Notch3 accumulation (Figure 2I).

Loss of pericytes is associated with BBB dysfunction

The function and integrity of the BBB is regulated by pericytes;[9,13,23] therefore, we examined the impact of pericyte loss on BBB integrity in TgNotch3^{R169C} mice. To test whether the progressive degeneration of pericytes in aged CADASIL mice affects the BBB, we measured the extravasation of albumin and fibrinogen, two plasma proteins that are not present in the brain parenchyma under normal conditions. Immunostaining revealed significant age-dependent extravasation and accumulation of albumin in the cortex of TgNotch3^{R169C} mice compared with wild-type littermates (Figure 3A-D). Age-dependent quantification of extravascular

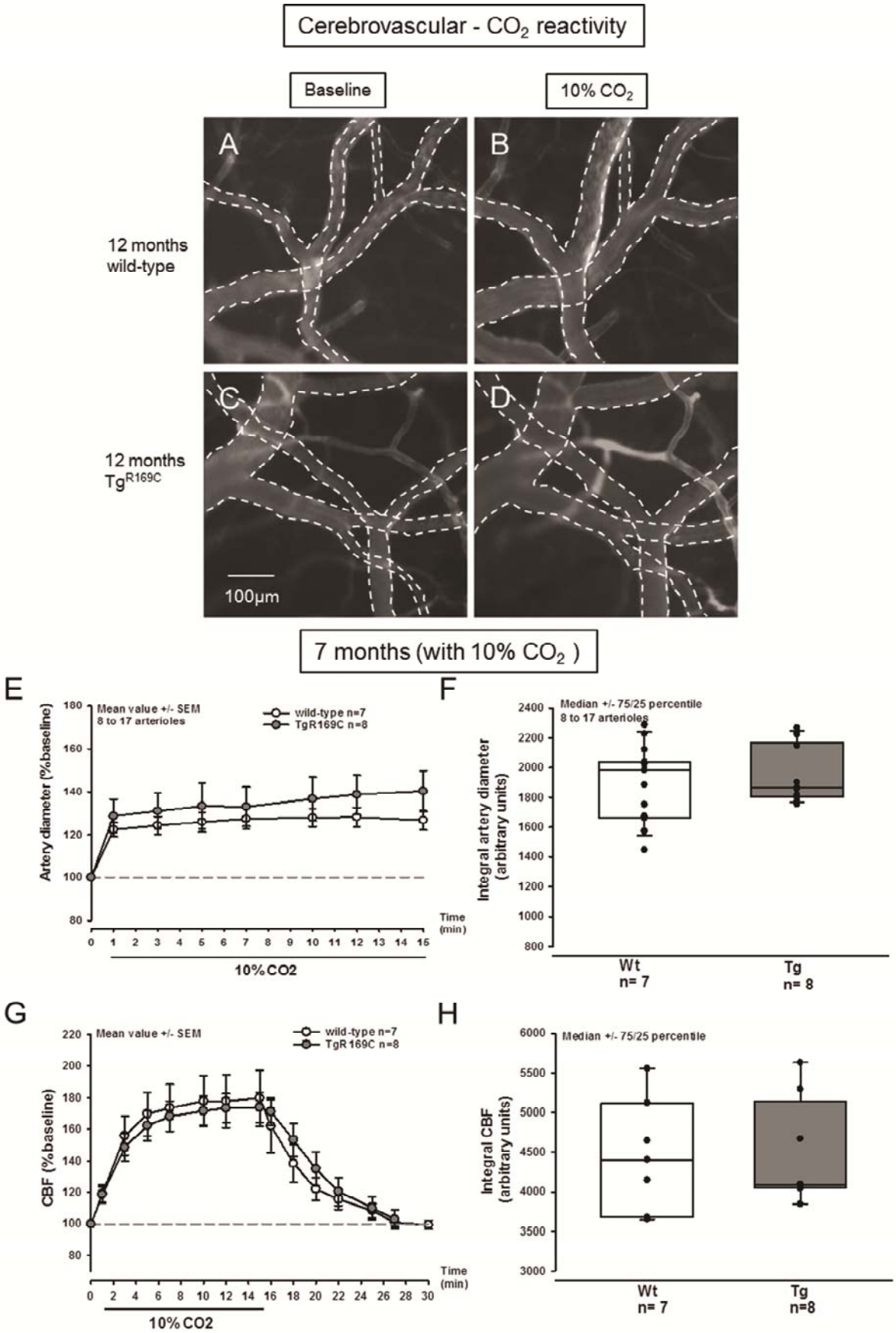
Cerebrovascular - CO_2 reactivity
Baseline
10% CO_2
A
B
C
D
12 months wild-type
12 months Tg^{R169C}
100µm
7 months (with 10% CO_2)
E
Mean value +/- SEM
8 to 17 arterioles
wild-type n=7
TgR169C n=8
Artery diameter (%baseline)
Time (min)
10% CO2
F
Median +/- 75/25 percentile
8 to 17 arterioles
Integral artery diameter (arbitrary units)
Wt n= 7
Tg n= 8
G
Mean value +/- SEM
wild-type n=7
TgR169C n=8
CBF (%baseline)
Time (min)
10% CO2
H
Median +/- 75/25 percentile
Integral CBF (arbitrary units)
Wt n= 7
Tg n=8

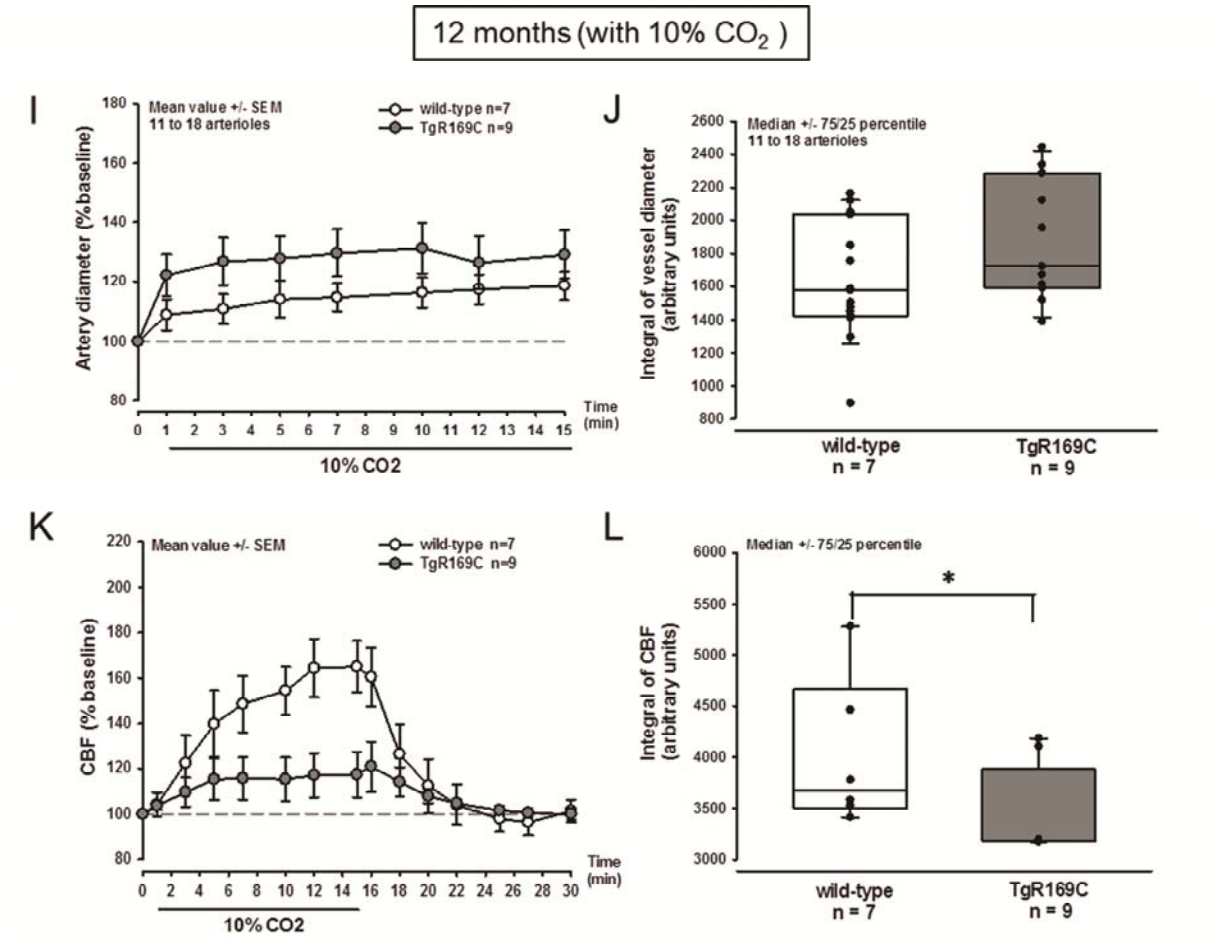

Figure 7. *In vivo* measurement of cerebrovascular reactivity in 7 month and 12-month-old mice. **(A-D)** Vessels were measured in 12-month-old TgNotch3^{R169C} and wild-type mice before (baseline) and during inhalation with 10% CO_2. **(E)** Summary of the time course of arterial diameter (normalized to baseline) in TgNotch3^{R169C} and wild-type during inhalation with 10% CO_2 in 7 month old mice. **(F)** Quantification of pial vessel diameter (measured from 8-17 arterioles/mouse, 7-8 mice/group) in TgNotch3^{R169C} and wild-type mice after inhalation with 10% CO_2 in 7 month old mice. **(G)** Summary of the time course of cerebral blood flow (CBF) in TgNotch3^{R169C} and wild-type mice during and after inhalation with 10% CO_2in 7 month old mice. **(H)** Quantification of CBF in 7-month-old TgNotch3^{R169C} and wild-type mice after inhalation with 10% CO_2. The data in E and G are presented as mean ± SEM; the data in F and H are presented as median ± the 75th and 25th percentiles. **(I)** Summary of the time course of arterial diameter (normalized to baseline) in TgNotch3^{R169C} and wild-type during inhalation with 10% CO_2 in 12 month old mice. **(J)** Quantification of pial vessel diameter (measured from 11-18 arterioles/mouse, 7-9 mice/group) in TgNotch3^{R169C} and wild-type mice after inhalation with 10% CO_2 in 12 month old mice. **(K)** Summary of the time course of cerebral blood flow (CBF) in TgNotch3^{R169C} and wild-type mice during and after inhalation with 10% CO_2 in 12 month old mice. **(L)** Quantification of CBF in 12-month-old TgNotch3^{R169C} and wild-type mice after inhalation with 10% CO_2. The data in **E** and **G** are presented as mean ± SEM; the data in **F** and **H** are presented as median ± the 75th and 25th percentiles. *P≤0.1

albumin deposits in TgNotch3^{R169C} mice compared to age-matched wild-type littermates show approximately a 3-fold and 4-fold increase at 7 and 12 months of age, respectively (Figure 3E). Moreover, we also observed increased levels of extravascular fibrinogen deposits in the cortex of TgNotch3^{R169C} mice compared with wild-type littermates (Figure 3F-I). Age-dependent quantification of extravascular fibrinogen deposits in TgNotch3^{R169C} mice show approximately 2-fold and 3-fold increase at 7 and 12 months of age, respectively (Figure 3J). This increase in albumin and fibrinogen extravasation developed in parallel with the age-dependent loss of pericytes, suggesting that pericyte loss is associated with the breakdown in the BBB in CADASIL mice

Loss of astrocytic end-foot coverage and redistribution of astrocyte polarized markers in CADASIL mice

In addition to pericytes, astrocytes are also an integral component of the neurovascular unit; specifically, astrocytic end-feet are in close contact with the vasculature.[13,24,25] We therefore investigated whether astrocytes are altered in CADASIL mice. GFAP immunostaining in wild-type mice showed a distinct protoplastic population of astrocytes in the cortex, with the astrocytic end-feet in contact with microvessels (Figure 4A). GFAP is expressed in the processes, cell bodies and end-feet of

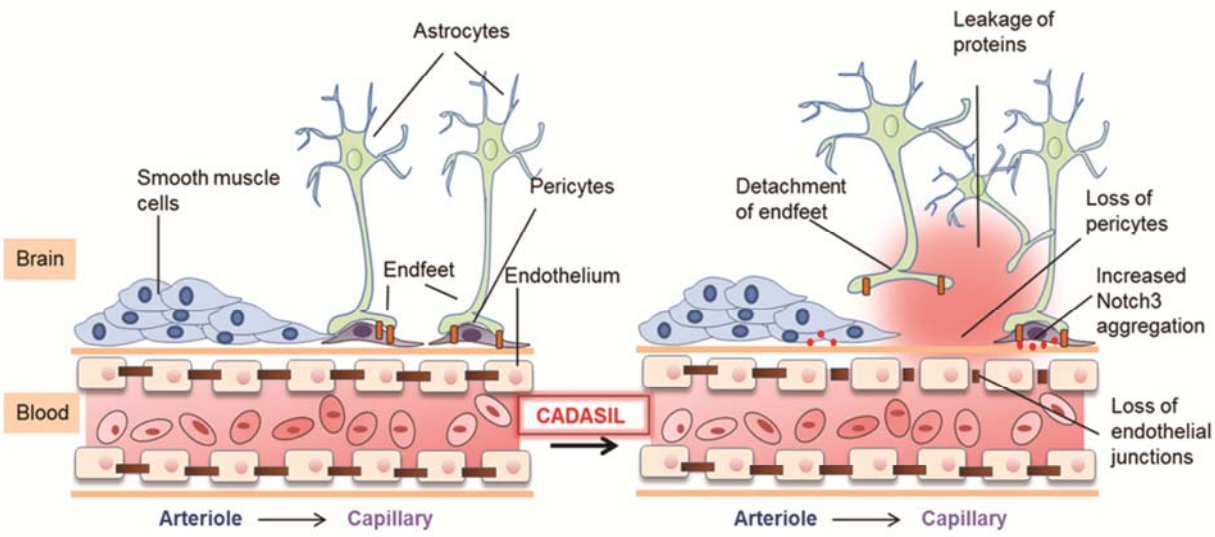

Figure 8. Model of microvascular changes in the cortex of CADASIL mice due to the progressive loss of pericytes and astrocytic end-feet. In the CADASIL mouse model (right), major changes occur in the neurovascular unit. These changes include a significant increase in Notch3 aggregation, significant pericyte loss, reduced pericyte coverage of the vessel, reduced astrocyte polarization, a loss of astrocytic end-foot coverage, a loss of endothelial junction proteins, and leakage of proteins through the BBB. In contrast, gap-junction proteins are not affected.

stellate astrocytes.[26,27] In 12-month-old TgNotch3^{R169C} mice, we found significantly reduced levels of astrocytic end-feet staining around the microvessels; this effect was observed throughout the cortex and was accompanied by a retraction of their end-feet (Figure 4B). Age-dependent quantification of astrocytic end-feet coverage in TgNotch3^{R169C} mice compared to age-matched wild-type littermates show approximately 50% and 70% reduction at 7 and 12 months of age, respectively (Figure 4C).

We also examined the expression of aquaporin-4, a specific marker for polarized astrocytic end-feet. Unlike GFAP, which predominantly stains astrocytic processes, end-feet and cell bodies, aquaporin-4 show uniform labeling of astrocytic end-feet around blood vessels (Figure 4D). Using aquaporin-4 staining, we found that the astrocytic end-feet are organized abnormally in TgNotch3^{R169C} mice. Specifically, aquaporin-4 staining was irregular in 12-month-old TgNotch3^{R169C} mice and we saw presence of the characteristic aquaporin-4-positive bridge-like projections[13] between adjacent lectin-positive vessels (Figure 4E). Using triple immunostaining for fibrinogen (labeled in magenta), GFAP (labeled in red), and lectin (labeled in green), we found that fibrinogen extravasation occurred in close proximity to retracted astrocytic end-feet near the blood vessels, indicating that the BBB is compromised at the site of pathology (Figure 4F).

Decreased endothelial adherens-junction proteins in CADASIL mice

Endothelial adherens junction proteins form a barrier that controls the passage of molecules from the blood to the brain and their expression is markedly reduced when the BBB is compromised.[13,16] We therefore investigated whether expression of the adherens junction protein VE-cadherin is altered in TgNotch3^{R169C} mice. Using western blot analysis, we found a significant progressive decrease in VE-cadherin levels in the cortex of TgNotch3^{R169C} mice compared to age-matched wild-type littermates (Figure 5A & B). We also measured the levels of connexin-43, an astrocytic gap junction protein [28-30], in our CADASIL model; however, we found no change in connexin-43 expression in the cortex of TgNotch3^{R169C} mice (Figure 5C & D).

No change in smooth muscle cells coverage and capillary density in CADASIL mice

CADASIL is also known as a SMC degenerative disease. [3,5] We therefore examined the coverage of SMC on cortical arterioles by performing staining for alpha smooth muscle actin (α-SMA). However, we found no α-SMA-positive cells in the capillaries. Moreover, although CADASIL is generally believed to be primarily a disease of vascular smooth muscle cells, we found no difference in SMC coverage of cortical vessels in TgNotch3^{R169C} mice compared to age-matched wild-type littermates (representative brain sections at 12 months of age are shown in Figure 6A & B). To determine whether the increased Notch3 accumulation in the TgNotch3^{R169C} mice is accompanied by a change in capillary morphology and/or density, we measured the lectin-positive capillary profiles in the TgNotch3^{R169C} and wild-type mice; we found no difference between the mouse lines at any age (representative brain sections at 12 months age are shown in Figure 6C & D). Age-dependent no change in SMCs coverage and capillary density in TgNotch3^{R169C} mice were respectively

seen in Figure 6E & F.

TgNotch3^{WT} transgenic mice were also analyzed for Notch3 aggregation, SMCs coverage, capillary density, pericyte coverage and albumin extravasation. Similar results (data not shown) as wild-type mice were obtained. This showed that overexpression itself did not induce any pathological characteristics.

Morphological changes in the cortex precede functional vascular impairment in CADASIL mice

To examine the consequences of pericyte loss at a functional level, we measured the vascular response to inhaled CO_2 in 7- and 12-month-old TgNotch3^{R169C} mice; inhalation of CO_2 induces vasodilatation via relaxation of the smooth muscle cells by a process that is dependent on the basal activity of nitric oxide synthase and soluble guanylate cyclase. We measured the increase in pial vessel diameter and cerebral blood flow (CBF) in response to inhalation of 10% CO_2. In 7-month-old mice (8 to 17 arterioles per group were analysed) and 12-month-old mice (11 to 18 arterioles per group were analysed), inhalation of 10% CO_2 caused a similar increase in vessel diameter in TgNotch3^{R169C}and wild-type mice (Figure 7A-D) showing viability and vasoreactivity of the vessels. At 7 months of age, 10% CO_2 induced a small increase in vessel diameter (not significant) and also no significant change in CBF in the TgNotch3^{R169C}and wild-type mice (Figure 7E-H); however, at 12 months of age, inhalation of 10% CO_2 caused a similar increase in vessel diameter in TgNotch3^{R169C}and wild-type mice as seen in 7 months aged mice but the TgNotch3^{R169C} mice had a significant increase in CBF in response to 10% CO_2 compared to age-matched wild-type littermates (Figure 7I-L). Hence, at 7 months there was no significant reduction in reactive hyperemia at the time when pericyte pathology was already present and that pericyte, astrocyte, and BBB pathology precedes functional vascular impairment in CADASIL mice.

DISCUSSION

Using a mouse model of CADASIL, we report that mutant Notch3 accumulates in pericytes; moreover, we report that progressive pericyte loss and BBB leakage in the cerebral cortex precede the functional impairments in cerebral vessels. These findings suggest that pericyte dysfunction and loss occur early in the pathogenesis of CADASIL, and pericyte dysfunction causes a disruption of the neurovascular unit and leakage of the blood-brain barrier (Figure 8).

Consistent with previous studies, we found an age-dependent increase in Notch3 aggregation, but no loss of SMCs.[5] The preservation of smooth muscle cell integrity in contrast to the pericyte is one of the most important findings of our study. In addition, we found no reduction in capillary density in TgNotch3^{R169C} mice. However, while investigating PDGFRβ in 12-month-old TgNotch3^{R169C} mice, we observed a significant reduction in the number of cortical pericytes, as well as a decrease in pericyte coverage around the endothelial wall of cortical microvessels, compared with aged-matched wild-type controls. Moreover, the age-dependent decrease in pericytes was proportional to the increase of Notch3 aggregates. These findings re-confirm previous observations by other groups who used electron microscopy to detect ultrastructural changes in pericytes in postmortem tissue samples from CADASIL patients.[17,18] To rule out the possibility that overexpressing mutant Notch3 merely caused a down-regulation of PDGFRβ in well-preserved pericyte processes, we used a second pericyte-specific marker, desmin, confirming that pericyte coverage of the microvasculature decreases with age. In contrast to previous reports using PDGFRβ-knockout mice,[9,13] the age-dependent loss of microvascular pericyte coverage in our CADASIL mouse model was not accompanied by a decrease in capillary density or vascular diameter. This difference in results may be due to the earlier, more severe loss of pericytes in PDGFRβ-knockout mice and may suggest that pericytes play a more important role in vascular formation during embryonic development than in microvascular maintenance in the adult brain.

The reduction in neurovascular pericyte coverage and the loss of pericytes were correlated with the extent of BBB breakdown in the cerebral cortex as measured by the extravasations of two intrinsic plasma-proteins, albumin and fibrinogen. In addition, we observed a decrease in astrocytic end-foot coverage on microvessels; this decrease was confirmed using GFAP staining. Conformational changes in the neurovascular unit were also confirmed by the reorganization of polarized markers of astrocytic end-feet and by presence of the characteristic bridges. We also provide the first evidence that pericytes directly communicate with astrocytes in order to maintain the BBB. We found a significant reduction in the endothelial adherens junction protein VE-cadherin in TgNotch3^{R169C} mice, but we found no reduction in the gap junction protein connexin-43. These results are consistent with reports that BBB breakdown does not involve a reduction in connexins.[31] Other groups reported the reorganization of connexin-43 in astrocytic gap junctions but no change in connexin-43 protein levels in response to injury.[32,33] Therefore, connexin-43 may be reorganized in CADASIL mice, which would correlate nicely with the reorganization of polarized markers of astrocytic end-feet. Using *in vivo* imaging, we also found that cerebral flood flow is not altered in TgNotch3^{R169C} mice at 7 months of age, despite significant changes in microvascular morphology changes at this age. Consistent with previous reports, at 12 months of age, the CO_2-induced response in CBF was significantly reduced in TgNotch3^{R169C} mice.[5] Experiments on somatosensory stimulation show no difference between 7 and 12 month old CADASIL mutant mice and respective controls (unpublished data). Also, our data may suggest a selective dysfunction of pial versus intra-parenchymal arterioles. However, CBF integrates the response of the whole neurovascular tree. Therefore, a normal (or even augmented) response of pial arterioles in CADASIL mutant mice together with a significantly reduced CBF response clearly points towards dysfunction of

parenchymal arterioles and/or capillaries. This interpretation is well in line with our findings that CADASIL mutant mice show reduced pericyte coverage and opening of the BBB in intra-parenchymal arterioles. Taken together, these results confirm that changes in cortical morphology precede functional vascular dysfunction in CADASIL.

Our results provide important clues regarding the mechanisms that underlie the changes in cortical morphology that occur during the progression of CADASIL. Specifically, progressive pericyte loss causes progressive changes in microvascular structure and a disruption in the BBB. BBB damage has been implicated in many neurological disorders, including Alzheimer´s disease, multiple sclerosis, and AIDS dementia complex.[16] Understanding the mechanisms underlying BBB dysfunction in such neurological disorders can reveal therapies designed to reverse and/or reduce neuronal damage that occurs secondary to is accelerated by BBB damage. Here, we show that early changes in cortical morphology are followed by late-onset vascular functional impairment. Several vascular defects have been reported to occur in several types of neurodegenerative disorders; however, whether these defects are the cause or the consequence of the disease remains largely unknown.[23,33] Consistent with a previous report in which pericyte loss mediates BBB disruption and vascular dysfunction precedes neuronal degeneration in Alzheimer's disease,[9] we found that pericyte loss mediates BBB disruption in our CADASIL mouse model, and this effect precedes functional vascular impairment. Another important hallmark of CADASIL are white matter lesions [3,5]. The opening of the BBB and neurovascular dysfunction are features of the disease which precede white matter damage[5] by several months in this model. This also suggest that blood brain barrier permeability could be an important trigger for white matter lesions and progression, as also suggested by others.[34] Taken together, these results provide an important clue suggesting that vascular defects are the cause rather than the consequence of neurodegenerative diseases, including CADASIL. Based on these findings, we conclude that CADASIL is initiated by pericyte dysfunction and disruption of the BBB, which subsequently may lead to neuronal dysfunction, eventually giving rise to dementia and other CADASIL-related symptoms. However, the precise sequence of events is a matter of debate and requires further study. Nevertheless, our results open new avenues for studying other vascular components, including endothelial cells, the basal membrane, and various signaling cascades. Finally, aging has a well-documented effect on the progression of cerebral small-vessel disease;[24,35] consistent with this effect, we found that aging significantly affects both the onset and course of CADASIL in our TgNotch3^{R169C} mouse model. So far CADASIL mutant mice were not evaluated regarding their behavior because they were generated in the genetic FVB/N background and behavior is difficult to assess in these mice due to their well-known hyperactivity and visual impairments.[36]

Therefore, our results suggest that Notch3 accumulation and the subsequent dysfunction of pericytes are early steps in the pathogenesis of CADASIL. Therefore, pericytes may represent a novel therapeutic target in CADASIL. Moreover, this vascular view of CADASIL pathogenesis could have profound implications with respect to our understanding of neurological disorders and other forms of vascular-related dementia.

ACKNOWLEDGEMENTS

This work was supported by the Deutsche Forschungsgemeinschaft (German Research Foundation) within the framework of the Munich Cluster for Systems Neurology (EXC 1010 SyNergy). We thank Dr. Norbert Hübner for kindly providing the R169C transgenic mice. We thank Dr. Anne Joutel for helpful discussions and for kindly providing the Notch3 ECD antibody (5E1).

AUTHORSHIP

M.G. designed the study, performed experiments, analyzed the data, and wrote the manuscript; M.B. performed experiments, analyzed the data, and helped prepare the manuscript; F.H. helped in data analysis and was involved in the preparation of the manuscript; M.D. initiated the study and was involved in the preparation of the manuscript; U.L. designed the study, aided in data analysis and helped prepare the manuscript; N.P. designed the study, aided in data analysis, and wrote the manuscript.

POTENTIAL CONFLICTS OF INTEREST

None to report.

REFERENCES

1. Chabriat H, Bousser MG, Pappata S. Cerebral autosomal dominant arteriopathy with subcortical infarcts and leukoencephalopathy: a positron emission tomography study in two affected family members. Stroke; a journal of cerebral circulation. 1995 Sep;26(9):1729-30.
2. Dichgans M, Mayer M, Uttner I, et al. The phenotypic spectrum of CADASIL: clinical findings in 102 cases. Annals of neurology. 1998 Nov;44(5):731-9.
3. Chabriat H, Joutel A, Dichgans M, Tournier-Lasserve E, Bousser MG. Cadasil. Lancet neurology. 2009 Jul;8(7):643-53.
4. Joutel A, Corpechot C, Ducros A, et al. Notch3 mutations in CADASIL, a hereditary adult-onset condition causing stroke and dementia. Nature. 1996 Oct 24;383(6602):707-10.
5. Joutel A, Monet-Lepretre M, Gosele C, et al. Cerebrovascular dysfunction and microcirculation rarefaction precede white matter lesions in a mouse genetic model of cerebral ischemic small vessel disease. The Journal of clinical investigation. 2010 Feb;120(2):433-45.
6. Viswanathan A, Gray F, Bousser MG, Baudrimont M, Chabriat H. Cortical neuronal apoptosis in CADASIL. Stroke; a journal of cerebral circulation. 2006 Nov;37(11):2690-5.
7. Jouvent E, Mangin JF, Duchesnay E, et al. Longitudinal changes of cortical morphology in CADASIL. Neurobiology of aging. 2012 May;33(5):1002 e29-36.

8. Duering M, Righart R, Csanadi E, et al. Incident subcortical infarcts induce focal thinning in connected cortical regions. Neurology. 2012 Nov 13;79(20):2025-8.
9. Bell RD, Winkler EA, Sagare AP, et al. Pericytes control key neurovascular functions and neuronal phenotype in the adult brain and during brain aging.Neuron.2010 Nov4;68(3):409-27
10. Winkler EA, Bell RD, Zlokovic BV. Central nervous system pericytes in health and disease. Nature neuroscience. 2011 Nov;14(11):1398-405.
11. Sengillo JD, Winkler EA, Walker CT, Sullivan JS, Johnson M, Zlokovic BV. Deficiency in mural vascular cells coincides with blood-brain barrier disruption in Alzheimer's disease. Brain pathology. 2013 May;23(3):303-10.
12. Armulik A, Genove G, Mae M, et al. Pericytes regulate the blood-brain barrier. Nature. 2010 Nov 25;468(7323):557-61.
13. Armulik A, Genove G, Betsholtz C. Pericytes: developmental, physiological, and pathological perspectives, problems, and promises. Developmental cell. 2011 Aug 16;21(2):193-215.
14. Fernandez-Klett F, Offenhauser N, Dirnagl U, Priller J, Lindauer U. Pericytes in capillaries are contractile in vivo, but arterioles mediate functional hyperemia in the mouse brain. Proceedings of the National Academy of Sciences of the United States of America. 2010 Dec 21;107(51):22290-5.
15. Hall CN, Reynell C, Gesslein B, et al. Capillary pericytes regulate cerebral blood flow in health and disease. Nature. 2014;508(7494):55-60.
16. Zlokovic BV. The blood-brain barrier in health and chronic neurodegenerative disorders. Neuron. 2008 Jan 24;57(2):178-201.
17. Dziewulska D, Lewandowska E. Pericytes as a new target for pathological processes in CADASIL. Neuropathology : official journal of the Japanese Society of Neuropathology. 2012 Oct;32(5):515-21.
18. Gu X, Liu XY, Fagan A, Gonzalez-Toledo ME, Zhao LR. Ultrastructural changes in cerebral capillary pericytes in aged Notch3 mutant transgenic mice. Ultrastructural pathology. 2012 Feb;36(1):48-55.
19. Schwarzmaier SM, Kim SW, Trabold R, Plesnila N. Temporal profile of thrombogenesis in the cerebral microcirculation after traumatic brain injury in mice. Journal of neurotrauma. 2010 Jan;27(1):121-30.
20. Thal SC, Plesnila N. Non-invasive intraoperative monitoring of blood pressure and arterial pCO2 during surgical anesthesia in mice. Journal of neuroscience methods. 2007 Jan 30;159(2):261-7.
21. Schwarzmaier SM, Zimmermann R, McGarry NB, Trabold R, Kim SW, Plesnila N. In vivo temporal and spatial profile of leukocyte adhesion and migration after experimental traumatic brain injury in mice. Journal of neuroinflammation. 2013;10:32.
22. Diaz-Flores L, Gutierrez R, Madrid JF, et al. Pericytes. Morphofunction, interactions and pathology in a quiescent and activated mesenchymal cell niche. Histology and histopathology. 2009 Jul;24(7):909-69.
23. Quaegebeur A, Segura I, Carmeliet P. Pericytes: blood-brain barrier safeguards against neurodegeneration? Neuron. 2010 Nov 4;68(3):321-3.
24. Iadecola C. The pathobiology of vascular dementia. Neuron. 2013 Nov 20;80(4):844-66.
25. Abbott NJ, Ronnback L, Hansson E. Astrocyte-endothelial interactions at the blood-brain barrier. Nature reviews Neuroscience. 2006 Jan;7(1):41-53.
26. Ballabh P, Braun A, Nedergaard M. The blood-brain barrier: an overview: structure, regulation, and clinical implications. Neurobiology of disease. 2004 Jun;16(1):1-13.
27. El-Khoury N, Braun A, Hu F, et al. Astrocyte end-feet in germinal matrix, cerebral cortex, and white matter in developing infants. Pediatric research.2006 May;59(5):673-9.
28. Sohl G, Maxeiner S, Willecke K. Expression and functions of neuronal gap junctions. Nature reviews Neuroscience. 2005 Mar;6(3):191-200.
29. Yamamoto T, Ochalski A, Hertzberg EL, Nagy JI. LM and EM immunolocalization of the gap junctional protein connexin 43 in rat brain. Brain research. 1990 Feb 5;508(2):313-9.
30. Oguro K, Jover T, Tanaka H, et al. Global ischemia-induced increases in the gap junctional proteins connexin 32 (Cx32) and Cx36 in hippocampus and enhanced vulnerability of Cx32 knock-out mice. The Journal of neuroscience: the official journal of the Society for Neuroscience. 2001 Oct 1;21(19):7534-42.
31. Hossain MZ, Peeling J, Sutherland GR, Hertzberg EL, Nagy JI. Ischemia-induced cellular redistribution of the astrocytic gap junctional protein connexin43 in rat brain. Brain research. 1994 Aug 1;652(2):311-22
32. Alonso A, Reinz E, Jenne JW, et al. Reorganization of gap junctions after focused ultrasound blood-brain barrier opening in the rat brain. Journal of cerebral blood flow and metabolism: official journal of the International Society of Cerebral Blood Flow and Metabolism. 2010 Jul;30(7):1394-402
33. Quaegebeur A, Carmeliet P. Oxygen sensing: a common crossroad in cancer and neurodegeneration. Current topics in microbiology and immunology. 2010;345:71-103
34. Wardlaw JM, Smith C, Dichgans M. Mechanisms of sporadic cerebral small vessel disease: insights from neuroimaging. Lancet neurology. 2013 May;12(5):483-97.
35. Tucsek Z, Toth P, Tarantini S, et al. Aging Exacerbates Obesity-induced Cerebromicrovascular Rarefaction, Neurovascular Uncoupling, and Cognitive Decline in Mice. The journals of gerontology Series A, Biological sciences and medical sciences. 2014 Jun 3.
36. Cognat E, Cleophax S, Domenga-Denier V, Joutel A. Early white matter changes in CADASIL: evidence of segmental intramyelinic oedema in a pre-clinical mouse model. Acta neuropathologica communications. 2014;2:49.

5 Characterization of cerebrovascular function in a mouse model of small vessel disease – CARASIL

5.1 Summary

CARASIL is a rare form of familial small vessel disease and the recessive counterpart to CADASIL, yet this is the first study characterizing the vascular function in this genetically determined small vessel disease animal model. Endothelium-dependent response to CO_2 inhalation resulted in an increased dilation in parenchymal vessels of 24-month-old CARASIL mice compared to healthy, age-matched controls, with no difference in response visible in pial vessels. Forepaw stimulation using repetitive stimuli (16s on, 40s off) resulted in impaired neurovascular coupling in terms of parenchymal vessel dilation but not regional CBF (rCBF) response. Continuous forepaw stimulation for 1 minute proofed enough to expose neurovascular impairment in the rCBF response. These mutation-related disruptions in neurovascular coupling may be the result of impaired TGF-β signaling in fibroblasts, lower levels of CTGF or of the contractile protein alphaSMA, all consequences of the HtrA1 deficiency characteristic of the CARASIL mutation. These results reveal a need to analyze contractile elements of parenchymal and pial vessels to probe for histological basis for impairments in neurovascular function.

Characterization of cerebrovascular function in a mouse model of small vessel disease – CARASIL

Matilde Balbi[1,2], Martin Dichgans[1,2,3] and Nikolaus Plesnila[1,2,3]

[1]Institute for Stroke and Dementia Research (ISD), University of Munich Medical Center & [2]Graduate School of Systemic Neurosciences (GSN), Ludwig-Maximilians University (LMU), Munich, Germany and [3]Munich Cluster for Systems Neurology, Munich, Germany. Correspondence: Professor, Dr Nikolaus Plesnila, Institute for Stroke and Dementia Research (ISD), University of Munich Medical Center, Feodor-Lynen Straße 17, Munich 81377, Germany. E-mail: nikolaus.plesnila@med.uni-muenchen.de

CARASIL is a rare form of inherited cerebral small vessel disease. Disturbances in neurovascular reactivity have been observed in one other model of small vessel disease and as a result of healthy aging, which may compromise the metabolic status of neurons and result in brain damage. This study aims to characterize the functional vascular reactivity in small vessel disease in order to clarify the pathophysiology and progression over time of the condition and may lead to identifying targets for potential therapeutic strategies. Neurovascular function was found impaired in terms of parenchymal vessel dilation in response to CO_2 inhalation. Parenchymal vessel dilation as well as CBF response were impaired in neurovascular coupling. The findings of the current study suggest for the first time that the HtrA1 loss of function leads to alterations in cerebral vessels.

Key words: CARASIL, neurovascular coupling, CO2, parenchymal vessels, in vivo

INTRODUCTION

Cerebral autosomal-recessive arteriopathy with subcortical infarcts and leukoencephalopathy (CARASIL) is a rare form of inherited cerebral small vessel disease—only 12 families identified—[1, 2] caused by a loss-of-function mutation in the high temperature requirement serine peptidase A1 gene (HTRA1). Patients with CARASIL suffer from early adult–onset dementia, gait disturbance, alopecia, and low back pain.[2] The diagnosis is confirmed if diffuse symmetrical white matter lesions are noticed on neuroradiological examination together with respective mutations in the HTRA1 gene. Studies have shown that loss of HtrA1 activity leads to an increase in transforming growth factor ß (TGF-ß) signaling.[3] TGF-ß is a cytokine that promotes cell differentiation and has an important role in angiogenesis and vascular homeostasis.[4, 5] The increased TGF-ß signaling consequent to loss of HtrA1 function leads to accumulation of the extra domain A of fibronectin and versican in the intima of cerebral small arteries, potentially leading to structural and/or functional vessel damage.[1]

Disturbances in neurovascular reactivity have been observed in one other model of small vessel disease and as a result of healthy aging, which may compromise the metabolic status of neurons and result in brain damage.[6] In order to determine whether mutations in the HTRA1 gene associated with CARASIL affect neurovascular reactivity, we used HtrA1 deficient mice and investigated neurovascular function assessing endothelium-dependent response to hypercapnia and neuronal-activity-driven response to somatosensory stimulation. These responses ensure a balance of supply and demand of metabolic substrates, critical for neuronal activity and survival. An increase in CO2 concentration in the blood triggers an endothelium-dependent dilation of blood vessels. This results in an increase cerebral blood flow (CBF), thus restoring required levels of oxygen supply. Neuronal activity elicits similar vessel dilation in order to replenish energy substrates metabolized during neuronal firing.[7] This "neurovascular coupling" (NVC) occurs through complex interactions between neurons, astrocytes, and cerebral vessels that are not yet fully understood.[8, 9]

The characterization of functional vascular reactivity in small vessel disease is necessary to clarify the pathophysiology and progression over time of the condition and may lead to identifying targets for potential therapeutic strategies.

MATERIALS AND METHODS

Subjects

Animal breeding, housing and all experimental procedures were conducted according to institutional guidelines of the University of Munich and were approved by the Ethical Review Board of the Government of Upper Bavaria. In vivo experiments were conducted on 24 month-old male and female C57BL/6 mice bread at the Center for Neuropathology, University of Munich (Munich, Germany) and are reported according to the ARRIVE criteria. The following lines of mice used for this study: wild-type; homozygous HTRA1 $^{-/-}$ mice (strain HTRA1^{tm1Ybf}) generated by Yingbin Fu. [10]

Anesthesia and physiological monitoring

The mice had free access to food and water before surgery. The surgical procedure was performed as previously described.[6] Shortly mice were initially anesthetized with 2% isoflurane in 70% N2O and 30% O2. Later on isoflurane was gradually reduced, and a continuous intra-arterial infusion of ketamine (30 mg/Kg/h,

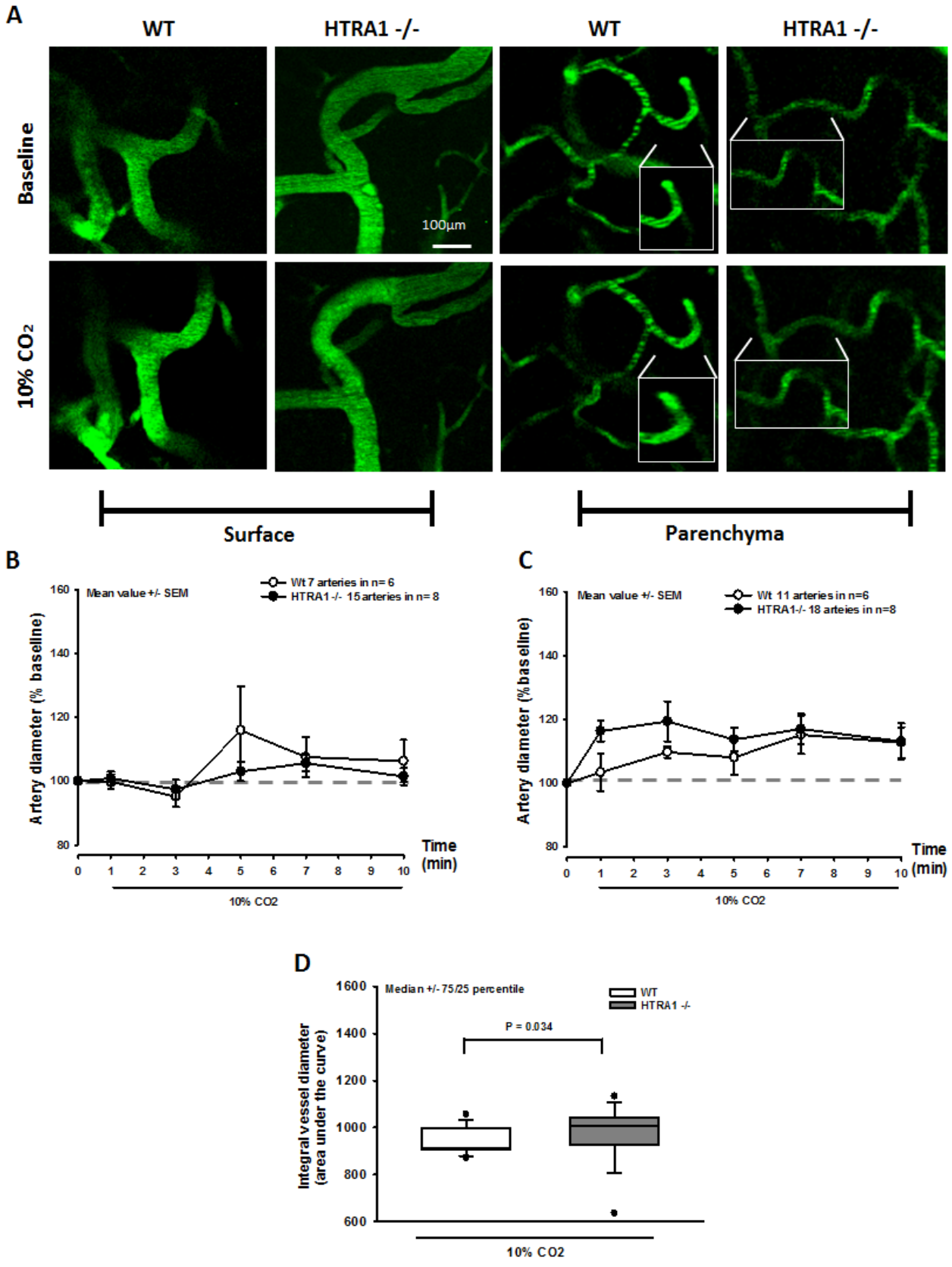

Figure 1. Pial and parenchymal arteries in response to hypercapnia in CARASIL mice. **(A)** Representative two-photon microscopy images of pial (left) and parenchymal arteries (right) of 2 year-old WT and CARASIL mice before and during 10% CO_2 inhalation. **(B)** Surface and **(C)** parenchymal artery diameter during hypercapnia of WT mice (white symbols) or CARASIL (gray symbols) and **(D)** quantification. Mean +/- SEM; Mann-Whitney Rank Sum test; 7 to 15 arteries **(B)** and 11 to 18 arteries **(C)** in n=6-8 mice per group.

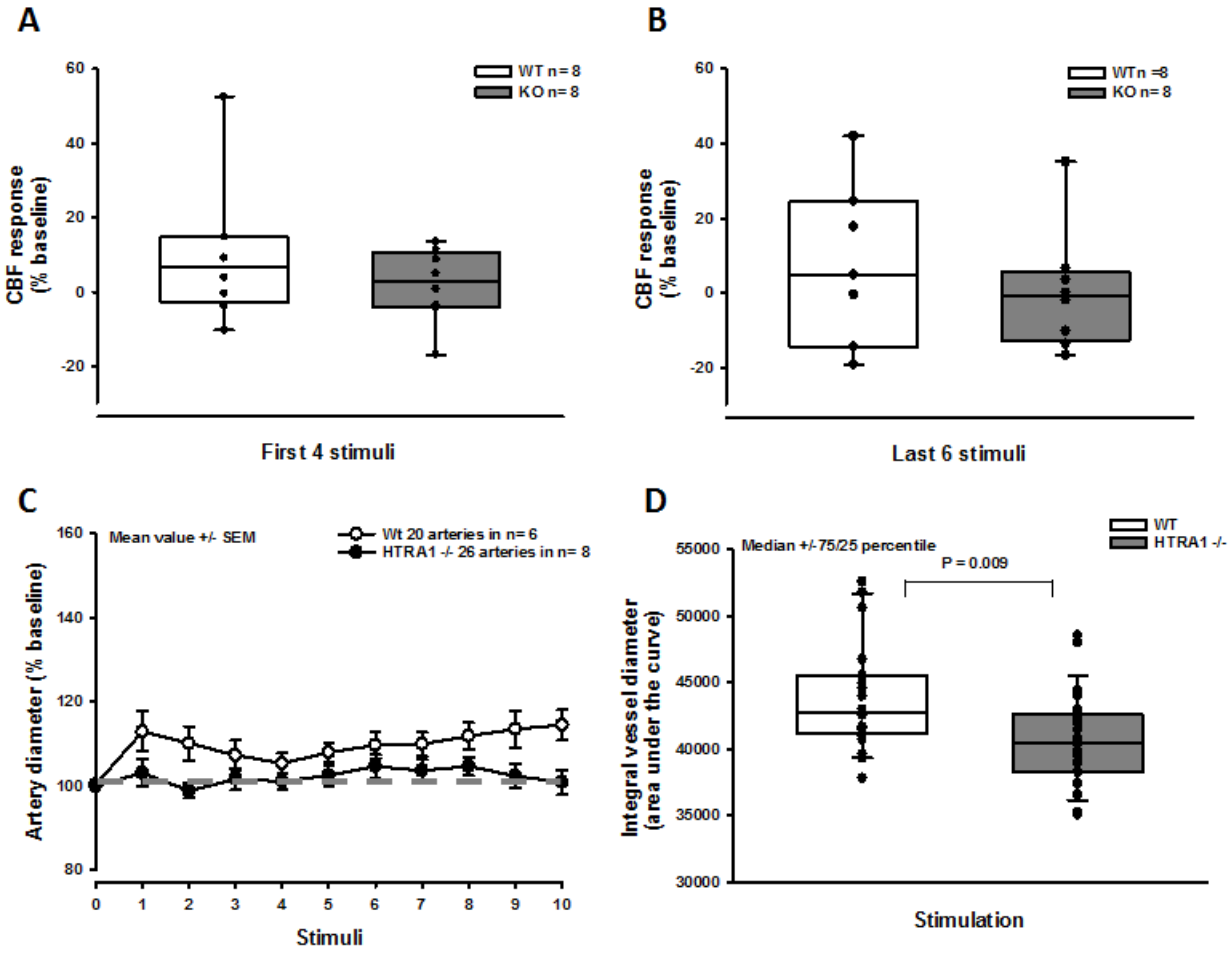

Figure 2. Neurovascular coupling in CARASIL mice. **(A-B)** Box plots showing CBF increase in response to the first four **(A)** and last six **(B)** discrete electrical stimuli to the forepaw, in WTC mice (white symbols) and CARASIL (gray symbols). No significant effect was found between the experimental groups. Median +/- 75/25, n=8 each. **(C)** Artery dilation and **(D)** integral vessel diameter in response to a discrete electrical stimulation show difference between experimental groups. Mean +/- SEM; 20 to 26 arteries from n=6-8 mice.

Inresa,Freiburg,Germany) was administrated. Mice were orotrachealy intubated and mechanically ventilated (Minivent, Hugo Sachs, Hugstetten, Germany). End-tidal pCO2 was measured with a microcapnometer (Capnograph, Hugo Sachs, Hugstetten, Germany) and kept constant between 30 and 40 mmHg by respective adjustments to the ventilation.16sah A thermostatically regulated, feedback-controlled heating pad (FHC, Bowdoin, ME, USA) was used to maintain body temperature at 37°C. The left femoral artery was cannulated for continuous blood pressure monitoring and for infusion of 240 µl/h physiological saline solution to prevent dehydration of the mice. Regional cerebral blood flow (rCBF) was measured with a laser Doppler probe placed over the right somatosensory cortex area.

Two-photon microscopy

A cranial window (2 x 1 mm) was drilled under constant cooling above the area of the somatosensory cortex associated to the fore paw leaving the dura mater intact as previously described.[6] Mice were placed under a two-photon microscope (Zeiss LSM-7 MP, Oberkochen, Germany) equipped with a Li:Ti laser (Chameleon, Coherent, USA) as described previously,[11] and the exposed dura mater was kept wet with isotonic saline. The fluorescent dye, fluorescein isothiocyanate (FITC-dextran; molecular weight 150 kDa) was introduced into the blood via intra-arterial injection (0.05 ml of a 0.5% solution; Sigma, Deisenhofen, Germany) and both parenchymal (diameter: up to 20 µm; depth: 100 µm) and pial vessels (diameter: 20 to 40 µm) were visualized using a 10x Zeiss EC Plan-NeoFluar objective.

Neurovascular reactivity to CO_2

Diameters of both parenchymal and pial arterioles were examined under physiological conditions in order to obtain baseline values. Thereafter, arteriolar diameter was observed during inhalation of 10% CO_2 for 10 minutes. The amount of inhaled CO_2 was measured by microcapnometry (Hugo-Sachs Elektronik, March-Hugstetten, Germany). Arteriolar diameters were quantified with calibrated image analysis software (Zen, Zeiss, Oberkochen, Germany) and expressed in percentage of baseline as previously described.[6]

Forepaw-evoked neurovascular coupling

Neurovascular coupling was evaluated as previously described.[6, 12] Briefly, The left forepaw was stimulated with two subdermally inserted needle electrodes with a diameter of 0.2 mm

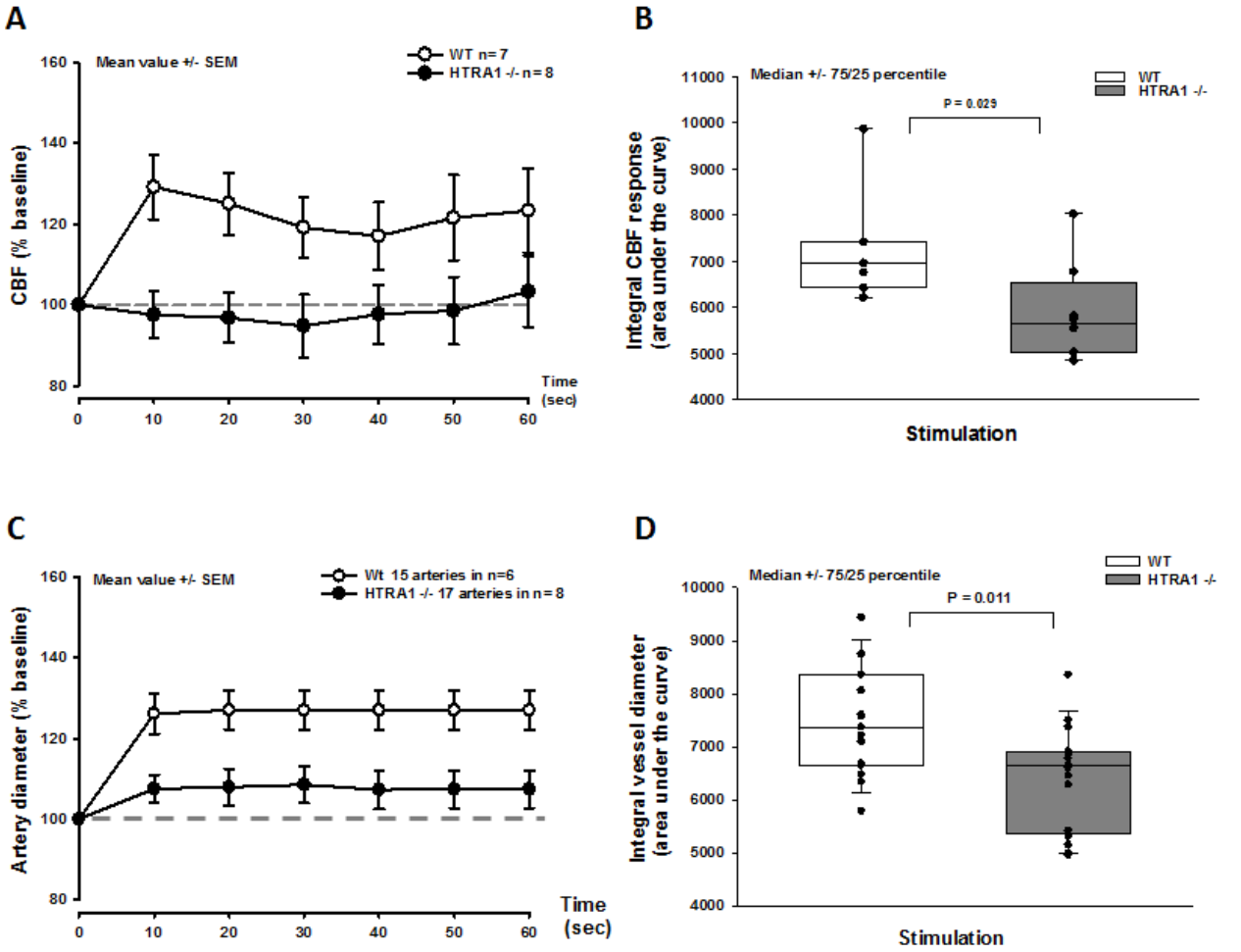

Figure 3. Neurovascular coupling in CARASIL mice **(A)** CBF increase in response to continuous electrical stimulation shows difference between WT mice and mice carrying the CARASIL mutation, as also showed in the quantification **(B)** Mean +/- SEM; Mann-Whitney Rank Sum test n=7 to 8 mice. **(E)** Artery dilation in response to a continuous electrical stimulation shows a significant difference between WT or CARASIL mice. Mean +/- SEM; Mann-Whitney Rank Sum test; 15 to 17 arteries from n=6 to 8 mice.

(Hwato,Suzho,China) at an intensity of 2mA for 0.3 ms (Digitimer Ltd, Hertfordshire, England). One stimulation cycle contained 96 stimulations and lasted 16 seconds (6Hz). The interval between two stimulation cycles was 40 seconds. CBF was assessed over five different locations within the cranial window placed over the somatosensory cortex in order to identify the exact location of the somatosensory cortex representing the left forepaw. The region with the strongest CBF response was then considered for analysis and further for assessment of the microvascular response by intravital microscopy.

Statistical analysis

Statistical analysis was performed with a standard statistical software package (Sigma Plot 12.5; Systat Software, Erkrath, Germany). Results are presented as median ± standard error of the mean (SEM).

Randomization and blinding

All animals were randomly assigned to the procedures; the surgical preparation and data analysis were performed by a researcher blinded towards the treatment of the animals.

RESULTS

In vivo physiological parameters

Body temperature, systemic blood pressure, blood pH, pCO_2 and pO_2 – factors with a strong impact on CBF [13] – were monitored in all investigated mice and did not differ between groups. (**Supplementary table 1)**

Neurovascular response to CO_2 *in vivo*

Inhalation of 10% CO_2 induces a delayed increase in pial artery diameter of WT and HTRA1$^{-/-}$ mice. A weak dilation of 5-10% was observed only 5 minutes after CO_2 administration and without differences between the two groups, indicating an affected reactivity of pial arteries related more to the age of these mice than the mutation itself (**Figure 1B**). On the other hand, parenchymal arteries retained their capacity to promptly dilate in response to CO_2. WT mice showed a maximal increase in artery diameter of 13-14%, which was significantly smaller than the response in arteries of HTRA1$^{-/-}$ mice that reached a maximal dilation of 20%. (**Figure 1C and D**). These results demonstrate

that reaction to CO_2 exposure is dramatically reduced in pial arterioles of all 24 month-old mice. Conversely, parenchymal vessels continue to respond to the stimulus, and mutated mice show a significant increase in vessel diameter compared to the WT group.

Effects of the mutation on neurovascular coupling

Sensory stimulation of the forepaw with ten consecutive stimulation cycles resulted in an increase in CBF in WT and HTRA1$^{-/-}$ mice (**Figure 2A-B**). In response to stimulation, increase in artery diameter of parenchymal vessels reached values of 15% in the WT group, (**Figure 2C, white symbols**) while in the mutated group this response is dramatically abolished (**Figure 2C, black symbols**) as evidenced by the quantification (**Figure 2D**). Continuous sensory stimulation of the forepaw for one minute increased CBF by 27-30% in the WT group, but showed a complete loss of response in HTRA1$^{-/-}$ mice, as illustrated in the quantification (**Figure 3A-B**). The diameter of parenchymal arteries in response to continuous sensory stimulation increased by 25% in WT mice (**Figure 3C, white symbols**) and approximately 7% in mutated mice (**Figure 3C, black symbols**). Box plots quantify the significant decrease in vessel diameter of HTRA1$^{-/-}$ mice. These results point to an impaired neurovascular coupling in mice carrying the CARASIL mutation.

DISCUSSION

Cerebral small vessel disease is a major cause of stroke and dementia. Hereditary forms such as CARASIL are of great interest as models to gain insight into the mechanisms underlying the disease. The findings of the current study suggest for the first time that the HtrA1 loss of function leads to alterations in cerebral vessels.

A significant difference in intraparenchymal artery diameter in response to CO_2 inhalation – a specific cerebral vasodilator – exposes vessel over-reactivity in HtrA1 deficient mice. By contrast, investigation of pial vessels showed only a very small response in all mice and therefore did not show any difference between groups. These results are well in line with our previous studies on aged mice, demonstrating that the dysfunctions induced by aging starts in pial arteries and precipitates down the neurovascular tree.[6] At the same time, neurovascular coupling, which refers to a function essential to proper brain functionality characterized by changes in CBF and vessel diameter in response to neuronal activation, is impaired in HtrA1 deficient mice. The decrease in cerebral blood flow upon neuronal activation limits the delivery of energy substrates and oxygen to activated neurons, inducing metabolic alterations and eventually neuronal damage, as reported in conditions like Alzheimer's disease.[14]

Using trains of repetitive stimuli, we could identify a reduction in artery diameter in CARASIL mice but we couldn't detect alterations in the CBF response. This discontinuous way to elicit neuronal activation, where a 16-second stimulus was followed by a 40-second pause, may not have been sufficient to bring to light any alteration in global, integrated response of the entire neurovascular tree, quantified as the CBF measurment. With continuous stimulation to the forepaw for a period of 1 minute, CBF alterations became evident in the corresponding area of the somatosensory cortex.

The alterations to vascular reactivity found in this study expose a functional consequence of HtrA1 deficiency. HtrA1 has been proposed to release transforming growth factor β (TGF–β), a well-defined regulator of angiogenesis and vascular homeostasis,[4,5] from the extracellular matrix, thus promoting TGF-β activity.[15] Accordigly, TGF-β signaling was strongly impaired in fibroblasts and brain tissue from HtrA1 deficient mice.[15] Furthermore, previous studies have shown a strong reduction in levels of the contractile protein alphaSMA in the cerebral vessels of CARASIL and CADASIL patients.[16] Both of these mechanisms might contribute to structural alterations in blood vessels, and affect neurovascular reactivity. Further research into the TGF-β pathway and status of contractile proteins may elucidate their contribution to small vessel disease.

Taken together, our results demonstrate for the first time that CARASIL mutation leads to an impaired neurovascular coupling accompained by alterations in the CO_2 reactivity.

AUTHOR CONTRIBUTIONS

MB: performed all *in vivo* experiments and wrote the manuscript.
MD: designed the study.
NP: designed the study, wrote and edited the manuscript

DISCLOSURE/CONFLICT OF INTEREST

No competing financial interests exist.

REFERENCES

1. Hara K, Shiga A, Fukutake T, Nozaki H, Miyashita A, Yokoseki A *et al.* Association of HTRA1 mutations and familial ischemic cerebral small-vessel disease. *The New England journal of medicine* 2009; 360(17)**:** 1729-39.
2. Fukutake T, Hirayama K. Familial young-adult-onset arteriosclerotic leukoencephalopathy with alopecia and lumbago without arterial hypertension. *European neurology* 1995; 35(2)**:** 69-79.
3. Oka C, Tsujimoto R, Kajikawa M, Koshiba-Takeuchi K, Ina J, Yano M *et al.* HtrA1 serine protease inhibits signaling mediated by Tgfbeta family proteins. *Development* 2004; 131(5)**:** 1041-53.
4. ten Dijke P, Arthur HM. Extracellular control of TGFbeta signalling in vascular development and disease. *Nature reviews. Molecular cell biology* 2007; 8(11)**:** 857-69.
5. Goumans MJ, Liu Z, ten Dijke P. TGF-beta signaling in vascular biology and dysfunction. *Cell research* 2009; 19(1)**:** 116-27.
6. Balbi M, Ghosh M, Longden TA, Jativa Vega M, Gesierich B, Hellal F *et al.* Dysfunction of mouse cerebral arteries during

early aging. *Journal of cerebral blood flow and metabolism : official journal of the International Society of Cerebral Blood Flow and Metabolism* 2015.

7. Moore CI, Cao R. The hemo-neural hypothesis: on the role of blood flow in information processing. *Journal of neurophysiology* 2008; 99(5)**:** 2035-47.
8. Iadecola C, Nedergaard M. Glial regulation of the cerebral microvasculature.*Nature neuroscience*2007;10(11)**:** 1369-76.
9. Attwell D, Buchan AM, Charpak S, Lauritzen M, Macvicar BA, Newman EA. Glial and neuronal control of brain blood flow. *Nature* 2010; 468(7321)**:** 232-43.

   Iadecola C. The pathobiology of vascular dementia. *Neuron* 2013; 80(4)**:** 844-66.
10. Jones A, Kumar S, Zhang N, Tong Z, Yang JH, Watt C *et al.* Increased expression of multifunctional serine protease, HTRA1, in retinal pigment epithelium induces polypoidal choroidal vasculopathy in mice. *Proceedings of the National Academy of Sciences of the United States of America* 2011; 108(35)**:** 14578-83.
11. Schwarzmaier SM, Zimmermann R, McGarry NB, Trabold R, Kim SW, Plesnila N. In vivo temporal and spatial profile of leukocyte adhesion and migration after experimental traumatic brain injury in mice. *Journal of neuroinflammation* 2013; 10**:** 32.
12. Balbi M; Koide M; Schwarzmaier SM; Wellman GC; Plesnila N. Acute changes in neurovascular reactivity after subarachnoid hemorrhage in vivo. *Journal of Cerebral Blood Flow and Metabolism* 2015; In press.
13. Faraci FM, Heistad DD. Regulation of the cerebral circulation: role of endothelium and potassium channels. *Physiological reviews* 1998; 78(1)**:** 53-97.
14. Niwa K, Araki E, Morham SG, Ross ME, Iadecola C. Cyclooxygenase-2 contributes to functional hyperemia in whisker-barrel cortex. *The Journal of neuroscience : the official journal of the Society for Neuroscience* 2000; 20(2)**:** 763-7
15. Beaufort N, Scharrer E, Kremmer E, Lux V, Ehrmann M, Huber R et al. Cerebral small vessel disease-related protease HtrA1 processes latent TGF-beta binding protein 1 and facilitates TGF-beta signaling. Proceedings of the National Academy of Sciences of the United States of America 2014; 111(46): 16496-501.
16. Oide T, Nakayama H, Yanagawa S, Ito N, Ikeda S, Arima K. Extensive loss of arterial medial smooth muscle cells and mural extracellular matrix in cerebral autosomal recessive arteriopathy with subcortical infarcts and leukoencephalopathy (CARASIL). Neuropathology : official journal of the Japanese Society of Neuropathology 2008; 28(2): 132-42.

SUPPLEMENTARY INFORMATION

Age	Genotype	N	MAP (mmHg)	pCO2 (mmHg)	pO2 (mmHg)	pH
2 years	WT	5	115 +/- 6 (n=6)	45 +/- 3	197 +/- 29	7.0 +/- 0.1
2 years	HTRA1 -/-	7	108 +/- 3	46 +/- 3	198 +/- 27	7.1 +/- 0.1

Mean value +/- SEM

Supplementary table 1. Blood gas analysis data of WT and CARASIL group.

6 Summary and conclusion

This work investigated cerebral vascular function under normal and pathological conditions. Endothelium-dependent response to hypercapnia and neuronal activity-dependent response to electrical stimulation of the forepaw were assessed using one- and two-photon intravital microscopy to gauge vessel dilation and laser Doppler fluxmetry to measure changes in CBF. First, I analyzed the effects of aging on the reactivity of the cerebral vasculature of mice. At 8 months, neurovascular coupling resulted in a blunted age-related response in terms of rCBF and vessel dilation. I was also able to detect an age-related impairment in endothelium-dependent vessel dilation that was not observed in the CBF response. These results point to differential effects of aging in neurovascular function, and breakdown in endothelial function in pial arteries before parenchymal arterioles. Next, I studied the effects of an acute event, namely subarachnoid hemorrhage, on vascular reactivity. While endothelium-dependent responses were completely blunted three hours after SAH was induced, activity-dependent responses remained unaffected in this time frame. This indicates that SAH initiates biochemical pathways that interfere with the endothelial response before they interfere with neurovascular coupling. Next, I used a model of small vessel disease, CADASIL, to study how the progression of the disease affects vessel functionality. At 12 months, hypercapnia resulted in a blunted response in terms of CBF, but an increased dilatory response in pial arteries. No discernible differences were observed in vascular function during neurovascular coupling. Finally, I looked at another model of small vessel disease, CARASIL. In 24-month-old mice, hypercapnia resulted in an increased dilatory response in parenchymal arteries and no discernible difference in pial arteries. Neurovascular coupling elicited blunted responses in terms of both parenchymal dilation and rCBF.

Functional hyperemia or the ability to supply nervous tissue with energy substrates via the blood flow proportional to their energy consumption is a vital function of the brain that has been found to be reduced by approximately 40% already in 12-month-old mice using the whisker stimulation paradigm (Park et al. 2007), suggesting a dysfunction in the neuron-astrocyte-pericyte/smooth muscle cell axis. My study reports impairment in neurovascular coupling starting at 8 months of

age. Under trains of repetitive stimuli, 6-week- and 8-month-old mice showed a normal reaction after the first stimulus in, while in 12-month-old mice presented a reduced CBF response. However, upon repeating the stimulation up to ten times, it became apparent that vessels in 6-week-old mice maintained their CBF response over time while vessels in 8 month and 12-month-old mice could not maintain their initial response level and showed almost no functional hyperemia. Furthermore, 6 of 16 of the old animals (38%) showed reductions in CBF as a result of NVC. Thus, NVC impairment seems to be a much earlier event than previously anticipated, as it occurs at as early as 8 months of age, the first third of a mouse's life. The vascular 'fatigue effect' observed could be explained by a structural damage to the NVU, impaired neuron–astrocyte–vascular signaling, or dysfunction within the vascular wall itself. To assess these hypotheses, capillary density, smooth muscle cell coverage of cerebral arterioles, pericyte and astrocytic end-foot coverage of capillaries and leakage of the BBB were quantified by three-dimensional immunohistochemistry. None of these parameters was altered up to an age of 12 months, suggesting that the structure of arterioles and capillaries plays no role in NVC breakdown. To clarify whether neuron–astrocyte–vascular signaling might be impaired, experiments were performed on isolated brain slices from aged mice. Vessels in control slices from young mice dilated robustly to neuronal activation induced by electrical field stimulation, while vessels in slices from aged mice showed a complete loss of NVC with a tendency toward vasoconstriction, similar to *in vivo* observations at 12 months. However, the increase of astrocytic end-foot Ca^{2+} upon neuronal activation was not significantly distinct across age groups. Accordingly, it may be concluded that aging principally affects the functionality of cerebral vessels without affecting neuronal–astrocytic signaling or the structure of the NVU, as previously suggested by others (Park et al. 2007; Faraci and Heistad 1998). Additionally, my results suggest that the mechanisms involved in NVC affected by aging are found downstream of astrocytic end-foot Ca^{2+} signaling. One such mechanism might be Ca^{2+}-driven release of K^+ from astrocytic end-feet plays a critical role in generating rapid vasodilation of cerebral parenchymal arterioles in response to neural activity (Filosa et al. 2006) through activation of smooth muscle cell potassium K_{ir}, driving membrane potential hyperpolarization and vasodilation (Straub et al. 2007). It has been previously shown that this mechanism is sensitive to

disruption at the level of the SMC K_{ir} channel (Longden et al. 2014). Future studies will need to explore the role of vascular K_{ir} channels in AVD in more detail.

An increase in CO_2 concentration in the blood induces nitric-oxide dependent vasodilation. Aging is associated with a decrease in resting CBF (Faraci and Heistad 1998) and a reduced response to endothelium-dependent vasodilators such as CO_2 (Mayhan et al. 1990). Until now, deficiencies in this pathway have only been detected in mice starting at 12 months of age, but previous studies have only measured CBF, a parameter which integrates the response of the whole neuro-vascular tree. Therefore, the response of individual subpopulations of cerebral vessels to hypercapnia remained unclear. Accordingly, my study took a different approach to detecting age related impairments: direct inspection of vessels on the brain surface—pial arteries—using intravital microscopy, and examining the global increase of CBF after inhalation of 5% or 10% CO_2. Visualization of pial vessels allowed me to detect neurovascular dysfunction at the earlier stage of 8 months. No global neurovascular dysfunction—CBF—in mice up to an age of 12 months was observed, consistent with findings by Park et al. (Park et al. 2007). This suggests that AVD starts in pial arteries and continues down the neurovascular tree during aging. This is supported by previous data showing that aging affects the global increase of CBF after inhalation of CO_2 only in mice older than 1.5 years (Park et al. 2007), and showing accelerated aging of pial arteries in a mouse model small-vessel disease (Joutel et al. 2010). Furthermore, since hypercapnia-induced vasodilation is mediated by endothelial NO synthases, the current data also suggest that AVD may be linked with disturbed NO signaling. It has been suggested that the main underlying mechanism is the production of reactive oxygen species (ROS) by NADPH oxidase in the vessel wall, where ROS convert NO to peroxynitrite, thereby reducing the bioavailability of NO and damaging vascular structures. (Park et al. 2007; Girouard et al. 2007) Taken together, results from aged mice show that age impairs neurovascular coupling at an unexpectedly young age in mice. The lack of vascular CO_2 reactivity suggests that defective constitutive NO signaling may represent a possible mechanism. Dysfunctions are not accompanied by any changes on the cellular composition of the NVU or by impaired astrocytic Ca^{2+} reactivity. My investigation identified the onset and location of age-related neurovascular

dysfunctions and suggests putative mechanisms, thereby paving the way for the development of novel strategies to maintain neurovascular function during aging.

The majority of studies investigating pial and parenchymal arterioles used in vitro systems (Kajita et al. 1996; Park et al. 2001; Koide et al. 2013) that require experimental conditions that do not necessarily reflect microvascular function *in vivo*. The few published studies investigating the cerebral microcirculation after SAH *in vivo* used conventional epi-fluorescence microscopy and were only able to explore pial vessels due to the limited penetration depth of this technology (Sun et al. 2009; Ishikawa et al. 2009; Friedrich et al. 2014). These vessels are of particular interest in the context of SAH given that these are the only cerebral microvessels coming into direct contact with extravasated blood after subarachnoid bleeding. Indeed, pial vessels were shown to constrict after SAH in experimental animals models and in SAH patients thereby suggesting that spasms of cerebral microvessels are one of the main reasons for the cerebral ischemia observed after SAH (Uhl et al. 2003; Friedrich et al. 2012). Pial microvessels, however, are morphologically distinct from parenchymal arterioles in that pial vessels have perivascular innervation and lack of astrocytic end-foot coverage (Cipolla 2009). Most importantly, parenchymal, not pial, arterioles are in direct contact with the brain parenchyma and communicate directly with astrocytes and neurons. However, parenchymal arterioles within the brain lie beyond the range of conventional epi-fluorescence microscopy.

Given that in the first five days following subarachnoid hemorrhage patients suffer persistent cerebral ischemia (Sun et al. 2009), this work focused on investigating the state of vascular function at this early stage. Previous data has shown that pial vessel reactivity to hypercapnia is impaired 3 hours after SAH (Friedrich et al. 2012). Mine is the first study investigating neurovascular coupling after SAH in vivo. SAH was induced using the intraluminal perforation model, a well-established model that mimics elevated ICP, cerebral ischemia, hippocampal damage, mortality and cerebral edema, all acute and long term processes induced by the rupture of an intracranial aneurysm (Feiler et al. 2010). SAH induction was verified in each animal by an increase in intracranial pressure following the post-hemorrhagic event. Considering the importance of this regulation for brain functionality, the attention brought on the topic by *ex vivo* studies reporting that, paradoxically, neuronal activity may lead to parenchymal arteriolar constriction

(Koide et al. 2014) and the shift in neurovascular coupling from vasodilation to vasoconstriction at 24 to 96 hours after SAH (Koide et al. 2014), I investigated *in vivo* early effects of SAH on neurovascular coupling. Neither repeated nor continuous sensory stimulation to the forepaw shows any impairment of the neurovascular coupling three hours after SAH induction; both sham-operated and SAH mice have a comparable increase in rCBF response as well as an increase in artery diameter. These data were also confirmed in *ex vivo* brain slices investigated four hours after SAH. In these experiments, electrical field stimulation evoked local neuronal activation which in turn induced a rise in astrocytic end-foot Ca^{2+} followed by vasodilation of the adjoining parenchymal arteriole in both sham-operated and SAH mice four hours after the hemorrhagic event. 24 to 96 hours after SAH the already increased basal perivascular potassium reaches excessive levels above 20 mM which causes smooth muscle depolarization and parenchymal arteriolar constriction in rat cortical brain slices (Koide et al. 2014). This inverted neurovascular coupling leads to a pathological hypoperfusion of the brain tissue after SAH which results in glucose and oxygen deprivation. The mechanisms underlying SAH-induced inversion of NVC are not fully understood, but are likely to involve an increase in the magnitude of spontaneous Ca^{2+} release events in astrocytic end-feet leading to elevation of K^+ in the restricted perivascular space around parenchymal arterioles (Koide et al. 2012). Seen that neurovascular coupling functionality does not show any sign of impairment during the first few hours point to a potential time window for viable intervention.

Results from these experiments show a complete loss of reactivity to CO_2 in pial arteries three hours after SAH. These data corroborated previous findings where cerebral arterioles covered in blood and affected by post-hemorrhagic microvasospasms lacked CO_2 reactivity (Friedrich et al. 2011). This loss in reactivity indicates an inability of the brain to increase blood flow in response to a stimulus, suggesting a severe inability of cerebral autoregulation to maintain adequate and stable cerebral blood flow after SAH. Given this lack of CO_2 reactivity in pial arteries and the fact that cerebral vessel reactivity had only been investigated in pial vessels, we decided to investigate deep parenchymal vessels using *in vivo* two-photon microscopy. The results show that not only microvessels located in the subarachnoid space and coming in direct contact with blood, but also arterioles in the parenchyma,

where blood is not present, lose their ability to dilate in the face of increased levels of CO_2. Thus the brain as a whole seems to lose its ability to regulate blood flow in response to metabolic stress and may thus become increasingly vulnerable to additional damage. Thus, the NOS signaling pathway may be a mechanism involved and therefore a novel target for potential therapeutic strategies after SAH. The differences in impairment of the endothelium-dependent and neural activity-dependent responses three hours after SAH induction suggest that CO_2 reactivity and NVC are at least partly mediated by different signaling pathways (Figure 3) and that these pathways are differentially affected by SAH. Further research is needed to decipher these pathways and pave the way for novel therapeutic strategies for SAH patients with both early and delayed cerebral ischemia.

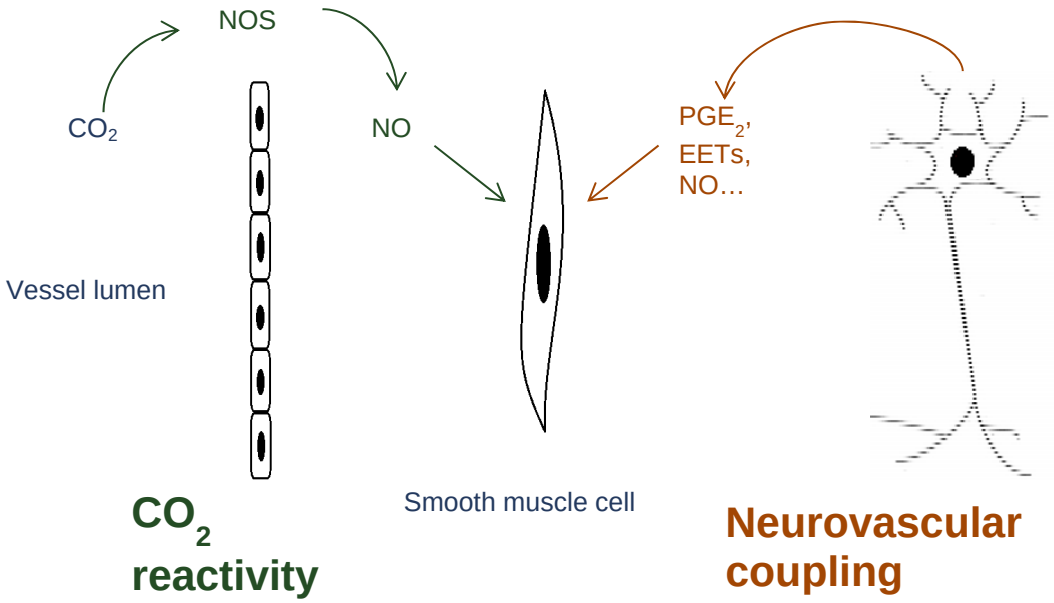

Figure 3. Vasoregulatory pathways. Endothelium dependent vasodilation in response to hypercapnia and neural-activity-dependent vasodilation are mediated by separate biochemical pathways and differentially affected by aging and SAH.

My investigation on CADASIL provides significant evidence implicating brain capillaries early on in the pathophysiology of CADASIL and possibly other small vessel disorders in the brain. We report that mutant Notch3 accumulates in pericytes; moreover, we report that progressive pericyte loss and BBB leakage in the cerebral cortex precede the functional impairments in cerebral vessels. These

findings suggest that pericyte dysfunction and loss occur early in the pathogenesis of CADASIL, and pericyte dysfunction causes a disruption of the neurovascular unit and leakage of the blood-brain barrier. The current study demonstrates that mutated Notch3 accumulates in pericytes and that evolving pericyte loss and BBB leakage in the cerebral cortex precede functional impairments of cerebral vessels in a mouse model of inherited small vessel disease. The study found age-dependent increase in Notch3 aggregation, but no SMCs degeneration, consistent with previous studies (Joutel et al. 2010). The preservation of smooth muscle cell integrity at this stage in contrast to pericyte integrity is one of the most important findings of our study. Additionally, no reduction in capillary density was observed in mice carrying the mutation. However, while investigating beta-type platelet-derived growth factor receptor (PDGF-Rβ), a pericyte marker, in 12-month-old CADASIL specimens, we observed a significant reduction in the number of cortical pericytes as well as pericyte coverage around the endothelial wall of cortical micro vessels in 12-month-old CADASIL mice compared to age-matched controls. Moreover, age-dependent reduction in pericyte population was inversely proportional to Notch3 aggregation. These findings corroborate previous observations using electron microscopy to detect structural abnormalities of pericytes in human postmortem CADASIL tissue samples (Dziewulska et al. 2012; Gu et al. 2012). In contrast to previous reports from PDGF-Rβ-knockout mice (Bell et al. 2010; Armuilik et al. 2010), age dependent loss of microvascular pericyte coverage in our CADASIL mouse model does not go along with a reduction in capillary density or vascular diameter. This difference in results may be due to the earlier, more severe loss of pericytes in PDGF-Rβ-knockout mice and may suggest that pericytes play a more important role in vascular formation during embryonic development than in the maintenance of microvessels in the adult brain. Reduced neurovascular pericyte coverage and loss of pericytes strongly correlated with extent of BBB breakdown in the cortex in terms of extravasation of two intrinsic plasma-proteins, albumin and fibrinogen. In addition, we observed a decrease in astrocytic end-foot coverage on microvessels; this decrease was confirmed using GFAP staining. Conformational changes in the neurovascular unit were also confirmed by the reorganization of polarized markers of astrocytic end-feet and by presence of the characteristic bridges. We also provide the first evidence that pericytes directly communicate with astrocytes in order to maintain the BBB. We

found a significant reduction in the endothelial adherens junction protein VE-cadherin in CADASIL mice, but we found no reduction in the gap junction protein connexin-43. These results are consistent with reports that BBB breakdown does not involve a reduction in connexins (Hossain et al. 1994). Other groups reported the reorganization of connexin-43 in astrocytic gap junctions but no change in connexin-43 protein levels in response to injury (Alonso et al. 2010; Quaegebeur et al. 2010). Therefore, connexin-43 may be reorganized in CADASIL mice, which would correlate nicely with the reorganization of polarized markers of astrocytic end-feet.

The finding of structural alterations to the microvasculature prompted the investigation of functional implications of these mutation-related deficiencies using *in vivo* imaging. No impairment to rCBF regulation was found in 7 months old aged CADASIL mice despite significant changes to the microvascular morphology and pericyte loss at this age. However, it was found that at 12 months, hypercapnia results in a significantly lower increase in rCBF as a result of the mutation, consistent with previous studies (Joutel et al. 2010). On the other hand, direct visualization of pial arteries found significantly stronger vasodilation in response to hypercapnia in CADASIL mice. Given that a decreased rCBF response points to a weaker perfusion across the entire neurovascular tree, resulting in a decrease in overall vessel diameter, and that pial arteries show an increase in vessel diameter, we may infer that parenchymal vessels decrease in vessel diameter in response to hypercapnia. This may be verified via two-photon microscopy analysis of parenchymal vessels. This interpretation is well in line with our findings that CADASIL mutant mice show reduced pericyte coverage and opening of the BBB in intra-parenchymal arterioles. Experiments on somatosensory stimulation show no difference between 7 and 12 month old CADASIL mice and respective controls (unpublished data). Taken together, these results confirm that early changes in cortical morphology are followed by late-onset vascular functional impairment. Our results provide important clues regarding the mechanisms that underlie the changes in cortical morphology that occur during the progression of CADASIL. Specifically, progressive pericyte loss causes progressive changes in microvascular structure and a disruption in the BBB. This is consistent with a previous report in which pericyte loss mediates BBB disruption and vascular dysfunction precedes neuronal degeneration in Alzheimer's disease (Bell et al. 2013). Understanding the mechanisms underlying BBB

dysfunction in such neurological disorders can reveal therapies designed to reverse and/or reduce neuronal damage accelerated by BBB damage. Based on these findings, we conclude that CADASIL is initiated by pericyte dysfunction and disruption of the BBB, which subsequently may lead to neuronal dysfunction, eventually giving rise to dementia and other CADASIL-related symptoms. However, the precise sequence of events is a matter of debate and requires further study. Finally, aging has a well-documented effect on the progression of cerebral small-vessel disease. (Iadecola et al. 2013; Tucsek et al. 2014) Accordingly, we found that aging significantly affects both the onset and course of CADASIL in our mouse model. These results provide novel insight into the pathobiology of cerebral small vessels in CADASIL, which are expected to also relate to other types of cerebral small vessel disease.

To date, there are no studies characterizing the vascular function in the mouse model of CARASIL, a recessively inherited small vessel disease characterized by mutations in the HTRA1 gene. The findings of my investigation suggest that the functionality of cerebral vessels is altered by the HTRA1 mutation. Similar to what was found in the CADASIL model, CO_2 stimulation resulted in an overreaction in terms of artery dilation. While in the dominant form of the disease pial artery response resulted in over-dilation, in the recessive form only parenchymal arteries responded with over-dilation. However, it is crucial to note for comparative analysis that observations in mice carrying the CARASIL mutation were performed at 24 months of age, and at 12 months of age in mice carrying the CADASIL mutation. It is also important to keep in mind that previous findings demonstrate that age-related dysfunctions start in pial arteries and precipitates down the neurovascular tree. Additionally, neurovascular coupling was found to be impaired in HTRA1$^{-/-}$ mice. This decrease in cerebral blood flow upon neuronal activation limits the delivery of energy substrates and oxygen to activated neurons, inducing metabolic alterations and neuronal damage as reported in conditions like Alzheimer's disease (Niwa et al. 2000). Using trains of repetitive stimuli, only a reduction in artery diameter in CARASIL mice was visible but not alterations in the rCBF response. Given that this discontinuous way to elicit neuronal activation may not have been sufficient to expose an alteration in the integrated response of the neurovascular tree, we stimulated the forepaw continuously for one minute. This mode of stimulation

revealed alterations in rCBF responses and parenchymal vessel dilation in the corresponding area of the somatosensory cortex. The alterations to vascular reactivity found in this study expose a functional consequence of the HTRA1$^{-/-}$ mutation. Mutant HtrA1 fails to cleave binding sites of TGF-β to the extracellular matrix of smooth muscle cells, resulting in a decrease of TGF-β activity (Beaufort et al. 2014) in animals carrying the mutation. Furthermore, studies have shown that a loss of HtrA1 function results in a 50% reduction in levels of connective tissue growth factor (CTGF). Reduced action of these growth factors, which are well-defined regulators of angiogenesis and vascular homeostasis (ten Dijke et al. 2007; Goumans et al. 2009), may lead to structural alterations in blood vessels and poor angiogenesis and thus explain the alterations observed in neurovascular reactivity. Further research into this pathway may elucidate the role of these growth factors in small vessel disease. Taken together, our results demonstrate for the first time that loss of function of HtrA1 as observed in CARASIL results in disruptions to neural-activity-dependent and endothelium-dependent vasodilation. Further analysis of contractile elements of parenchymal vessels would help elucidate mechanisms involved in these impairments.

This thesis explored neurovascular deficits in healthy aging, after SAH and in two models of small vessel disease. My data demonstrated previously conceived notions such as the progression of functional decay from pial arteries down the neurovascular tree in chronic conditions, lack of reactivity to hypercapnia after SAH, and early changes to vessel structure and morphology in CADASIL mice. Additionally, these results may help design novel therapeutic strategies such as targeting K_{ir} channels and the NO pathway in aging, intervening within an early time window following SAH, and addressing pericyte deficiencies in small vessel diseases. This together with a thorough characterization of cerebrovascular function at various levels in each of these conditions provides a comprehensive understanding and outlook for the cerebral regulation of blood flow in health and disease.

7 Reference list

Aaslid, R., K. F. Lindegaard, et al. (1989). "Cerebral autoregulation dynamics in humans." Stroke **20**(1): 45-52.

Abounader, R. and E. Hamel (1997). "Associations between neuropeptide Y nerve terminals and intraparenchymal microvessels in rat and human cerebral cortex." J Comp Neurol **388**(3): 444-453.

Abounader, R., J. G. Villemure, et al. (1995). "Characterization of neuropeptide Y (NPY) receptors in human cerebral arteries with selective agonists and the new Y1 antagonist BIBP 3226." Br J Pharmacol **116**(4): 2245-2250.

Adams, H. P., Jr., N. F. Kassell, et al. (1981). "Early management of aneurysmal subarachnoid hemorrhage. A report of the Cooperative Aneurysm Study." J Neurosurg **54**(2): 141-145.

Alonso A, Reinz E, Jenne JW, et al. Reorganization of gap junctions after focused ultrasound blood-brain barrier opening in the rat brain. Journal of cerebral blood flow and metabolism: official journal of the International Society of Cerebral Blood Flow and Metabolism. 2010 Jul;30(7):1394-402

Alkayed, N. J., E. K. Birks, et al. (1996). "Inhibition of brain P-450 arachidonic acid epoxygenase decreases baseline cerebral blood flow." Am J Physiol **271**(4 Pt 2): H1541-1546.

Alkayed, N. J., E. K. Birks, et al. (1997). "Role of P-450 arachidonic acid epoxygenase in the response of cerebral blood flow to glutamate in rats." Stroke **28**(5): 1066-1072.

Allt, G. and J. G. Lawrenson (2001). "Pericytes: cell biology and pathology." Cells Tissues Organs **169**(1): 1-11.

Ances, B. M. (2004). "Coupling of changes in cerebral blood flow with neural activity: what must initially dip must come back up." J Cereb Blood Flow Metab **24**(1): 1-6.

Armulik, A., G. Genove, et al. (2010). "Pericytes regulate the blood-brain barrier." Nature **468**(7323): 557-561.

Attwell, D. and C. Iadecola (2002). "The neural basis of functional brain imaging signals." Trends Neurosci **25**(12): 621-625.

Attwell, D. and S. B. Laughlin (2001). "An energy budget for signaling in the grey matter of the brain." J Cereb Blood Flow Metab **21**(10): 1133-1145.

Banerjee, S. and M. A. Bhat (2007). "Neuron-glial interactions in blood-brain barrier formation." Annu Rev Neurosci **30**: 235-258.

Baudrimont, M., F. Dubas, et al. (1993). "Autosomal dominant leukoencephalopathy and subcortical ischemic stroke. A clinicopathological study." Stroke **24**(1): 122-125.

Bederson, J. B., A. L. Levy, et al. (1998). "Acute vasoconstriction after subarachnoid hemorrhage." Neurosurgery **42**(2): 352-360; discussion 360-352.

Begley, D. J. and M. W. Brightman (2003). "Structural and functional aspects of the blood-brain barrier." Prog Drug Res **61**: 39-78.

Bell RD, Winkler EA, Sagare AP, et al. Pericytes control key neurovascular functions and neuronal phenotype in the adult brain and during brain aging. Neuron. 2010 Nov 4;68(3):409-27.

Brown, A. M. and B. R. Ransom (2007). "Astrocyte glycogen and brain energy metabolism." Glia **55**(12): 1263-1271.

Cahill, J. and J. H. Zhang (2009). "Subarachnoid hemorrhage: is it time for a new direction?" Stroke **40**(3 Suppl): S86-87.

Cauli, B. and E. Hamel (2010). "Revisiting the role of neurons in neurovascular coupling." Front Neuroenergetics **2**: 9.

Cauli, B., X. K. Tong, et al. (2004). "Cortical GABA interneurons in neurovascular coupling: relays for subcortical vasoactive pathways." J Neurosci **24**(41): 8940-8949.

Chabriat, H., A. Joutel, et al. (2009). "Cadasil." Lancet Neurol **8**(7): 643-653.

Chabriat, H., C. Levy, et al. (1998). "Patterns of MRI lesions in CADASIL." Neurology **51**(2): 452-457.

Chabriat, H., K. Vahedi, et al. (1995). "Clinical spectrum of CADASIL: a study of 7 families. Cerebral autosomal dominant arteriopathy with subcortical infarcts and leukoencephalopathy." Lancet **346**(8980): 934-939.
Chedotal, A., C. Cozzari, et al. (1994). "Distinct choline acetyltransferase (ChAT) and vasoactive intestinal polypeptide (VIP) bipolar neurons project to local blood vessels in the rat cerebral cortex." Brain Res **646**(2): 181-193.
Chedotal, A. and E. Hamel (1990). "Serotonin-synthesizing nerve fibers in rat and cat cerebral arteries and arterioles: immunohistochemistry of tryptophan-5-hydroxylase." Neurosci Lett **116**(3): 269-274.
Chillon, J. M., S. Ghoneim, et al. (1997). "Effects of chronic nitric oxide synthase inhibition on cerebral arterioles in rats." Hypertension **30**(5): 1097-1104.
Chow, N., R. D. Bell, et al. (2007). "Serum response factor and myocardin mediate arterial hypercontractility and cerebral blood flow dysregulation in Alzheimer's phenotype." Proc Natl Acad Sci U S A **104**(3): 823-828.
Cipolla, M. J. (2007). "Cerebrovascular function in pregnancy and eclampsia." Hypertension **50**(1): 14-24.
Cipolla, M. J., R. Li, et al. (2004). "Perivascular innervation of penetrating brain parenchymal arterioles." J Cardiovasc Pharmacol **44**(1): 1-8.
Cipolla MJ. In: The Cerebral Circulation: San Rafael (CA), 2009.
Cohen, Z., G. Molinatti, et al. (1997). "Astroglial and vascular interactions of noradrenaline terminals in the rat cerebral cortex." J Cereb Blood Flow Metab **17**(8): 894-904.
Cornell-Bell, A. H., S. M. Finkbeiner, et al. (1990). "Glutamate induces calcium waves in cultured astrocytes: long-range glial signaling." Science **247**(4941): 470-473.
Cox, S. B., T. A. Woolsey, et al. (1993). "Localized dynamic changes in cortical blood flow with whisker stimulation corresponds to matched vascular and neuronal architecture of rat barrels." J Cereb Blood Flow Metab **13**(6): 899-913.
De Michele, M., O. Touzani, et al. (2005). "Corticotropin-releasing factor: effect on cerebral blood flow in physiologic and ischaemic conditions." Exp Brain Res **165**(3): 375-382.
Dichgans, M. (2007). "Genetics of ischaemic stroke." Lancet Neurol **6**(2): 149-161.
Dichgans, M., M. Mayer, et al. (1998). "The phenotypic spectrum of CADASIL: clinical findings in 102 cases." Ann Neurol **44**(5): 731-739.
Drake, C. T. and C. Iadecola (2007). "The role of neuronal signaling in controlling cerebral blood flow." Brain Lang **102**(2): 141-152.
Duchemin, S., M. Boily, et al. (2012). "The complex contribution of NOS interneurons in the physiology of cerebrovascular regulation." Front Neural Circuits **6**: 51.
Dunn, K. M. and M. T. Nelson (2014). "Neurovascular signaling in the brain and the pathological consequences of hypertension." Am J Physiol Heart Circ Physiol **306**(1): H1-14.
Elhusseiny, A. and E. Hamel (2000). "Muscarinic--but not nicotinic--acetylcholine receptors mediate a nitric oxide-dependent dilation in brain cortical arterioles: a possible role for the M5 receptor subtype." J Cereb Blood Flow Metab **20**(2): 298-305.
Estrada, C., E. Mengual, et al. (1993). "Local NADPH-diaphorase neurons innervate pial arteries and lie close or project to intracerebral blood vessels: a possible role for nitric oxide in the regulation of cerebral blood flow." J Cereb Blood Flow Metab **13**(6): 978-984.
Faraci, F. M. and D. D. Heistad (1998). "Regulation of the cerebral circulation: role of endothelium and potassium channels." Physiol Rev **78**(1): 53-97.
Faraci, F. M. and C. G. Sobey (1998). "Role of potassium channels in regulation of cerebral vascular tone." J Cereb Blood Flow Metab **18**(10): 1047-1063.
Farkas, E. and P. G. Luiten (2001). "Cerebral microvascular pathology in aging and Alzheimer's disease." Prog Neurobiol **64**(6): 575-611.
Feiler, S., B. Friedrich, et al. (2010). "Standardized induction of subarachnoid hemorrhage in mice by intracranial pressure monitoring." J Neurosci Methods **190**(2): 164-170.

Feiler, S., N. Plesnila, et al. (2011). "Contribution of matrix metalloproteinase-9 to cerebral edema and functional outcome following experimental subarachnoid hemorrhage." Cerebrovasc Dis **32**(3): 289-295.
Filosa, J. A., A. D. Bonev, et al. (2004). "Calcium dynamics in cortical astrocytes and arterioles during neurovascular coupling." Circ Res **95**(10): e73-81.
Filosa, J. A., A. D. Bonev, et al. (2006). "Local potassium signaling couples neuronal activity to vasodilation in the brain." Nat Neurosci **9**(11): 1397-1403.
Franklin, J. L., D. J. Fickbohm, et al. (1992). "Long-term regulation of neuronal calcium currents by prolonged changes of membrane potential." J Neurosci **12**(5): 1726-1735.
Friedrich, B., F. Muller, et al. (2012). "Experimental subarachnoid hemorrhage causes early and long-lasting microarterial constriction and microthrombosis: an in-vivo microscopy study." J Cereb Blood Flow Metab **32**(3): 447-455.
Friedrich B, Michalik R, Oniszczuk A, Abubaker K, Kozniewska E, Plesnila N. CO2 has no therapeutic effect on early microvasospasm after experimental subarachnoid hemorrhage. Journal of cerebral blood flow and metabolism : official journal of the International Society of Cerebral Blood Flow and Metabolism 2014; 34(8): e1-6.
Frontera, J. A., T. Rundek, et al. (2006). "Cerebrovascular reactivity and vasospasm after subarachnoid hemorrhage: a pilot study." Neurology **66**(5): 727-729.
Fukutake, T. (2011). "Cerebral autosomal recessive arteriopathy with subcortical infarcts and leukoencephalopathy (CARASIL): from discovery to gene identification." J Stroke Cerebrovasc Dis **20**(2): 85-93.
Fukutake, T. and K. Hirayama (1995). "Familial young-adult-onset arteriosclerotic leukoencephalopathy with alopecia and lumbago without arterial hypertension." Eur Neurol **35**(2): 69-79.
Furchgott, R. F. and J. V. Zawadzki (1980). "The obligatory role of endothelial cells in the relaxation of arterial smooth muscle by acetylcholine." Nature **288**(5789): 373-376.
Garavito, R. M. and A. M. Mulichak (2003). "The structure of mammalian cyclooxygenases." Annu Rev Biophys Biomol Struct **32**: 183-206.
Gordon, G. R., S. J. Mulligan, et al. (2007). "Astrocyte control of the cerebrovasculature." Glia **55**(12): 1214-1221.
Gotoh, J., T. Y. Kuang, et al. (2001). "Regional differences in mechanisms of cerebral circulatory response to neuronal activation." Am J Physiol Heart Circ Physiol **280**(2): H821-829.
Goumans MJ, Liu Z, ten Dijke P (2009) TGF-beta signaling in vascular biology and dysfunction. Cell Res 19(1):116–127.
Grigg, M. M., M. A. Kelly, et al. (1987). "Electroencephalographic activity after brain death." Arch Neurol **44**(9): 948-954.
Gruetter, R. (2003). "Glycogen: the forgotten cerebral energy store." J Neurosci Res **74**(2): 179-183.
Hamel, E. (2006). "Perivascular nerves and the regulation of cerebrovascular tone." J Appl Physiol (1985) **100**(3): 1059-1064.
Hara, K., A. Shiga, et al. (2009). "Association of HTRA1 mutations and familial ischemic cerebral small-vessel disease." N Engl J Med **360**(17): 1729-1739.
Harder, D. R., R. J. Roman, et al. (1998). "A common pathway for regulation of nutritive blood flow to the brain: arterial muscle membrane potential and cytochrome P450 metabolites." Acta Physiol Scand **164**(4): 527-532.
Harder, D. R., C. Zhang, et al. (2002). "Astrocytes function in matching blood flow to metabolic activity." News Physiol Sci **17**: 27-31.
Hawkins, B. T. and T. P. Davis (2005). "The blood-brain barrier/neurovascular unit in health and disease." Pharmacol Rev **57**(2): 173-185.
Haydon, P. G. and G. Carmignoto (2006). "Astrocyte control of synaptic transmission and neurovascular coupling." Physiol Rev **86**(3): 1009-1031.

Heistad, D. D., M. L. Marcus, et al. (1978). "Experimental attempts to unmask effects of neural stimuli on cerebral blood flow." Ciba Found Symp(56): 97-118.
Helbok, R., S. B. Ko, et al. (2011). "Global cerebral edema and brain metabolism after subarachnoid hemorrhage." Stroke **42**(6): 1534-1539.
Herz, D. A., S. Baez, et al. (1975). "Pial microcirculation in subarachnoid hemorrhage." Stroke **6**(4): 417-424.
Heuser, D. (1978). "The significance of cortical extracellular H+, K+ and Ca2+ activities for regulation of local cerebral blood flow under conditions of enhanced neuronal activity." Ciba Found Symp(56): 339-353.
Hinkle, J. L. and L. Bowman (2003). "Neuroprotection for ischemic stroke." J Neurosci Nurs **35**(2): 114-118.
Hockel, K., R. Trabold, et al. (2012). "Impact of anesthesia on pathophysiology and mortality following subarachnoid hemorrhage in rats." Exp Transl Stroke Med **4**(1): 5.
Hoffmeyer, H. W., P. Enager, et al. (2007). "Nonlinear neurovascular coupling in rat sensory cortex by activation of transcallosal fibers." J Cereb Blood Flow Metab **27**(3): 575-587.
Hossain MZ, Peeling J, Sutherland GR, Hertzberg EL, Nagy JI. Ischemia-induced cellular redistribution of the astrocytic gap junctional protein connexin43 in rat brain. Brain research. 1994 Aug 1;652(2):311-22
Hossmann, K. A. (1994). "Glutamate-mediated injury in focal cerebral ischemia: the excitotoxin hypothesis revised." Brain Pathol **4**(1): 23-36.
Hossmann, K. A. (1994). "Viability thresholds and the penumbra of focal ischemia." Ann Neurol **36**(4): 557-565.
Hossmann, K. A. and V. Hossmann (1977). "Coagulopathy following experimental cerebral ischemia." Stroke **8**(2): 249-254.
Howarth, C., C. M. Peppiatt-Wildman, et al. (2010). "The energy use associated with neural computation in the cerebellum." J Cereb Blood Flow Metab **30**(2): 403-414.
Hungerhuber, E., S. Zausinger, et al. (2006). "Simultaneous bilateral laser Doppler fluxmetry and electrophysiological recording during middle cerebral artery occlusion in rats." J Neurosci Methods **154**(1-2): 109-115.
Iadecola, C. (1992). "Does nitric oxide mediate the increases in cerebral blood flow elicited by hypercapnia?" Proc Natl Acad Sci U S A **89**(9): 3913-3916.
Iadecola, C. (1993). "Regulation of the cerebral microcirculation during neural activity: is nitric oxide the missing link?" Trends Neurosci **16**(6): 206-214.
Iadecola, C. (1998). "Neurogenic control of the cerebral microcirculation: is dopamine minding the store?" Nat Neurosci **1**(4): 263-265.
Iadecola, C. (2004). "Neurovascular regulation in the normal brain and in Alzheimer's disease." Nat Rev Neurosci **5**(5): 347-360.
Iadecola, C. and M. Nedergaard (2007). "Glial regulation of the cerebral microvasculature." Nat Neurosci **10**(11): 1369-1376.
Ishikawa M, Kusaka G, Yamaguchi N, Sekizuka E, Nakadate H, Minamitani H et al. Platelet and leukocyte adhesion in the microvasculature at the cerebral surface immediately after subarachnoid hemorrhage. Neurosurgery 2009; 64(3): 546-53; discussion 553-4.
Itoh, Y. and N. Suzuki (2012). "Control of brain capillary blood flow." J Cereb Blood Flow Metab **32**(7): 1167-1176.
Johnston, S. C., S. Selvin, et al. (1998). "The burden, trends, and demographics of mortality from subarachnoid hemorrhage." Neurology **50**(5): 1413-1418.
Jones, E. G. (1970). "On the mode of entry of blood vessels into the cerebral cortex." J Anat **106**(Pt 3): 507-520.
Joutel, A., F. Andreux, et al. (2000). "The ectodomain of the Notch3 receptor accumulates within the cerebrovasculature of CADASIL patients." J Clin Invest **105**(5): 597-605.

Joutel, A., C. Corpechot, et al. (1996). "Notch3 mutations in CADASIL, a hereditary adult-onset condition causing stroke and dementia." Nature **383**(6602): 707-710.
Joutel, A., D. D. Dodick, et al. (2000). "De novo mutation in the Notch3 gene causing CADASIL." Ann Neurol **47**(3): 388-391.
Joutel, A., P. Favrole, et al. (2001). "Skin biopsy immunostaining with a Notch3 monoclonal antibody for CADASIL diagnosis." Lancet **358**(9298): 2049-2051.
Joutel, A., M. Monet-Lepretre, et al. (2010). "Cerebrovascular dysfunction and microcirculation rarefaction precede white matter lesions in a mouse genetic model of cerebral ischemic small vessel disease." J Clin Invest **120**(2): 433-445.
Joutel, A., K. Vahedi, et al. (1997). "Strong clustering and stereotyped nature of Notch3 mutations in CADASIL patients." Lancet **350**(9090): 1511-1515.
Kacem, K., P. Lacombe, et al. (1998). "Structural organization of the perivascular astrocyte end-feet and their relationship with the endothelial glucose transporter: a confocal microscopy study." Glia **23**(1): 1-10.
Kajita Y, Dietrich HH, Dacey RG, Jr. Effects of oxyhemoglobin on local and propagated vasodilatory responses induced by adenosine, adenosine diphosphate, and adenosine triphosphate in rat cerebral arterioles. Journal of neurosurgery 1996; 85(5): 908-16.
Kalaria, R. N. (1996). "Cerebral vessels in ageing and Alzheimer's disease." Pharmacol Ther **72**(3): 193-214.
Kalaria, R. N. (2009). "Linking cerebrovascular defense mechanisms in brain ageing and Alzheimer's disease." Neurobiol Aging **30**(9): 1512-1514.
Kalaria, R. N., G. E. Maestre, et al. (2008). "Alzheimer's disease and vascular dementia in developing countries: prevalence, management, and risk factors." Lancet Neurol **7**(9): 812-826.
Kalimo, H., M. Viitanen, et al. (1999). "CADASIL: hereditary disease of arteries causing brain infarcts and dementia." Neuropathol Appl Neurobiol **25**(4): 257-265.
Kety, S. S. and C. F. Schmidt (1948). "The Effects of Altered Arterial Tensions of Carbon Dioxide and Oxygen on Cerebral Blood Flow and Cerebral Oxygen Consumption of Normal Young Men." J Clin Invest **27**(4): 484-492.
Kim, K. J. and J. A. Filosa (2012). "Advanced in vitro approach to study neurovascular coupling mechanisms in the brain microcirculation." J Physiol **590**(Pt 7): 1757-1770.
Kimelberg, H. K. (2004). "Water homeostasis in the brain: basic concepts." Neuroscience **129**(4): 851-860.
Kirov, S. A. and K. M. Harris (1999). "Dendrites are more spiny on mature hippocampal neurons when synapses are inactivated." Nat Neurosci **2**(10): 878-883.
Kleinfeld, D., P. P. Mitra, et al. (1998). "Fluctuations and stimulus-induced changes in blood flow observed in individual capillaries in layers 2 through 4 of rat neocortex." Proc Natl Acad Sci U S A **95**(26): 15741-15746.
Ko, K. R., A. C. Ngai, et al. (1990). "Role of adenosine in regulation of regional cerebral blood flow in sensory cortex." Am J Physiol **259**(6 Pt 2): H1703-1708.
Koehler, R. C., D. Gebremedhin, et al. (2006). "Role of astrocytes in cerebrovascular regulation." J Appl Physiol (1985) **100**(1): 307-317.
Koide M, Wellman GC. SAH-induced suppression of voltage-gated K(+) (K (V)) channel currents in parenchymal arteriolar myocytes involves activation of the HB-EGF/EGFR pathway. Acta neurochirurgica. Supplement 2013; 115: 179-84.
Koide M DK, Bulkeley EA, Nelson MT, Wellman GC. In vivo and ex vivo dysfunction of neurovascular coupling in a mouse model of subarachnoid hemorrhage. FASEB 2014; 28 (1 Supplement), 676.3.
Kontos, H. A., E. P. Wei, et al. (1978). "Responses of cerebral arteries and arterioles to acute hypotension and hypertension." Am J Physiol **234**(4): H371-383.
Kontos, H. A., E. P. Wei, et al. (1977). "Local mechanism of CO2 action of cat pial arterioles." Stroke **8**(2): 226-229.

Kubota, Y., R. Hattori, et al. (1994). "Three distinct subpopulations of GABAergic neurons in rat frontal agranular cortex." Brain Res **649**(1-2): 159-173.
Kulik, T., Y. Kusano, et al. (2008). "Regulation of cerebral vasculature in normal and ischemic brain." Neuropharmacology **55**(3): 281-288.
Lacombe, P., C. Oligo, et al. (2005). "Impaired cerebral vasoreactivity in a transgenic mouse model of cerebral autosomal dominant arteriopathy with subcortical infarcts and leukoencephalopathy arteriopathy." Stroke **36**(5): 1053-1058.
Li, J. and C. Iadecola (1994). "Nitric oxide and adenosine mediate vasodilation during functional activation in cerebellar cortex." Neuropharmacology **33**(11): 1453-1461.
Lierse, W. and E. Horstmann (1965). "Quantitative anatomy of the cerebral vascular bed with especial emphasis on homogeneity and inhomogeneity in small ports of the gray and white matter." Acta Neurol Scand Suppl **14**: 15-19.
Lindauer, U., D. Megow, et al. (1999). "Nitric oxide: a modulator, but not a mediator, of neurovascular coupling in rat somatosensory cortex." Am J Physiol **277**(2 Pt 2): H799-811.
Long, J. B., D. D. Rigamonti, et al. (1992). "Somatostatin causes vasoconstriction, reduces blood flow and increases vascular permeability in the rat central nervous system." J Pharmacol Exp Ther **260**(3): 1425-1432.
Lopez-Bayghen, E. and A. Ortega (2011). "Glial glutamate transporters: new actors in brain signaling." IUBMB Life **63**(10): 816-823.
Macdonald, R. L. and B. K. Weir (1991). "A review of hemoglobin and the pathogenesis of cerebral vasospasm." Stroke **22**(8): 971-982.
Mayhan WG, Faraci FM, Baumbach GL, Heistad DD. Effects of aging on responses of cerebral arterioles. AmJ Physiol 1990; 258: H1138–H1143.
Malonek, D., U. Dirnagl, et al. (1997). "Vascular imprints of neuronal activity: relationships between the dynamics of cortical blood flow, oxygenation, and volume changes following sensory stimulation." Proc Natl Acad Sci U S A **94**(26): 14826-14831.
Markus, H. S. (2004). "Cerebral perfusion and stroke." J Neurol Neurosurg Psychiatry **75**(3): 353-361.
Markus, H. S., R. J. Martin, et al. (2002). "Diagnostic strategies in CADASIL." Neurology **59**(8): 1134-1138.
Martin, L. J., N. A. Al-Abdulla, et al. (1998). "Neurodegeneration in excitotoxicity, global cerebral ischemia, and target deprivation: A perspective on the contributions of apoptosis and necrosis." Brain Res Bull **46**(4): 281-309.
Mc, D. D. and J. M. Potter (1951). "The distribution of blood to the brain." J Physiol **114**(3): 356-371.
Mellander, S. (1989). "Functional aspects of myogenic vascular control." J Hypertens Suppl **7**(4): S21-30; discussion S31.
Mendelow, A. D. (1993). "Mechanisms of ischemic brain damage with intracerebral hemorrhage." Stroke **24**(12 Suppl): I115-117; discussion I118-119.
Mendioroz, M., I. Fernandez-Cadenas, et al. (2010). "A missense HTRA1 mutation expands CARASIL syndrome to the Caucasian population." Neurology **75**(22): 2033-2035.
Miao, Q., T. Paloneva, et al. (2004). "Fibrosis and stenosis of the long penetrating cerebral arteries: the cause of the white matter pathology in cerebral autosomal dominant arteriopathy with subcortical infarcts and leukoencephalopathy." Brain Pathol **14**(4): 358-364.
Moncada, S. (1992). "Nitric oxide gas: mediator, modulator, and pathophysiologic entity." J Lab Clin Med **120**(2): 187-191.
Mulligan, S. J. and B. A. MacVicar (2004). "Calcium transients in astrocyte end-feet cause cerebrovascular constrictions." Nature **431**(7005): 195-199.
Nguyen, T. S., H. R. Winn, et al. (2000). "ATP-sensitive potassium channels may participate in the coupling of neuronal activity and cerebrovascular tone." Am J Physiol Heart Circ Physiol **278**(3): H878-885.
Nishimura, N., C. B. Schaffer, et al. (2007). "Penetrating arterioles are a bottleneck in the perfusion of neocortex." Proc Natl Acad Sci U S A **104**(1): 365-370.

Niwa, K., E. Araki, et al. (2000). "Cyclooxygenase-2 contributes to functional hyperemia in whisker-barrel cortex." J Neurosci **20**(2): 763-770.
Niwa, K., C. Haensel, et al. (2001). "Cyclooxygenase-1 participates in selected vasodilator responses of the cerebral circulation." Circ Res **88**(6): 600-608.
Niwa, M., H. Maruyama, et al. (2000). "Affinity selection of cDNA libraries by lambda phage surface display." Gene **256**(1-2): 229-236.
Ohta, S., E. Meyer, et al. (1992). "Oxygen consumption of the living human brain measured after a single inhalation of positron emitting oxygen." J Cereb Blood Flow Metab **12**(2): 179-192.
Opherk, C., N. Peters, et al. (2004). "Long-term prognosis and causes of death in CADASIL: a retrospective study in 411 patients." Brain **127**(Pt 11): 2533-2539.
Osol, G., J. F. Brekke, et al. (2002). "Myogenic tone, reactivity, and forced dilatation: a three-phase model of in vitro arterial myogenic behavior." Am J Physiol Heart Circ Physiol **283**(6): H2260-2267.
Palay, S. L. (1991). "The founding of The Journal of Comparative Neurology." J Comp Neurol **314**(1): 1-8.
Pantoni, L. (2010). "Cerebral small vessel disease: from pathogenesis and clinical characteristics to therapeutic challenges." Lancet Neurol **9**(7): 689-701.
Park KW, Metais C, Dai HB, Comunale ME, Sellke FW. Microvascular endothelial dysfunction and its mechanism in a rat model of subarachnoid hemorrhage. Anesthesia and analgesia 2001; 92(4): 990-6.
Pelligrino, D. A., F. Vetri, et al. (2011). "Purinergic mechanisms in gliovascular coupling." Semin Cell Dev Biol **22**(2): 229-236.
Peng, X., J. R. Carhuapoma, et al. (2002). "Suppression of cortical functional hyperemia to vibrissal stimulation in the rat by epoxygenase inhibitors." Am J Physiol Heart Circ Physiol **283**(5): H2029-2037.
Peppiatt, C. M., C. Howarth, et al. (2006). "Bidirectional control of CNS capillary diameter by pericytes." Nature **443**(7112): 700-704.
Petzold, G. C. and V. N. Murthy (2011). "Role of astrocytes in neurovascular coupling." Neuron **71**(5): 782-797.
Pobereskin, L. H. (2001). "Incidence and outcome of subarachnoid haemorrhage: a retrospective population based study." J Neurol Neurosurg Psychiatry **70**(3): 340-343.
Poels, M. M., E. W. Steyerberg, et al. (2012). "Assessment of cerebral small vessel disease predicts individual stroke risk." J Neurol Neurosurg Psychiatry **83**(12): 1174-1179.
Prayer, D., G. Kasprian, et al. (2006). "MRI of normal fetal brain development." Eur J Radiol **57**(2): 199-216.
Quaegebeur A, Carmeliet P. Oxygen sensing: a common crossroad in cancer and neurodegeneration. Current topics in microbiology and immunology. 2010;345:71-103
Razvi, S. S., R. Davidson, et al. (2005). "The prevalence of cerebral autosomal dominant arteriopathy with subcortical infarcts and leucoencephalopathy (CADASIL) in the west of Scotland." J Neurol Neurosurg Psychiatry **76**(5): 739-741.
Reivich, M. (1964). "Arterial Pco2 and Cerebral Hemodynamics." Am J Physiol **206**: 25-35.
Riggs, H. E. and C. Rupp (1963). "Variation in form of circle of Willis. The relation of the variations to collateral circulation: anatomic analysis." Arch Neurol **8**: 8-14.
Ringelstein, E. B. and D. G. Nabavi (2005). "Cerebral small vessel diseases: cerebral microangiopathies." Curr Opin Neurol **18**(2): 179-188.
Robertson, B. E., R. Schubert, et al. (1993). "cGMP-dependent protein kinase activates Ca-activated K channels in cerebral artery smooth muscle cells." Am J Physiol **265**(1 Pt 1): C299-303.
Ruchoux, M. M., D. Guerouaou, et al. (1995). "Systemic vascular smooth muscle cell impairment in cerebral autosomal dominant arteriopathy with subcortical infarcts and leukoencephalopathy." Acta Neuropathol **89**(6): 500-512.

Sa-Pereira, I., D. Brites, et al. (2012). "Neurovascular unit: a focus on pericytes." Mol Neurobiol **45**(2): 327-347.
Santello, M., C. Cali, et al. (2012). "Gliotransmission and the tripartite synapse." Adv Exp Med Biol **970**: 307-331.
Schubert, G. A., M. Seiz, et al. (2009). "Acute hypoperfusion immediately after subarachnoid hemorrhage: a xenon contrast-enhanced CT study." J Neurotrauma **26**(12): 2225-2231.
Scremin, O. U., A. A. Rovere, et al. (1973). "Cholinergic control of blood flow in the cerebral cortex of the rat." Stroke **4**(2): 233-239.
Sehba, F. A., V. Friedrich, Jr., et al. (2007). "Acute cerebral vascular injury after subarachnoid hemorrhage and its prevention by administration of a nitric oxide donor." J Neurosurg **106**(2): 321-329.
Sehba, F. A., G. Mostafa, et al. (2005). "Acute microvascular platelet aggregation after subarachnoid hemorrhage." J Neurosurg **102**(6): 1094-1100.
Silva, A. C., S. P. Lee, et al. (2000). "Early temporal characteristics of cerebral blood flow and deoxyhemoglobin changes during somatosensory stimulation." J Cereb Blood Flow Metab **20**(1): 201-206.
Skrifvars, M. B. and M. J. Parr (2012). "Incidence, predisposing factors, management and survival following cardiac arrest due to subarachnoid haemorrhage: a review of the literature." Scand J Trauma Resusc Emerg Med **20**: 75.
Smith, W. L., R. M. Garavito, et al. (1996). "Prostaglandin endoperoxide H synthases (cyclooxygenases)-1 and -2." J Biol Chem **271**(52): 33157-33160.
Sobey, C. G. and F. M. Faraci (1997). "Effects of a novel inhibitor of guanylyl cyclase on dilator responses of mouse cerebral arterioles." Stroke **28**(4): 837-842; discussion 842-833.
Sokoloff, L. (1977). "Relation between physiological function and energy metabolism in the central nervous system." J Neurochem **29**(1): 13-26.
Strandgaard, S. and O. B. Paulson (1990). "Pathophysiology of stroke." J Cardiovasc Pharmacol **15 Suppl 1**: S38-42.
Strbian, D., A. Durukan, et al. (2008). "Rodent models of hemorrhagic stroke." Curr Pharm Des **14**(4): 352-358.
Szabo, C., J. E. Hardebo, et al. (1991). "An amplifying effect of exogenous and neurally stored 5-hydroxytryptamine on the neurogenic contraction in rat tail artery." Br J Pharmacol **102**(2): 401-407.
Sun BL, Zheng CB, Yang MF, Yuan H, Zhang SM, Wang LX. Dynamic alterations of cerebral pial microcirculation during experimental subarachnoid hemorrhage. Cellular and molecular neurobiology 2009; 29(2): 235-41.
Takano, T., G. F. Tian, et al. (2006). "Astrocyte-mediated control of cerebral blood flow." Nat Neurosci **9**(2): 260-267.
Talman, W. T. and D. Nitschke Dragon (2007). "Neuronal nitric oxide mediates cerebral vasodilatation during acute hypertension." Brain Res 1139: 126-132.
ten Dijke P, Arthur HM (2007) Extracellular control of TGFbeta signalling in vascular development and disease. Nat Rev Mol Cell Biol 8(11):857–869.
Thal, S. C., S. Sporer, et al. (2009). "Brain edema formation and neurological impairment after subarachnoid hemorrhage in rats. Laboratory investigation." J Neurosurg **111**(5): 988-994.
Titova, E., R. P. Ostrowski, et al. (2009). "Experimental models of subarachnoid hemorrhage for studies of cerebral vasospasm." Neurol Res **31**(6): 568-581.
Truebestein, L., A. Tennstaedt, et al. (2011). "Substrate-induced remodeling of the active site regulates human HTRA1 activity." Nat Struct Mol Biol **18**(3): 386-388.
Tsai, P. S., J. P. Kaufhold, et al. (2009). "Correlations of neuronal and microvascular densities in murine cortex revealed by direct counting and colocalization of nuclei and vessels." J Neurosci **29**(46): 14553-14570.

Tucsek Z, Toth P, Tarantini S, et al. Aging Exacerbates Obesity-induced Cerebromicrovascular Rarefaction, Neurovascular Uncoupling, and Cognitive Decline in Mice. The journals of gerontology Series A, Biological sciences and medical sciences. 2014 Jun 3.

Uhl, E., J. Lehmberg, et al. (2003). "Intraoperative detection of early microvasospasm in patients with subarachnoid hemorrhage by using orthogonal polarization spectral imaging." Neurosurgery **52**(6): 1307-1315; disacussion 1315-1307.

Vander Eecken, H. M. and R. D. Adams (1953). "The anatomy and functional significance of the meningeal arterial anastomoses of the human brain." J Neuropathol Exp Neurol **12**(2): 132-157.

Vaucher, E., X. K. Tong, et al. (2000). "GABA neurons provide a rich input to microvessels but not nitric oxide neurons in the rat cerebral cortex: a means for direct regulation of local cerebral blood flow." J Comp Neurol **421**(2): 161-171.

Villringer, A. and U. Dirnagl (1995). "Coupling of brain activity and cerebral blood flow: basis of functional neuroimaging." Cerebrovasc Brain Metab Rev **7**(3): 240-276.

Wardlaw JM, Smith C, Dichgans M. Mechanisms of sporadic cerebral small vessel disease: insights from neuroimaging. Lancet neurology. 2013 May;12(5):483-97Wang, H., I. M. Hitron, et al. (2005). "Synaptic and vascular associations of neurons containing cyclooxygenase-2 and nitric oxide synthase in rat somatosensory cortex." Cereb Cortex 15(8): 1250-1260.

Weir, B., M. Grace, et al. (1978). "Time course of vasospasm in man." J Neurosurg **48**(2): 173-178.

Weiss, N., F. Miller, et al. (2009). "The blood-brain barrier in brain homeostasis and neurological diseases." Biochim Biophys Acta **1788**(4): 842-857.

Westermaier, T., A. Jauss, et al. (2011). "The temporal profile of cerebral blood flow and tissue metabolites indicates sustained metabolic depression after experimental subarachnoid hemorrhage in rats." Neurosurgery **68**(1): 223-229; discussion 229-230.

Wu, L., F. Shen, et al. (2006). "The neuroprotection conferred by activating the mitochondrial ATP-sensitive K+ channel is mediated by inhibiting the mitochondrial permeability transition pore." Neurosci Lett **402**(1-2): 184-189.

Yaksh, T. L., J. Y. Wang, et al. (1987). "Cortical vasodilatation produced by vasoactive intestinal polypeptide (VIP) and by physiological stimuli in the cat." J Cereb Blood Flow Metab **7**(3): 315-326.

Yamagata, K., K. I. Andreasson, et al. (1993). "Expression of a mitogen-inducible cyclooxygenase in brain neurons: regulation by synaptic activity and glucocorticoids." Neuron **11**(2): 371-386.

Zlokovic, B. V. (2005). "Neurovascular mechanisms of Alzheimer's neurodegeneration." Trends Neurosci **28**(4): 202-208.

Zlokovic, B. V. (2008). "The blood-brain barrier in health and chronic neurodegenerative disorders." Neuron **57**(2): 178-201.

Zonta, M., M. C. Angulo, et al. (2003). "Neuron-to-astrocyte signaling is central to the dynamic control of brain microcirculation." Nat Neurosci **6**(1): 43-50.

MATILDE BALBI

Schmuzerstrasse 3
Munich, Bavaria, Germany
(+49) 174 630 9589 matilde.balbi@med.uni-muenchen.de

EDUCATION

LUDWIG MAXIMILLIANS UNIVERSITY — Munich, Germany
Institute for Stroke and Dementia
Graduate School of Systemic Neurosciences
October 2011 – Present — ***PhD in Neuroscience***

LITE COLLEGE — London, United Kingdom
November 2009 – July 2010 — ***English language course***

UNIVERSITY OF NAPLES "FEDERICO II" — Naples, Italy
October 2007 – July 2009 — ***Master of Science in Medical Biotechnology; Grade: 110/110***

UNIVERSITY OF NAPLES "FEDERICO II" — Naples, Italy
October 2004 – October 2007 — ***Bachelor of Science – Biotechnology for healthcare***

WORK HISTORY

Research Assistant
Royal College of Surgeons in Ireland (RCSI)
Department of Neurodegeneration — November 2010 – September 2011
Dublin, Ireland

I worked on a project on the possible therapeutic effects of Lithium on Traumatic Brain Injury (TBI), described below.

MAIN PROJECT EXPERIENCE

Regulation of cerebral blood flow in health and disease
Ludwig Maximillians University, PhD Thesis
October 2011 – Present

The first aim of this project is to identify early micro-vascular dysfunctions in hereditary small-vessel diseases using the CADASIL and CARASIL animal models in order to accelerate the development of novel therapeutic strategies. I set up systems to measure vessel response to hypercapnia and neurovascular coupling. The scope of the project was expanded to investigate vessels of mice under subarachnoid hemorrhage as well as normal aging.

Lithium chloride effect on acute lesion expansion and brain swelling after TBI in mice
Royal College of Surgeons in Ireland, Research Assistant
October 2010 – September 2011

I investigated the effect of both chronic and acute lithium treatment on secondary brain damage 24 hours after TBI. Neither chronic intraperitoneal administration of lithium chloride nor acute intracerebroventricular administration in different concentrations had an effect on brain swelling or secondary lesion expansion 24 hours after trauma compared to saline. Lithium does not seem to mediate acute neuroprotection following experimental TBI.

Assessment of the effects of gliadin peptides on innate immunity
University of Naples "Federico II", Master thesis
January 2008 – July 2009

I investigated the role of gliadin in general and the role of peptide P31-43 on the EGFR and interleukin fifteen pathway in intestinal epithelial cell model CaCo2. It was found that proliferation induced by P31- 43 in CaCo2 cells depends on EGFR and IL15 activity. P31-43 treatment induces the formation and phosphorylation of a IL15R-α/EGFR complex, and these effects are dependent on EGFR and IL15 activity.

Selection of menin knockout cells
University of Naples "Federico II", Bachelor thesis
January 2007 – September 2007

I worked in a group to generate and select menin knockout frog cells for future use in experiments involving regulation of mitosis. This was my first lab experience and I had the chance to learn techniques such as Western blotting and cell culturing.

SKILLS

Animal physiology and pharmacology	Experience with several **mouse models** (small-vessel disease, SAH, aging, controlled cortical impact). Experience with pharmacological studies in rodents. In depth experience with **handling** and **breeding** of trasngenic mice. Various non-standard animal physiology techniques in mice, e.g. **intubation**, ventilation, and **long term anesthesia** (up to 6 h), microcapnometry, invasive (**catheterization**) and non-invasive blood pressure monitoring. Measurement of regional cerebral blood flow by laser Doppler flow in mice. Design and execution of neurovascular coupling experiments by **forepaw stimulation**. **Two-photon** and **intravital fluorescence microscopy** for the study of cerebral microvessels in the living brain.
Biochemistry/Molecular biology	siRNA, RT-PCR, DNA electrophoresis, Western blotting, immunohistochemistry, histology, fluorescence microscopy, Golgi staining
Cell culturing	Hands-on experience with the preparation and culturing of CaCo2 cells and fibroblasts from mice embryos.
Software	LabChart, SigmaPlot, ImageJ Microsoft Office
Operating Systems	Linux. Mac and Windows
Languages	Fluent in Italian and English. Conversant in Spanish and German.

CONFERENCE POSTERS

1. **Balbi M**, Koide M, Wellman G, Plesnila N
   "Neurovascular coupling after Subarachnoid Hemorrhage (SAH) in vivo"
   XXVIIth International Symposium on Cerebral Blood Flow Metabolism and Function, Vancouver, Canada, June 27th -30th,2015

2. **Balbi M***, Ghosh M*, Longden T, Jativa M, Gesierich B, Hellal F, Nelson M, Plesnila N
   Dysfunction of mouse cerebral arteries during early aging
   XXVIIth International Symposium on Cerebral Blood Flow Metabolism and Function, Vancouver, Canada, June 27th -30th,2015

3. **Balbi M,** Plesnila N
   "Characterization of cerebrovascular function in mice with cerebral small vessel disease"
   Society for Neuroscience, Washington DC, USA, November 15-19, 2014

4. **Balbi M,** Schwarzmaier S, Plesnila N
   "Therapeutic effect of chronic and acute lithium application following traumatic brain injury in mice"
   XXVIth International Symposium on Cerebral Blood Flow Metabolism and Function
   Shanghai, China, May 20-23, 2013

5. Meissner L, Gallozzi M, **Balbi M,** Schwarzmaier S, Terpolilli N, Plesnila N
   "MicroRNA expression profile during secondary lesion expansion after traumatic brain injury"
   XXVIth International Symposium on Cerebral Blood Flow Metabolism and Function
   Shanghai, China, May 20-23, 2013

6. Barone MV, Nakayakkara M, Lania G, Zanzi D, Santagata S, Saputo M, Discepolo V, Kosova R, Russo A, **Balbi M,** Troncone R, Auricchio S
   "Gliadin P31-43 prompts IL15 R ALFA and EGFR cooperation to induce cell proliferation in CaCo2 cells"
   13th International Coeliac Disease Symposium. Amsterdam, Netherlands, April 6-8, 2009

7. Nakayakkara M, Lania G, Vitale V, Discepolo V, Kosova R, Marino I, **Balbi M,** Troncone R, Auricchio S, Barone MV
   "The gliadin peptide P31-43 delays the activation of the EGFR (Epidermal Growtor Factor Receptor) interfering with the endocytotic pathway"
   Scientific day of Pediatric department, University of Naples "Federico II" Naples, Italy, 2009

8. Lania G, Nakayakkara M, Saputo M, Marino I, Vitale V, **Balbi M,** Kosova R, Barone MV
   "Alteration in actin rearrangement, adhesion and motility can discriminate cutaneous fibroblasts of coeliac patients from controls"
   Scientific day of Pediatric department, University of Naples "Federico II" Naples, Italy, 2009

Publications

1. **Balbi M***, Ghosh M*, Longden T, Jativa M, Gesierich B, Hellal F, Nelson M, Plesnila N
   Dysfunction of mouse cerebral arteries during early aging
   Journal of Cerebral Blood Flow and Metabolism, advance online publication June 10, 2015;

2. **Balbi M**, Koide M, Wellman G, Plesnila N
   Neurovascular coupling after Subarachnoid Hemorrhage(SAH) in vivo
   Journal of Cerebral Blood Flow and Metabolism *(Accepted for publication)*

3. Ghosh M*, **Balbi M***,Farida Hellal, Martin Dichgans, Lindauer U, Plesnila N
   Pericytes are involved in the pathogenesis of CADASIL
   Annals of Neurology *(Under revision)*

4. Meissner L*, Gallozzi M*, **Balbi M***, Schwarzmaier S, Terpolilli NA, Plesnila N
   Temporal profile of microRNA expression in contused cortex following experimental TBI in mice,
   Journal of Neurotrauma *(Under revision)*

6. **Balbi M,** Dichgans M, Plesnila N
   Characterization of cerebrovascular function in a mouse model of cerebral small vessel disease – CARASIL *(Manuscript in preparation)*

7. Prades R, Oller-Salvia B, Schwarzmaier SM, Selva J, Moros M, **Balbi M**, Grazú V, de La Fuente, JM, Egea G, Plesnila N, Teixidó M, Giralt E
   Applying the retro-enantio approach to obtain a peptide capable of overcoming the blood-brain barrier.
   Angew Chem Int Ed Engl. 2015 Mar 23; 54(13):3967-72.

* Equally contributed

Eidesstattliche Versicherung/Affidavit

Hiermit versichere ich an Eides statt, dass ich die vorliegende Dissertation **“Regulation of cerebral blood flow in health and disease”** selbstständig angefertigt habe, mich außer der angegebenen keiner weiteren Hilfsmittel bedient und alle Erkenntnisse, die aus dem Schrifttum ganz oder annähernd übernommen sind, als solche kenntlich gemacht und nach ihrer Herkunft unter Bezeichnung der Fundstelle einzeln nachgewiesen habe.

I hereby confirm that the dissertation **“Regulation of cerebral blood flow in health and disease”** is the result of my own work and that I have only used sources or materials listed and specified in the dissertation.

München, den
Munich, date Unterschrift signature

List of author contribsutions

Dysfunction of mouse cerebral arteries during early aging

Balbi M, Ghosh M, Longden T, Jativa M, Gesierich B, Hellal F, Nelson M, Plesnila N

M.B. performed all in vivo experiments and wrote the manuscript.

M.G. performed all immunohistochemical staining

T.L. performed all in vitro experiments,contributed wiring, and edited the manuscript.

M.J. and **B.G.** analyzed data on neuronal firing

F.H. worked as a statistical consultant and edited the manuscript.

A.L. worked as a statistical consultant

M.N. edited the manuscript.

N.P. designed the study, wrote, and edited the manuscript

Neurovascular coupling after Subarachnoid Hemorrhage (SAH) in vivo

Balbi M, Koide M, Schwarzmaier S, Wellman G, Plesnila N

M.B. performed all *in vivo* experiments and wrote the manuscript

M.K. performed all ex vivo experiments and wrote the manuscript

S.S. provided technical input

G.W. designed the study and edited the manuscript

N.P. designed the study, wrote and edited the manuscript

Pericytes are involved in the pathogenesis of CADASIL

Ghosh M, Balbi M, Farida Hellal, Martin Dichgans, Lindauer U, Plesnila N

M.G. designed the study, performed experiments, analyzed the data, and wrote the manuscript

M.B. performed experiments, analyzed the data, and helped prepare the manuscript

F.H. helped in data analysis and was involved in the preparation of the manuscript

M.D. initiated the study and was involved in the preparation of the manuscript

U.L. designed the study, aided in data analysis and helped prepare the manuscript

N.P. designed the study, aided in data analysis, and wrote the manuscript

Characterization of cerebrovascular function in a mouse model of cerebral small vessel disease – CARASIL

Balbi M, Dichgans M, Plesnila N

M.B. performed all the experiments, analyzed the data and wrote the manuscript

M.D. initiated the study, designed the study

N.P. designed the study, aided in data analysis, and wrote the manuscript

Acknowledgments

I was a young and inexperienced girl when somebody saw in me motivation and enthusiasm and decided to give me an opportunity to transform what was potential into action, and that is how it all started. With this thesis I am not only celebrating a successful PhD but also all the people who were or became part of my life in these years, the people who enjoyed with me moments of happiness and shared my frustration when things were not going as expected, the same people who made me realize that in difficulty lies opportunity.

This thesis is of Nick, for betting on that young girl and opening for her the door of the opportunities, for teaching me about science, for without his guidance this work would not have been possible.

This thesis is of Farida, for seeing the fire in my eyes and keeping the flame alive like only somebody who has the same passion can do.

This thesis is of the people I discovered as more than just colleagues: Stefan for all the time he was there as only a friend can be; Thanasis, always ready to push me.

This thesis is of Uta, Susanne, Mitrajit, Kathrin, Sepiede, Gemma, Arthur, Vikram, Kathrin, Steffen, Pat, Caro, Jessi, Eva, Barbara, Nati, Nathalie, Manu, for teaching me the basis, for the time they took to answer all my questions, for using the right word in the right moment, for the daily support, for the laughs and the drama.

Questa tesi è dei miei genitori, perchè solo io conosco i sacrifici fatti durante questi anni, e quanto ancora per loro pesi la distanza che ci separa, ma in silenzio guardano me realizzarsi, ed è questo che rende loro felici.

Questa tesi è di mio fratello per tutte le volte che con uno sgurado carico d’orgoglio è li pronto a sostenermi.

Questa tesi è di mia nonna e dei miei zii perche non c’è stato un solo giorno in cui non mi abbiano dimostrato quanto fieri fossero di me.

Questa tesi è di Valerio, il mio punto fermo, il mio sostegno.

This thesis is of Elsa, Martin, Silvia, Thea, for the support they always showed me in this years, and never judge my choices.

Esta tesis es de Max, porque sin su amor y apoyo incondicional no podría haberlo logrado. Gracias por las aventuras de estos años.

This thesis is also a bit mine, wishing to keep a spirit of adventure in regard to research.

“Only a burning patience will lead to the attainment of a splendid happiness”

Neruda